



DISSERTATION

# Comprehensive Visualization of Cardiac MRI Data

ausgeführt zum Zwecke der Erlangung des akademischen Grades  
eines Doktors der technischen Wissenschaften unter der Leitung von

Ao. Univ. Prof. Dipl.-Ing. Dr. techn. Eduard Gröller  
Institut für Computergraphik und Algorithmen  
Abteilung für Computergraphik

eingereicht an der Technischen Universität Wien

Fakultät für Informatik

von

Dipl.-Ing. Maurice Alain Termeer  
Matrikelnummer 0827082  
Lange Gasse 14 / 2 / 27  
1080 Wien  
Österreich

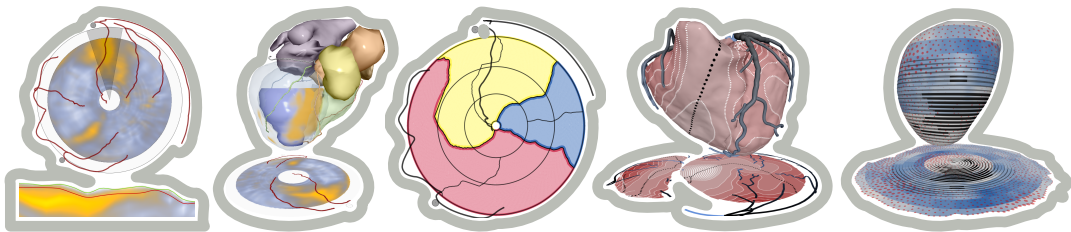
Wien, im Dezember 2008



---

# Comprehensive Visualization of Cardiac MRI Data

---



---

**Maurice Termeer**

---





# Abstract

Coronary artery disease is one of the leading causes of death in the western world. The continuous improvements in magnetic resonance imaging technology facilitate more accurate diagnoses by providing increasingly more detailed information on the viability, functioning, perfusion, and anatomy of a patient's heart. This increasing amount of information creates the need for more efficient and more effective means of processing these data.

This thesis presents several novel techniques that facilitate a more comprehensive visualization of a patient's heart to assist in the diagnosis of coronary artery disease using magnetic resonance imaging (MRI). The volumetric bull's eye plot is introduced as an extension of an existing visualization technique used in clinical practice—the bull's eye plot. This novel concept offers a more comprehensive view on the viability of a patient's heart by providing detailed information on the transmural scar while not suffering from discontinuities.

Anatomical context is often lost due to abstract representations of data, or may be scarce due to the nature of the scanning protocol. Several techniques to restore the relation to anatomy are presented. The primary coronary arteries are segmented in a whole heart scan and mapped onto a volumetric bull's eye plot, adding anatomical context to an abstract representation. Similarly, segmented late enhancement data are rendered along with a three-dimensional segmentation of the patient-specific myocardial and coronary anatomy. Additionally, coronary supply territories are computed from patient-specific data as an improvement over models based on population averages.

Information on the perfusion of the myocardium provided by MRI is typically of fairly low resolution. Using high-resolution anatomical data, an approach to visualize simulated myocardial perfusion is presented, taking full advantage of the detailed information on perfusion. Finally, a truly comprehensive visualization of a cardiac MRI exam is explored by combining whole heart, late enhancement, functional, and perfusion scans in a single visualization. The concepts introduced help to build a more comprehensive view of the patient and the additional information may prove to be beneficial for the diagnostic process.



# Kurzfassung

Koronare Herzkrankheit ist eine der führenden Todesursachen in der westlichen Welt. Die kontinuierliche Verbesserung der Magnetresonanztomographie (MRT) erleichtert genauere Diagnosen, indem sie immer detailliertere Informationen über die Lebensfähigkeit, das Funktionieren, die Durchblutung und die Anatomie des Herzens eines Patienten liefert. Diese zunehmende Menge an Informationen schafft die Notwendigkeit für effizientere und effektivere Mittel der Verarbeitung dieser Daten.

Diese Dissertation präsentiert mehrere neue Techniken, die eine umfassendere Visualisierung des Patienten bei der Diagnose von Erkrankungen der Herzkranzgefäße mittels MRT unterstützen. Das volumetrische Polardiagramm wird als Erweiterung des Polardiagramms, welches eine bestehende Visualisierungstechnik in der klinischen Praxis ist, eingeführt. Dieses neuartige Konzept bietet eine umfassendere Sicht auf die Lebensfähigkeit des Herzens eines Patienten, indem detaillierte Informationen über die Transmuralität der Narbe ohne Diskontinuitäten bereitgestellt werden.

Anatomische Zusammenhänge gehen in abstrakten Darstellungen von Daten häufig verloren. Darüberhinaus liefern einige Arten von Scans relativ wenig anatomischen Kontext. Mehrere Techniken zur Wiederherstellung des anatomischen Bezugs werden vorgestellt. Die primären Koronararterien sind in einem Scan des ganzen Herzens segmentiert und werden auf ein volumetrisches Polardiagramm abgebildet. Hierbei wird der abstrakten Repräsentation anatomischer Kontext hinzugefügt. Ebenso, werden segmentierte spätere Anreicherungsdaten zusammen mit einer drei-dimensionalen Segmentierung des patientenspezifischen Herzmuskels und koronarer Anatomie dargestellt. Darüberhinaus werden koronare Versorgungsgebiete aus den patientenspezifischen Daten berechnet. Dies bedeutet eine Verbesserung gegenüber Modellen welche auf Bevölkerungsdurchschnitten basieren.

Informationen über die Durchblutung des Herzmuskels welche aus MRT-Aufnahmen abgeleitet werden können sind in der Regel von relativ geringer Auflösung. Unter Verwendung hochauflösender anatomischer Daten wird ein Konzept für die Visualisierung simulierter Durchblutung des Herzmuskels präsentiert. Dabei wird die detaillierte Information über die Durchblutung genutzt. Schließlich, wird eine wirklich umfassende Visualisierung einer Herz-MRT-Untersuchung erforscht. Dabei werden

Scans des ganzen Herzens, der Herzvitalität, der Herzfunktion und der Durchblutung in einer einzigen Visualisierung kombiniert. Die eingeführten Konzepte fördern den Aufbau eines umfassenderen Überblicks über den Patienten. Die dabei zusätzlich gewonnene Information kann für den Diagnoseprozess von Nutzen sein.

# Contents

<b>Preface</b>	<b>xiii</b>
<b>1 Introduction</b>	<b>1</b>
1.1 The Human Heart . . . . .	1
1.2 Coronary Artery Disease . . . . .	3
1.3 Magnetic Resonance Imaging . . . . .	5
1.3.1 Cardiac MRI . . . . .	6
1.3.2 Whole Heart Imaging . . . . .	7
1.3.3 Functional Imaging . . . . .	8
1.3.4 Late Enhancement Imaging . . . . .	10
1.3.5 First-Pass Perfusion Imaging . . . . .	11
1.4 Visualization of Cardiac MRI Data . . . . .	12
1.5 Scope of this Thesis . . . . .	14
<b>2 The Volumetric Bull’s Eye Plot</b>	<b>15</b>
2.1 Introduction . . . . .	15
2.2 Related Work . . . . .	17
2.2.1 The Bull’s Eye Plot . . . . .	17
2.2.2 Combinations with Other Visualization Techniques	18
2.2.3 Segmentation of the Myocardium . . . . .	19
2.3 The Volumetric Bull’s Eye Plot . . . . .	20
2.3.1 Unfolding the Myocardium . . . . .	23
2.3.2 Overall Distribution of Scar . . . . .	24
2.3.3 Transmurality of Scar . . . . .	25
2.3.4 Preservation of Wall Thickness . . . . .	27
2.3.5 Overlaying Coronary Arteries . . . . .	30
2.3.6 Implementation Details . . . . .	30
2.4 Summary and Conclusions . . . . .	30
<b>3 Viability in an Anatomical Context</b>	<b>33</b>
3.1 Introduction . . . . .	33
3.2 Related Work . . . . .	34
3.3 Overview of the Framework . . . . .	34
3.4 Viability in an Anatomical Context . . . . .	37
3.4.1 Visualization of Coronary Arteries . . . . .	39

3.4.2	Resolving Occlusion of Scar . . . . .	40
3.4.3	Visualizing Slice Data . . . . .	41
3.4.4	Integration of Diverse Rendering Techniques . . . . .	43
3.5	Interactive Exploration with Linked Views . . . . .	44
3.5.1	Standard Views . . . . .	44
3.5.2	Interactive Navigation . . . . .	45
3.5.3	Automatic Viewpoint Control . . . . .	45
3.6	Summary and Conclusions . . . . .	46
<b>4</b>	<b>Patient-Specific Coronary Territories</b>	<b>49</b>
4.1	Introduction . . . . .	49
4.2	Related Work . . . . .	51
4.3	Computation of Coronary Territories . . . . .	52
4.3.1	Mesh of the Epicardium . . . . .	53
4.3.2	Projection of the Coronary Arteries . . . . .	54
4.3.3	Computation of the Voronoi Diagram . . . . .	54
4.3.4	Projection onto a Bull's Eye Plot . . . . .	56
4.4	Patient-Specific Coronary Territories . . . . .	56
4.4.1	A Patient-Specific 17-Segment Model . . . . .	58
4.4.2	Unconstrained Coronary Territories . . . . .	60
4.5	Medical Expert Evaluation . . . . .	60
4.5.1	Application to CT Data . . . . .	62
4.5.2	Application to Late Enhancement Data . . . . .	62
4.6	Discussion . . . . .	63
4.7	Summary and Conclusions . . . . .	66
<b>5</b>	<b>Visualization of Simulated Myocardial Perfusion</b>	<b>67</b>
5.1	Introduction . . . . .	67
5.2	Related Work . . . . .	68
5.3	Computation of Coronary Flow . . . . .	70
5.3.1	Perfusion through the Coronary Arteries . . . . .	71
5.3.2	Modeling of a Stenosis . . . . .	73
5.3.3	Diffusion of Flow . . . . .	73
5.4	Visualization of Coronary Flow . . . . .	75
5.4.1	Bull's Eye Plot Representation . . . . .	76
5.4.2	Blood Supply Area and Underperfused Regions . . . . .	77
5.4.3	Coronary Artery Territories . . . . .	79
5.4.4	Separate Coronary Artery Territories . . . . .	80
5.4.5	Querying Supplying Coronary Arteries . . . . .	81
5.5	Simulation and Visualization of a Stenosis . . . . .	82
5.5.1	Supply and Underperfused Regions . . . . .	83
5.5.2	Coronary Artery Territories . . . . .	83
5.5.3	Querying Supplying Coronary Arteries . . . . .	83
5.6	Discussion . . . . .	85

---

5.6.1	Feedback from Expert Clinicians . . . . .	86
5.6.2	Implementation Details . . . . .	87
5.7	Summary and Conclusions . . . . .	88
<b>6</b>	<b>Comprehensive Cardiac MRI Visualization</b>	<b>89</b>
6.1	Introduction . . . . .	89
6.2	Medical Background . . . . .	90
6.3	Simultaneous Visualization of Multiple Quantitative Analyses	93
6.3.1	Visualizing Viability using Textures . . . . .	95
6.3.2	Visualizing Function using Color Coding . . . . .	96
6.3.3	Visualizing Perfusion using Glyphs . . . . .	97
6.4	Comprehensive Visualization using Decision Trees . . . . .	98
6.5	Summary and Remaining Challenges . . . . .	99
<b>7</b>	<b>Summary and Conclusions</b>	<b>101</b>
<b>A</b>	<b>Coronary Territory Questionnaire</b>	<b>103</b>
A.1	Manually Defined Territories . . . . .	104
A.2	Territories Based on the 17-Segment Model . . . . .	105
A.3	Territories Based on an Adapted 17-Segment Model . . . . .	106
A.4	Territories Based on the Patient-Specific Coronary Anatomy	107
	<b>Bibliography</b>	<b>109</b>
	<b>Curriculum Vitae</b>	<b>119</b>





Die Viel-zu-vielen, deren  
Untergang man weder bedauern  
noch aufhalten sollte.

---

frei nach Friedrich Nietzsche

## Preface

**T**HIS WORK would not have been possible without the help and support of many people. I would like to thank Meister Eduard Gröller, Javier Oliván Bescós, and Marcel Breeuwer for sharing their knowledge, expertise, and inspiration and for the many fruitful discussions we have had. Furthermore I would like to thank Anna Vilanova and Frans Gerritsen for their scientific contributions and additional support, Eike Nagel for his contributions as a medical expert, and the people of the Philips Healthcare, Healthcare Informatics, Clinical Science & Advanced Development group. Last but not least I would like to express my thanks for providing a motivating and fun working environment to the people of the Visualization Group of the Vienna University of Technology, including Stefan Bruckner, Raphael Fuchs, Martin Haidacher, Peter Kohlmann, Muhammad Muddassir Malik, Matej Mlejnek, Daniel Patel, Peter Rautek, Ivan Viola, and Erald Vuçini.

This work was performed in the scope of the COMRADE project<sup>1</sup> funded by Philips Healthcare, Best, The Netherlands. Several datasets used during this project were provided by Hyogo BHC at Himeji, Japan, the Tokyo Metro Police Hospital, Japan, the Medical Satellite Yaesu Clinic, Japan, and the Kumamoto Cyon Hospital, Japan.

Vienna, Austria, December 2008

*Maurice Termeer*

---

<sup>1</sup><http://www.cg.tuwien.ac.at/research/vis/comrade>



Experience is what you get if  
you didn't get what you wanted.

---

Dan Stanford

# 1

## Introduction

Heart disease is one of the leading causes of death in the western world [4]. Most patients, especially at later age, suffer from coronary artery disease. The continuous improvement in tomographic imaging technology is enabling the early detection and accurate diagnosis of this disease. With a continuously increasing amount of data produced by modern scanning technology, there is a need for more efficient and effective methods for processing these data. This chapter gives a brief introduction into the anatomy of the human heart, coronary artery disease, how magnetic resonance imaging can be used to diagnose this disease, and currently common approaches to process and visualize the resulting tomographic cardiac data.

### 1.1 The Human Heart

**T**HE HUMAN HEART is one of the first organs to form in a human embryo. It maintains the circulation of blood throughout the body from three weeks after conception and continues to do so until the very end of a human life. This muscular organ is located slightly left of the center of the thorax, beneath the breastbone and is surrounded by the lungs. The majority of the heart is formed by a body of muscle tissue called the myocardium. The myocardium is surrounded by the pericardium on the outside and the endocardium on the inside of the heart. Figure 1.1 depicts an annotated anterior view of a human heart, while Figure 1.2 show the inside of the heart.

A human heart can be divided into a left and a right part. Each half consists of an atrium and a ventricle, giving the heart four chambers in total. The left and right halves are separated by the septum. The right

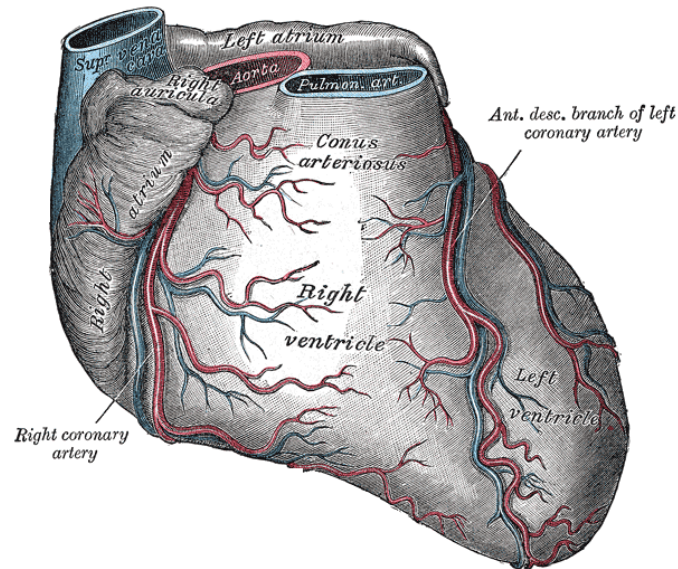


Figure 1.1: Anterior view of the heart depicting the atria, ventricles, connecting vessels, and the coronary arteries. Image courtesy of Gray [73].

heart is responsible for circulating blood through the lungs, while the left heart supplies the remainder of the body with oxygen-rich blood. As the left ventricle has to pump blood through a much larger part of the body than the right ventricle, the left ventricle has a thicker, stronger muscular wall. The tip of the left ventricle is called the apex, while the area near the top is called the base.

The repeating process of pumping blood through the heart by a series of muscle contractions is called the cardiac cycle. This cycle can be divided into two phases. The first phase is when the ventricles are in a relaxed state and are being filled with blood. This phase is called diastole. During the second phase the ventricles contract to pump out blood. This phase is called systole.

Each cardiac cycle, oxygen-depleted blood flowing through the inferior and superior vena cava enters the heart in the right atrium. It is then pumped through the tricuspid valve into the right ventricle. From there it flows through the pulmonary valve into the pulmonary artery, which leads the blood through the lungs. Inside the lungs gas exchange between carbon dioxide and oxygen occurs. The now oxygen-rich blood then flows through the pulmonary vein into the left atrium. Passing through the mitral valve, it enters the left ventricle, which finally pumps it through the aortic valve into the aorta.

Near the beginning of the aorta, two smaller vessels branch off. These are called the left and right coronary artery. These coronary arteries branch into a network of smaller arteries that supply the heart with oxygenated

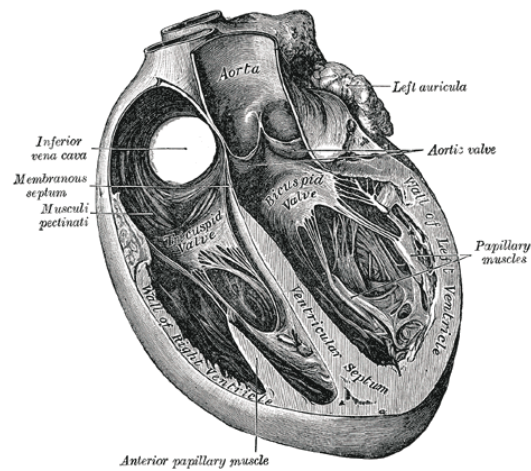


Figure 1.2: Anterior view of the heart exposing the inside of the ventricles, the valves, and the septum. Image courtesy of Gray [73].

blood. In Figure 1.1 the right coronary artery and left anterior descending are well visible. These two arteries are often abbreviated RCA and LAD, respectively. On the posterior side of the heart there also is the left circumflex, another branch of the left coronary artery often abbreviated LCX. These three arteries are the three main coronary arteries. They each branch into a network of smaller vessels. The exact shape and location of the coronary artery network differs greatly among individuals.

## 1.2 Coronary Artery Disease

Coronary artery disease is a collection of diseases related to a deficiency in one or more of the coronary arteries. It is sometimes also referred to as coronary heart disease and is commonly abbreviated CAD or CHD. Coronary artery disease is caused by the accumulation of atheromatous plaques on the walls of the coronary arteries. These plaques may form due to a number of reasons, including smoking, diabetes, high cholesterol, old age, and obesity. Over time a plaque may calcify and remain within the vessel wall. These plaques are relatively harmless since they do not cause a significant narrowing of the vessel. More harmful are lipid core plaques, which do not calcify. These plaques gradually increase in size and expand into the lumen of the vessel. Due to inflammation they can eventually rupture, which may obstruct the blood flow in the vessel. The acute rupture of a plaque is a common cause of sudden death, usually due to an infarction of the myocardium. Such an infarction is however not necessarily fatal. Plaques extending into the lumen of the vessel can also cause problems without rupturing. They may cause a partial or complete

obstruction of the vessel known as a stenosis. It can take several years before the effects of such an accumulation of plaque becomes noticeable.

Both an acute and chronically developed obstruction of a coronary artery can trigger a myocardial infarction, an event also known as heart attack. During this event myocardial tissue becomes infarcted due to a lack of supply of oxygenated blood. Without a quick response, the tissue in the affected area will receive irreversible damage. After an infarction the dead tissue will turn into scar. If the infarcted area does not extend through the entire wall of the ventricle, the healthy part of the wall can thicken while the scar thins over time. This degree of how far scar extends into the wall is called the transmural of the scar.

Within the area of coronary artery disease, the following three types of diseases, each caused by a partial or complete obstruction of the blood flow in one or more of the coronary arteries, are commonly distinguished.

**Ischemia** or ischemic heart disease is a condition where part of the myocardium does no longer receive sufficient oxygenated blood to contract, but is not yet infarcted, i.e. the muscle tissue is still alive. Tissue with reduced perfusion is said to be hypoperfused, which can also occur without a decrease in contractility. When contractility is decreased, this type of tissue is commonly called hibernating myocardium. Reduced wall contraction lowers the cardiac output, an indicator for how much blood the heart can pump. Ischemia can be caused by both partial and complete obstructions of a vessel. Restoring the proper supply of oxygenated blood through revascularization will restore the proper functioning of the myocardium.

**Chronic infarction** refers to a condition where the patient has already experienced one or more myocardial infarctions. An infarction occurs when part of the myocardium receives too little oxygenated blood to remain viable and is more commonly caused by complete than partial obstructions of a vessel. The muscle tissue dies and proper functioning of this tissue can no longer be restored. Over time the dead tissue will turn into scar. Myocardial tissue surrounding an area of scar can be ischemic. This tissue may show reduced wall contraction, but is not yet scar and can thus still benefit from restoring the blood flow by revascularization.

**Acute infarction** refers to an acute rupture of a plaque, causing a sudden block of oxygenated blood and preventing part of the myocardium to contract. Without a supply of oxygenated blood, infarction will occur after about 20 minutes. If the blood flow can be restored quickly enough, the affected area, called the area at risk, may still recover. The time frame in which revascularization is considered to be useful is around six hours.

The care cycle of coronary artery disease starts with a proper diagnosis. If it is concluded that the patient would benefit from intervention, several techniques exist for restoring the blood flow, a process known as revascularization. Bypass surgery consists of grafting vessels from another part of the body to bypass the obstructed part of a vessel. Coronary angioplasty involves placing a small balloon inside the obstructed vessel and then inflating it to widen the vessel. A stent can be placed to maintain the vessel shape after the balloon is removed. Finally, a blood clot causing obstruction can be diluted through pharmacological means by a technique called thrombolysis.

### 1.3 Magnetic Resonance Imaging

Magnetic resonance imaging (MRI) is a non-invasive [23] tomographic imaging technique based on spin properties of hydrogen nuclei. While a brief introduction into the basics of MRI follows, the reader is directed to other sources for a more thorough description of the technology behind MRI [32, 34].

An MRI scanner generates a strong, static magnetic field. The common field strength in current clinical practice is 1.5 Tesla, although a transition towards 3.0 Tesla is in progress [27, 58]. The organic compounds found in a human body contain relatively many hydrogen nuclei. These subatomic particles possess the quantum mechanical property of spin. When a body is placed inside the scanner, the spins of these hydrogen nuclei align themselves to the magnetic field in either a low or a high energy state. Under normal conditions, there are slightly more nuclei in the low energy state than in the high energy state. Nuclei in the low energy state can absorb a photon that has an energy that matches the difference in energy between the low and high energy states. Thus a radio frequency pulse can be used to excite the nuclei in the low energy state and throw them in the high energy state. This phenomenon is called resonance and explains the name magnetic resonance imaging. The exact frequency of the required radio frequency pulse is called the Larmor frequency and depends on many factors, including the strength of the magnetic field.

When the radio frequency pulse is stopped, the ratio between nuclei in the low and high energy states will restore itself. During this process nuclei that jump from the high energy state back to the low energy state emit the previously absorbed energy in the form of a radio frequency wave. It is this energy that can be detected using receiver coils, giving the MRI signal. Since different tissues have a different proton density, the MRI signal they cause also differs. Besides the proton density, two other tissue-specific characteristics can be read from the MRI signal. These two properties are related to the net magnetization of the nuclei. The

first is the rate at which the equilibrium of energy states is restored, the spin lattice relaxation time or  $T_1$ . This is the time for the longitudinal magnetization, the component aligned with the magnetic field, to increase by a factor of  $e$ . The second is the rate at which the spins of the nuclei dephase, the spin-spin relaxation time or  $T_2$ . This is the time for the transverse magnetization, the component orthogonal to the magnetic field, to decrease by a factor of  $e$ . Inhomogeneities in the magnetic field of the scanner affect the measurement of  $T_2$ . The measured decay factor, which is always less than  $T_2$ , is referred to as  $T_2^*$ .

Three magnetic gradients inside the scanner can locally change the magnetic field strength. Since the Larmor frequency depends on magnetic field strength, these gradients can be used to control which nuclei react to a radio frequency pulse. A slice selection gradient defines an imaging plane in which the nuclei react. A phase-encoding and frequency-encoding gradient are then used to further control the way the nuclei within the imaging plane react to the radio frequency pulse. The type of pulse used and the rate at which it is repeated affect the contribution of proton density,  $T_1$  and  $T_2$  to the final image. A phase-frequency image is constructed and using an inverse Fourier transformation, a two-dimensional image visualizing the anatomy can finally be obtained.

The main advantages of MRI compared to other imaging modalities are that it offers excellent soft tissue contrast and a high spatial and temporal resolution on an imaging plane of any orientation with a good signal-to-noise ratio. Since MRI uses harmless magnetic fields, it is also well suited for screening purposes. This is less true for some other tomography techniques. Computed tomography (CT) is based on X-ray technology and thus uses harmful ionizing radiation. Nuclear medicine methods including single photon emission computed tomography (SPECT) and positron emission tomography (PET) use harmful radioactive compounds. Disadvantages of MRI include the relatively high cost of the scanner. Furthermore since an MRI tube is rather narrow, some patients may experience claustrophobia. Also the presence of ferro-magnetic implants in a patient can be a reason not to undergo an MRI exam [23], although the acceptance of patients with pacemakers is being reconsidered [52].

### 1.3.1 Cardiac MRI

MRI is a powerful diagnostic imaging technique for the diagnosis of coronary artery disease [47, 19, 66, 69]. MRI in the context of diagnosing heart diseases is commonly called cardiac MRI. Given a patient with suspected coronary artery disease, making an accurate diagnosis and adequate treatment planning requires information on several aspects of the heart. MRI can provide information on the contractile functionality of the myocardium, the viability of myocardial tissue, changes in the perfusion



of the myocardium and changes in the myocardial and coronary arteries anatomy. These are all important factors for the diagnosis of coronary artery disease. This diversity is one of the main strengths of cardiac MRI. The sections below give a brief introduction to the individual cardiac MRI scanning protocols that are used to assess these properties.

Although MRI is an attractive technique for the diagnosis of coronary artery disease, in current clinical practice echocardiography, X-ray angiography, and nuclear medicine are still more prevalent than both MRI and CT. Reasons include MRI being rather expensive and relatively young. Good correlations between MRI perfusion imaging, X-ray angiography, and SPECT have been reported [81, 55] and the popularity of MRI in cardiac medicine is expected to increase.

### 1.3.2 Whole Heart Imaging

Whole heart imaging [88] provides a high resolution scan of the cardiac anatomy. A typical resolution for a whole heart scan is 160 slices of 512 by 512 voxels each. While it reveals little about the actual functioning of the heart, it provides detailed anatomical information on the shape and size of the ventricles and the location of the coronary arteries. Current whole heart MRI technology is however not yet capable of imaging the coronary arteries at a quality level that can compete with X-ray coronary angiography or coronary CT. Magnetic resonance angiography (MRA) is a related scanning protocol specifically for imaging the coronary arteries [9, 71, 90]. Since the coronary arteries can be hard to detect in a regular whole heart scan, a contrast agent is occasionally used to emphasise the coronary arteries. While the current clinical standard remains X-ray angiography, the less invasive nature and good correlations of MRA to X-ray angiography make it an attractive alternative angiography technique [1, 17, 41]. However, due to its higher spatial resolution, coronary CT angiography is also becoming more prevalent [33].

An example of two reformats from a whole heart scan are shown in Figure 1.3. This figure depicts two common orientations of the imaging plane in cardiac tomography. In the short-axis view (see Figure 1.3a) the imaging plane is perpendicular to the long axis, one of the two standard cardiac axes that runs from the base of the left ventricle to the apex. The 4-chamber long-axis view shown in Figure 1.3b is aligned to both the long and short axes. The latter axis runs approximately from the mitral valve to the tricuspid valve.

Due to its relatively high resolution a whole heart scan is well suitable for segmentation purposes [20]. A high quality segmentation is useful for visualization purposes, as will be demonstrated in this thesis. Due to continuous improvements of MRI technology [82, 38], the additional

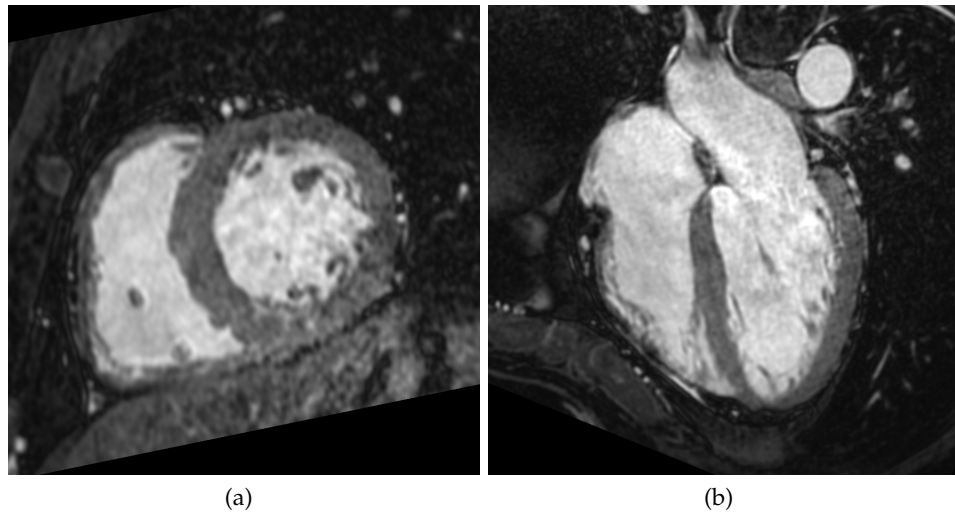


Figure 1.3: Two reformatted images from a whole heart scan showing (a) a short-axis view and (b) a 4-chamber long-axis view.

scanning time required for a whole heart scan is decreasing to a single breathhold.

### 1.3.3 Functional Imaging

Directly assessing the functionality of the heart provides information on whether any pathology already has had an effect. Capturing this type of information is possible with functional imaging, also called cine MRI. A cine scan provides dynamic image data of a beating heart. It has proven to be an effective method for detecting abnormalities in cardiac functionality [86, 54, 56] and has been shown to have increased sensitivity and specificity compared to echocardiography [68]. Common exams consist of the acquisition of a stack of short-axis slices, a 2-chamber long-axis view, and a 4-chamber long axis view. Figure 1.4 shows three short-axis slices from a cine-scan at the same slice scanning location but at different phases of the cardiac cycle. In order to deal with cardiac motion, an electrocardiogram (ECG) is used to determine the phase of each slice during scanning. Once all slices are acquired, this information can be used to place the slices in the correct order. Current MRI technology allows for the acquisition of a cine-sequence of a full heart beat in a single breathhold, but due to time restrictions such scans are typically limited to three to five slices [47]. Free-breathing cine allows for the acquisition of more slices through the use of respiratory gated scanning techniques, where in addition to an ECG also the lung-liver interface is monitored

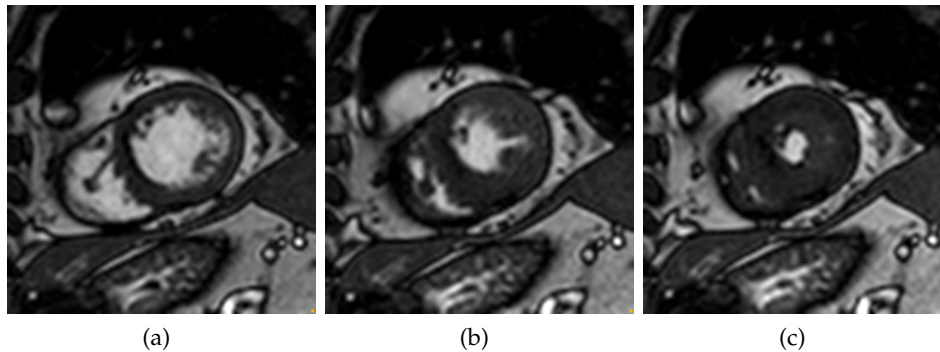


Figure 1.4: Three short-axis slices from a functional scan of different phases of the cardiac cycle ranging from (a) end-diastole to (c) end-systole.

to ensure all slices are scanned at approximately the same phase of the respiratory cycle.

A functional scan can be quantitatively analyzed to provide absolute measurements on the functioning of the heart [67]. Quantitative analysis requires a segmentation of the myocardium. Automatic segmentation techniques can greatly reduce the required amount of work of making this segmentation [29]. Several measures are commonly used to assess the relative health of a patient's heart. Stroke volume is the difference in volume of the left ventricular blood pool between end-diastole and end-systole. Ejection fraction is the stroke volume divided by the end-diastolic volume. Cardiac output is the stroke volume multiplied by the heart rate. Wall thickening is the difference in wall thickness at end-diastole and end-systole divided by the end-diastolic wall thickness [11]. The results of a quantitative analysis can be presented graphically by first dividing the myocardium in a number of segments on each slice. These segments can then be visually arranged into a single diagram called a bull's eye plot, showing a quantitative measure, for example wall thickening, for the entire left ventricle in a single image. The bull's eye plot is further discussed in Section 1.4.

While an MRI exam virtually always contains a functional scan at rest, functional scans at different stress levels can also optionally be acquired. A common stress inducing agent is dobutamine [86, 44]. The type of exam to measure function under stress using this contrast agent is often called dobutamine stress MRI. At a higher stress level the myocardium requires more oxygen. Any decreased functionality due to an obstructed supply of oxygenated blood may therefore be more pronounced at higher stress levels.

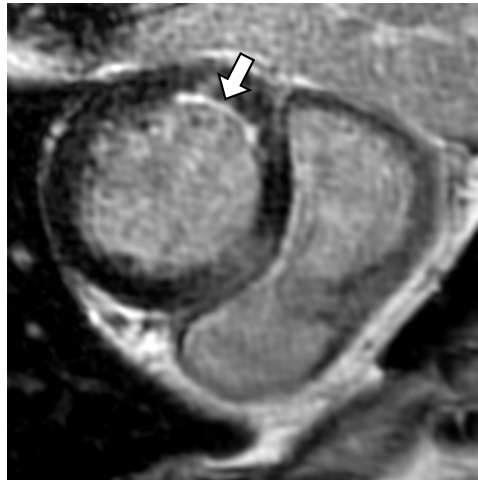


Figure 1.5: A slice from a late enhancement scan. The arrow indicates an area showing hyperenhancement near the endocardium.

### 1.3.4 Late Enhancement Imaging

Myocardial tissue that has died due to a prolonged lack of supply of oxygenated blood can be detected using late enhancement imaging, also referred to as delayed enhancement or delayed contrast enhancement imaging [89, 42, 16, 12, 8]. A contrast agent, most often gadolinium-based, that shows up bright on an MRI image is injected into the patient. Approximately 15 to 20 minutes after injection a scan is made. A scan typically consists of 15 to 20 short-axis slices, a 2-chamber long axis slices, and optionally a 4-chamber long-axis slice. All slices are taken at approximately the end diastolic phase of the cardiac cycle. An example of a short-axis late enhancement slice is shown in Figure 1.5. The injected contrast agent accumulates in infarcted tissue, while washing out of the well-perfused, viable parts of the myocardium. In the resulting scan hyperenhancement, an increase in signal strength due to contrast agent accumulation, is therefore observed in infarcted tissue. Some other tissues, such as the fat surrounding the heart, also show up bright in a late enhancement scan.

When assessing viability, the location and size of the infarcted region are relevant attributes to determine. The degree to which an infarcted region covers the myocardial wall, the transmural extent of infarction, is also important [15]. Scar can occur for example only near the endocardium, only near the epicardium, or in the middle of the myocardial wall. The exact location provides information on the nature of the infarct. If there is sufficient healthy tissue remaining, the infarcted tissue may thin over time and the wall can recover. Obtaining detailed information on the

transmurality of scar as well as the absolute amount of healthy tissue remaining is thus important for making an accurate diagnosis.

Also a late enhancement scan can be quantitatively analyzed. A common approach consists of first segmenting the myocardium. Since the scan consists of relatively few slices and only a single time step, a manual segmentation approach is feasible. Similar to the quantitative analysis of functional data, also this segmentation can be used to divide the myocardium in a number of segments. For each segment the percentage of scar and the transmural extent of infarction can then be visually presented in a bull's eye plot.

### 1.3.5 First-Pass Perfusion Imaging

Decreased contractility and scar are both the results of a reduced oxygen supply to the myocardium. The perfusion of the myocardium itself can also be visualized using first-pass perfusion imaging [55, 72, 2, 13, 35]. Similar to late enhancement imaging, this protocol relies on the use of a contrast agent. Instead of letting the contrast agent accumulate, the first pass of the contrast agent through the heart is captured. Since this imposes severe timing constraints—the scan has to be completed after the contrast agent has passed through the heart—the number of slices is typically limited to three to five at a temporal resolution of 10 to 30 time steps. The scanner, the patient's heart rate, and the duration a patient is capable of holding his breath all influence these limitations. A perfusion scan is always scanned under artificially induced stress. In contrast to functional imaging, a vasodilator, e.g. adenosine, is used to widen the vessels, simulating the effects of stress while keeping the heart rate low. Optionally a rest perfusion scan is made after the stress perfusion scan.

Figure 1.6 shows a few slices from a first-pass perfusion scan. A proper perfusion scan shows the contrast agent first enter the right ventricular blood pool, then enter the left ventricular blood pool and finally diffuse into the myocardium. In the latter phase a perfusion defect manifests itself as an area that lights up less bright—or not at all—than the rest of the myocardium. This is indicated by the white arrows in Figure 1.6d.

Due to the breathing motion from the patient during scanning, a perfusion scan often suffers from motion artifacts. Therefore the quantitative analysis of a perfusion scan often requires a registration between the various time steps of each slice. Note that registration can only compensate for motion parallel to the imaging plane. After the myocardium is segmented in the registered scan, a time-intensity curve can be constructed for each voxel of the scanned myocardium. Many parameters can be derived from this curve, including the average speed with which the signal strength increases, the time it takes to reach maximum signal strength and the maximum signal strength itself. These values are known as mean or maxi-

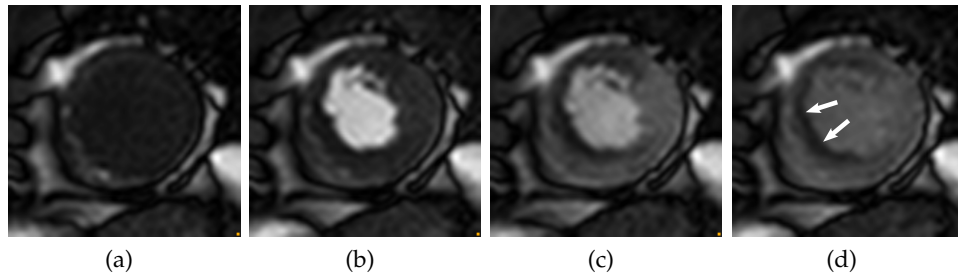


Figure 1.6: Four short-axis slices from a first-pass perfusion scan showing (a) no enhancement, (b) the contrast agent entering the left ventricular blood pool, and (c) & (d) diffusing into the myocardium. The darker area in the myocardium indicates a perfusion defect.

imum upslope, time-to-peak, and peak enhancement, respectively. When both a stress and rest scan are available, the myocardial perfusion reserve index (MPRI) can be computed, which is the ratio between the maximum upslope of the stress and rest scan. This measure has been shown to be an accurate indicator for coronary artery disease [55].

## 1.4 Visualization of Cardiac MRI Data

Visualization techniques can help reduce the workload by presenting data in a more accessible manner. Much work has been done on visualization techniques for cardiac MRI data. In this section a few of the most commonly applied techniques are mentioned. The remaining chapters contain a more complete discussion of relevant related work.

In current clinical practice, the primary methods of analyzing data from an MRI exam are based on visual inspection of the reconstructed slices. This requires much expertise from the clinician, for example in discriminating scanning artifacts from pathologies. It also means that combining the information provided by the scans of the various protocols has to be done mentally, by examining scans successively or side-by-side.

Segmentation is being applied increasingly, as it not only facilitates taking quantitative measurements but also creates possibilities for more advanced visualization techniques. Segmenting the left ventricular myocardium in a functional scan enables the computation of local wall thickness and subsequently related measurements including wall thickening, stroke volume, and ejection fraction. Segmenting the left ventricular myocardium in a late enhancement scan allows to depict the viability of the entire left ventricle in a two-dimensional schematic visualization called a bull's eye plot. Figure 1.7 shows two bull's eye plots of late enhancement data. Each concentric ring depicts data from one short-axis slice. The

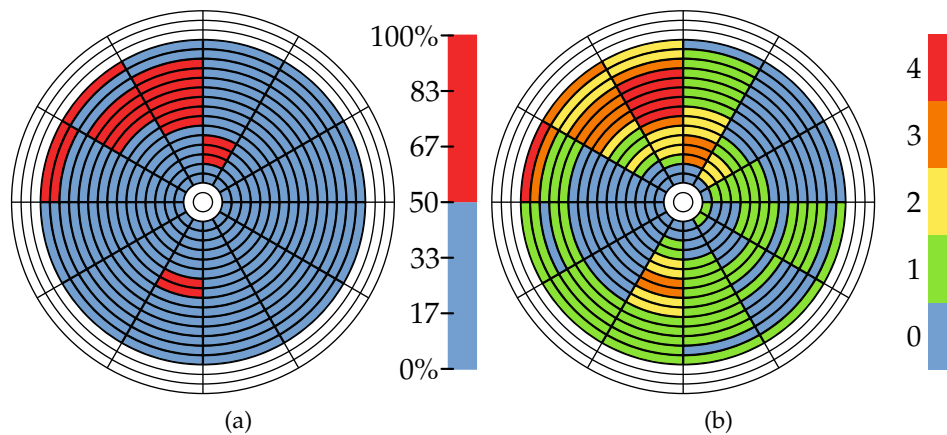


Figure 1.7: Two bull's eye plots of a late enhancement scan representing (a) percentage of scar and (b) transmural extent.

quantitative analysis results of both functional and perfusion scans are also commonly depicted in bull's eye plots. A more thorough description of the bull's eye plot is given in Chapter 2.

In a whole heart scan the individual parts of the heart can be segmented fully automatically [20]. This provides a patient-specific model of the heart, suitable as anatomical context in visualizations. The centerlines of the coronary arteries can also be segmented in a whole heart scan [50]. Current MRI scans do not yet offer sufficient level of detail to provide accurate vessel diameter measurements. Since the coronary arteries have a complex shape, examining them in two-dimensional slices is a tedious task that requires a lot of training. Once segmented, the coronary arteries can be visualized while preserving their complex shape by reformatting the whole heart scan on a three-dimensional surface that intersects the coronary arteries [21, 83]. Abstracting from their complex shape by virtually stretching the arteries and visualizing the reformatted whole heart scan has the advantage that the image data covering the entire artery can be observed in two dimensions [39].

The abundance of information provided by the available scanning protocols is one of the main advantages of cardiac MRI over other tomographic imaging technologies. Combining the information contained within the data of the multiple scans provides a more detailed understanding of the patient and allows for a more accurate diagnosis. It has been shown that combining perfusion and viability information [12, 30], optionally with coronary arteries [31], or combining functional and viability information [59, 26], provides an accurate discrimination between viable, ischemic, and infarcted tissue and also facilitates the detection of hibernating myocardium.

## 1.5 Scope of this Thesis

The large amount of mental processing involved in current diagnostic work flows seems to be partially caused by not explicitly visualizing relations between different types of data. This thesis explores several visualization approaches that present various types of data in a rich anatomical context. Several data types can be combined to increase spatial correlation between them. Data can also be represented differently, to easier extract desired information. Together these visualization approaches aim towards a comprehensive visualization of cardiac MRI data, combining the anatomy of the myocardium and the coronary arteries with various measurements about viability, function, and perfusion of the myocardium.

Chapter 2 introduces the volumetric bull's eye plot, an extension of the bull's eye plot that is continuous, preserves the volumetric nature of the myocardium, and adds anatomical context to the otherwise rather abstract representation of the left ventricle. This technique also provides a much more detailed visualization of transmural scar. This work was presented at IEEE Visualization 2007 [79] and the SCMR 11th annual scientific sessions [77]. Patent applications on this concept were filed under application number PH-008909-EP-1 (ID 680295) and PCT/IB2008/053464.

Chapter 3 presents the visualization of viability in a three-dimensional anatomical context, providing a more detailed relation between scar and coronary arteries than is common in previous methods. This work was presented at IEEE Visualization 2007 [79].

Chapter 4 investigates computing patient-specific coronary territories, i.e., computing which parts of the myocardium are supplied by which coronary arteries based on anatomical data from the patient. This work was filed as a technical report [75] and accepted for a poster publication at the SCMR 12th annual scientific sessions [78]. A patent application on this concept was filed under application number PH-010411-EP-1 (ID 676667).

Chapter 5 shows how ideal perfusion data could be visualized. The input for these methods is given by a simulation of myocardial perfusion based on patient-specific anatomy. Using simulation data provides several interesting new possibilities for visualization and also provides another detailed visualization of the patient's anatomy. This work was presented at IEEE VisWeek 2008 [80].

Chapter 6 discusses an approach to provide a comprehensive view of a patient by integrating anatomical, functional, viability, and perfusion data into a single image.

Finally, Chapter 7 presents a summary and the conclusion of the work in this thesis.



Any sufficiently advanced  
technology is indistinguishable  
from magic.

---

Arthur C. Clarke

# 2

## The Volumetric Bull's Eye Plot

The bull's eye plot is an accepted medical visualization technique commonly used during the diagnosis of patients with suspected coronary artery disease. It provides a visual representation of a quantitative measure for the entire left ventricle in a two-dimensional diagram. This chapter presents an extension of this technique in the context of assessing viability using a late enhancement cardiac MRI scan. The extended concept is based on an unfolding the left ventricular myocardium along the long axis. The improved diagram does not suffer from discontinuities, preserves the volumetric nature of the left ventricular wall, and adds anatomical context. The preservation of wall thickness facilitates a direct and detailed visualization of the transmural of scar. These improvements provide a more comprehensive view of the viability of the left ventricular myocardium of a patient in a way that can more easily be related to the patient-specific anatomy.

### 2.1 Introduction

**T**HE DETECTION and quantification of infarcted myocardial tissue, also called scar, is of importance for the assessment of the infarct location and severity. The severity of scar is partially determined by the transmural, a measure for how far the scar extends into the left ventricular wall. Quantification of scar is also important for the selection and planning of therapy such as revascularization via the placement of a stent or a bypass.

Late enhancement imaging is an MRI protocol suitable for the assessment of myocardial viability [89, 8]. It uses a contrast agent to visualize

scar. A late enhancement scan is made 15 to 20 minutes after injection of a contrast agent. Because scar can contain more contrast agent than healthy tissue and experiences a delayed wash in of the contrast agent, it shows up brighter in the scan than healthy tissue. For each MRI scanning protocol, the scanning time is minimized such that the desired information for that protocol is still obtained. Therefore the atria are for example not covered by a late enhancement scan, as they are not relevant for the assessment of viability. Late enhancement scans commonly consist of much fewer slices than whole heart scans, although the in-plane resolutions of both protocols are approximately equal. Due to the scanning protocol used, the coronary arteries are often not well visible. Late enhancement scans thus exhibit less anatomical detail than an whole heart scan.

In current clinical practice the results of MRI-based scar quantification methods are examined using solely two-dimensional visualization techniques. Apart from examining the individual slices, bull's eye plots are often used to obtain a schematic representation of the scar in a patient. A bull's eye plot maps the left ventricular wall to a set of concentric rings, the middle ring corresponding to the apex and the outer ring corresponding to the base. This two-dimensional visualization technique gives an overview of the entire late enhancement scan and eliminates shape variations of the left ventricle between patients. A common approach for assessing the left ventricular viability using bull's eye plots is to show several diagrams simultaneously, for example one showing the relative amount of scar and another showing the transmural extent of scar. The bull's eye plot has two important drawbacks. First it is difficult to make a relation to the three-dimensional anatomy. Even when using the late enhancement slices, all relations have to be constructed mentally. Second it is impossible to relate scar to specific coronary arteries—which may be the cause of the scar—in a patient-specific way, because those are not well visible in a late enhancement scan.

This chapter presents the volumetric bull's eye plot, a novel visualization technique for the diagnosis of patients with coronary artery disease, that overcomes the aforementioned limitations. This technique extends the bull's eye plot by unfolding the myocardium while preserving the volumetric nature of the left ventricular wall. This approach preserves continuity, is better scalable in the number of slices of the late enhancement scan, and allows for a more detailed visualization of transmural extent. The latter advantage may allow for a more detailed assessment of the severity of scar. Finally, the diagram is annotated with anatomical context to allow for a better relation to anatomy and other tomographic data of the patient.

This chapter is structured as follows. Section 2.2 discusses related work. Section 2.3 discusses the improved visualization techniques in detail. Finally, Section 2.4 concludes this chapter.

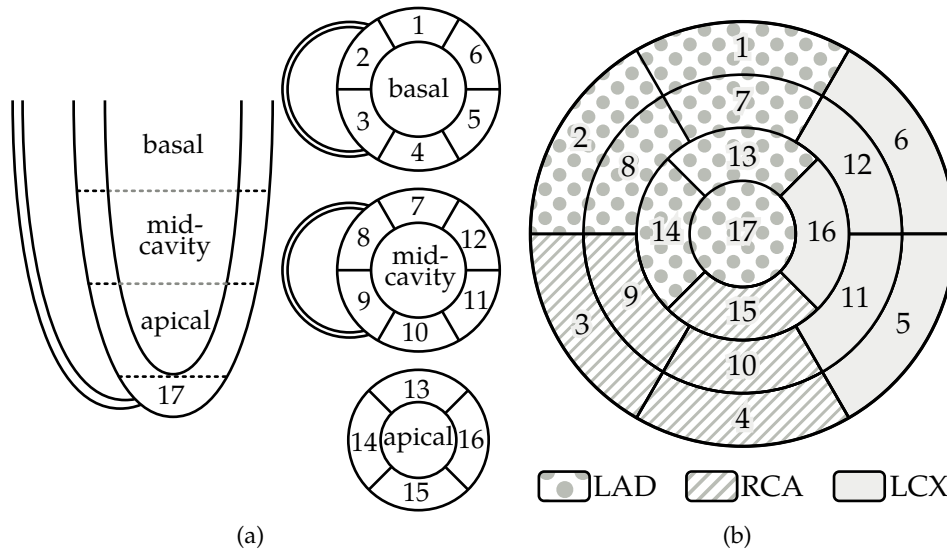


Figure 2.1: The 17-segment model as proposed by the American Heart Association [14]: (a) The division of the left ventricular myocardium into 17 segments; (b) the 17 segments displayed in a bull's eye plot.

## 2.2 Related Work

The American Heart Association has developed a standardized model for dividing the myocardium into segments for use among various tomography techniques in clinical practice [14]. The model aims at greatly increasing the comparability and reproducibility of diagnoses. The model is illustrated in Figure 2.1. It divides the left ventricle into a basal, a mid-cavity, and an apical part along the long axis. These three parts are further divided into segments, as is shown in Figure 2.1a. A separate segment is allocated to the apex. The model also suggested a mapping between these segments and the coronary arteries, shown in Figure 2.1b. This mapping is based on population averages. Later studies have investigated this mapping [65, 64] and have found that it should be used with care, as there are large variations in the anatomy of the coronary arteries among individuals.

### 2.2.1 The Bull's Eye Plot

Besides the segmentation model, the American Heart Association also presented a schematic approach to represent the left ventricle in a single diagram. This diagram is called a bull's eye plot [36]. It is a mapping of the myocardium to a set of concentric rings. The bull's eye plot in the model proposed by the American Heart Association consists of three rings, but the concept can be extended to any number of rings. Each ring

represents the segmented left ventricular myocardium on one slice of a short-axis scan. The apex, represented by the middle of the bull's eye plot, is often represented by a separately scanned long-axis slice. For each slice of the short-axis late enhancement scan, the left ventricular myocardium is reformatted to a ring. The inner ring represents the region near the apex, the bottom of the left ventricle, while the outer ring represents the area near the base, the top of the left ventricle. Each ring is divided into a number of segments, which can subsequently be colored according to a measured property. While the bull's eye plot as a visualization concept can be applied to various types of measurements, this chapter focuses on viability information provided by a late enhancement scan. An example of a bull's eye plot of late enhancement data is shown in Figure 2.3a. The bull's eye plot is popular in medical practice as it is intuitive and gives a standardized, global overview of the property being measured.

The left ventricular myocardium, apart from the apex, has approximately the shape of a cylinder. It is however not perfectly circular and the wall thickness varies throughout the left ventricle. These properties, as well as the general shape, size, and orientation, differ for each patient. The bull's eye plot was developed to allow for a structured and reproducible analysis that is easily comparable between different patients, or different scans of the same patients, by eliminating all shape variations.

Although the bull's eye plot eliminates all the inter- and intra-patient shape variations of the left ventricle, it has three main drawbacks. First the quantization of the data into segments gives a less accurate view than a continuous one. Implementations exist that provide more detail by using a high number of segments or interpolation. However, the bull's eye plot is discontinuous at the borders between the rings of the different slices. The second, more severe drawback is that it provides no information on the distribution of scar tissue throughout the ventricle wall—the transmural of scar. This problem is sometimes solved by displaying two bull's eye plots simultaneously: one that visualizes the amount of scar and one that visualizes the transmural of scar. The third drawback is that it provides very little anatomical information. The bull's eye plot is a two-dimensional, abstract representation of the late enhancement data, but relating it to anatomical information is necessary. Even with an additional view that provides anatomical information, the relation between these two views would have to be done mentally.

## 2.2.2 Combinations with Other Visualization Techniques

Noble *et al.* [59] combine late enhancement data with information on myocardial contraction to identify regions of the myocardium that suffer from ischemia but are not yet scarred. Such regions can still be revived and identification thereof is thus useful. They propose both the use of a bull's

eye plot and a projection onto the left ventricular wall as visualization of the resulting parameters. The latter aims to visualize the measurements in an anatomical context, since the bull's eye plot is an abstract representation without anatomical information. In their work the results were limited to providing shape information of the left ventricular myocardium, since only a segmentation of the left ventricle was available.

Besides the bull's eye plot, more visualization methods for the analysis of cardiac tomography data have been proposed, although most of these techniques have not yet been accepted in medical practice. Kuehnel *et al.* [43] designed software assistants for the analysis of cardiac CT and MRI data. Using segmentations of the coronary arteries and the left ventricle, they provide orthogonal cross-sections on the coronary arteries to inspect vessel diameters, bull's eye plots and color-coded slices of perfusion data, and an integrated visualization showing a three-dimensional left ventricle with perfusion data and the coronary arteries. In the same context Oeltze *et al.* [62] presented various visualization techniques for the analysis of perfusion data. There an integration of visualizations of perfusion measurements with anatomical information is proposed. This allows perfusion defects to be easily related to coronary artery branches feeding the affected area. Both these approaches propose the use of schematic visualization techniques such as the bull's eye plot in combination with three-dimensional visualization techniques to visualize the data in an anatomical context. A limitation of both approaches is that the schematic visualizations still contain fairly little anatomical detail themselves. The separate visualizations therefore still need to be combined mentally to put the schematic data into anatomical context.

### 2.2.3 Segmentation of the Myocardium

The construction of a bull's eye plot—or a volumetric bull's eye plot—requires the myocardium to be segmented in the late enhancement images. In this work manual contouring was used. Endocardial and epicardial contours were drawn by the user on each short-axis late enhancement slice where these structures are visible. An example of a late enhancement slice with manually drawn contours is given in Figure 2.2. For the volumetric bull's eye plot these contours are then interpolated using uniformly sampled Catmull-Rom splines to form a three-dimensional quadrilateral mesh. This mesh, which typically does not include the apex, forms a segmentation of the relevant parts of the left ventricular myocardium.

Besides a segmentation, a method is needed to discriminate scar from healthy tissue. This is commonly accomplished with the definition of image intensity ranges for both scar and viable tissue. In this work user-defined ranges are used. Inside the manually drawn contours, the user specifies two regions; one that clearly represents healthy tissue and one

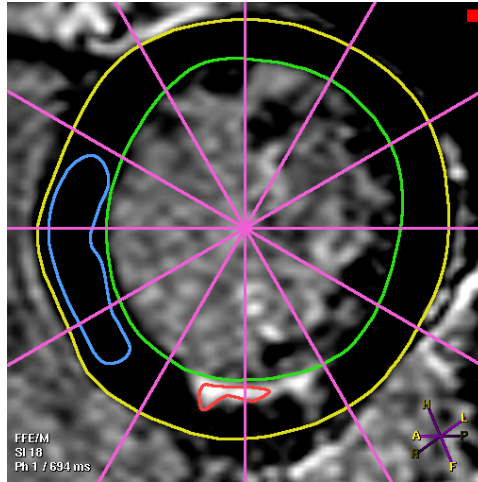


Figure 2.2: A late enhancement slice with manually drawn contours on the endocardium (green) and epicardium (yellow), healthy region (blue), and scar region (red).

that clearly represents scar. These two regions are shown in blue and red respectively in Figure 2.2. For both regions,  $[\mu - 2\sigma, \mu + 2\sigma]$  is used as the intensity range that represents either healthy tissue or scar. In this formula  $\mu$  denotes the mean intensity and  $\sigma$  denotes the standard deviation. In case these two intervals do not overlap, a linear transition is defined on the interval  $[\mu_{\text{healthy}} + 2\sigma_{\text{healthy}}, \mu_{\text{scar}} - 2\sigma_{\text{scar}}]$ . For some cases with little scar or good image contrast between scar and viable tissue a fuzzy thresholding approach was used instead. Here the user interactively specifies values  $\mu_{\text{mid}}$  and  $\sigma_{\text{mid}}$ . Then all intensity values below  $\mu_{\text{mid}} - \sigma_{\text{mid}}$  are considered viable tissue, all intensity values above  $\mu_{\text{mid}} + \sigma_{\text{mid}}$  are considered scar and a linear transition is used in between.

### 2.3 The Volumetric Bull's Eye Plot

The limitations of the bull's eye plot mentioned in Section 2.2.1 are overcome by the volumetric bull's eye plot; a three-dimensional extension of the bull's eye plot that is continuous, provides transmural information and is annotated with anatomical information. An example of a volumetric bull's eye plot is shown in Figure 2.3b.

The volumetric bull's eye plot is an unfolding of the myocardium along the long axis. This unfolding is illustrated in Figure 2.4 and discussed in detail in Section 2.3.1. The bottom of the cylinder corresponds to the epicardium and the top corresponds to the endocardium. The volumetric nature of the left ventricular wall is preserved. Similar to the bull's eye plot, the contours are reformatted to concentric rings to mask any shape

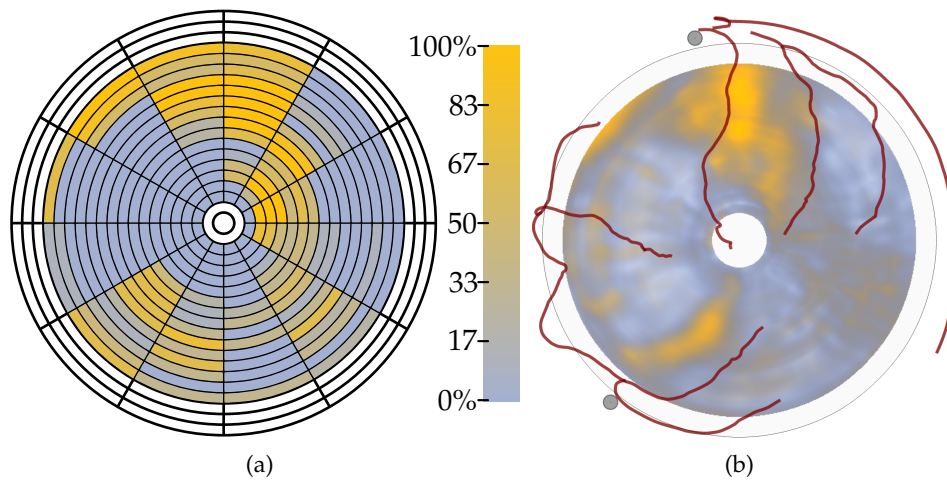


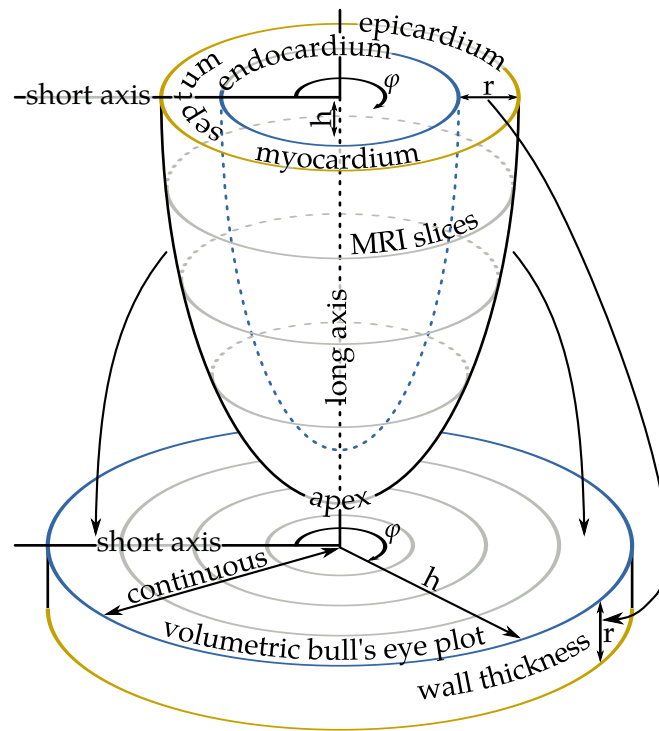
Figure 2.3: A comparison between (a) a bull's eye plot and (b) a volumetric bull's eye plot. The rings in (a) represent the reformatted contours. These are not present in (b), as the volumetric bull's eye plot is a continuous volume. The empty rings correspond to late enhancement slices where the myocardium was not present or could not be identified. In both figures blue corresponds to healthy tissue and orange corresponds to scar.

variations. There are however two important differences, that, combined with the additional anatomical context, solve the three aforementioned disadvantages of the bull's eye plot.

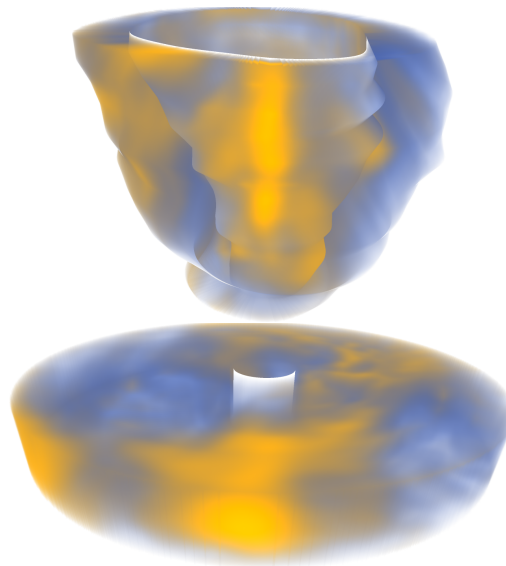
The first difference is that, as shown in Figure 2.4, the distance between the epicardium and endocardium is mapped to the thickness of the cylinder. This means that the volumetric nature of the left ventricular wall is preserved. The transmural information, which is lost in the bull's eye plot, is thus preserved in the volumetric bull's eye plot.

The second difference is that there are no discontinuities between the contours since the volumetric bull's eye plot is a continuous volume. Therefore there is also no need for quantization.

The addition of anatomical information solves the last disadvantage. As shown in Figure 2.3b, the coronary arteries are mapped on top of the epicardial side of the volumetric bull's eye plot. This allows scar to be related to coronary arteries. It also allows the orientation of the volumetric bull's eye plot with respect to the heart to be perceived. Since a late enhancement scan exhibits too little anatomical detail, the centerlines of the three primary coronary arteries are extracted from a whole heart scan of the same patient using a currently experimental prototype [50]. As additional orientation aid, two dots are drawn on the side of the volumetric bull's eye plot that indicate the locations where the right ventricle joins the left ventricle.



(a)



(b)

Figure 2.4: A volumetric bull's eye plot is constructed by unfolding and reformatting the myocardium to a cylinder, where the volumetric nature of the ventricle wall is preserved. Figure 2.4b shows a volume rendering of segmented late enhancement data in both original and unfolded form.



### 2.3.1 Unfolding the Myocardium

A parameterization of the left ventricle based on cylindrical coordinates is used for the unfolding of the myocardium. As illustrated in Figure 2.4, each point in either the myocardium or the volumetric bull's eye plot can be represented by a point in parameterized form  $\vec{x}_{\text{parm}} = (\varphi, h, r)$ . In this parameterization  $\varphi$  represents the angle with the short axis, which is mapped to the positive  $y$ -axis in the volumetric bull's eye plot, pointing upward in Figure 2.3b. The variable  $h$  represents the distance to the long axis in the myocardium, which is mapped to the distance to the center of the cylinder in the volumetric bull's eye plot. Finally, the variable  $r$  represents the distance to the long axis in the myocardium. In the volumetric bull's eye plot it represents the displacement along the cylinder axis. Given values for  $\varphi$  and  $h$ , the difference between  $r$  of the endo- and epicardium corresponds to the wall thickness, which varies throughout the left ventricle. This wall thickness is normalized in Figure 2.3b, to obtain a more uniform appearance. More on this matter is discussed in Section 2.3.4.

The contours segmenting the myocardium are sampled non-uniformly to compensate for distortions. Let  $f(p)$  denote the angle between the short axis and a line through both  $p$  and the point on the long axis closest to  $p$ . The contours are defined as piece-wise cubic Bézier splines  $C(\alpha)$  with  $\alpha \in [0, 2\pi]$ . These splines are sampled such that  $f(C(\alpha)) = \alpha$  for any  $\alpha \in \{\frac{i2\pi}{N} : 0 \leq i < N\}$  and a predefined integer  $N$ . For any  $\alpha \in (\frac{i2\pi}{N}, \frac{(i+1)2\pi}{N})$  with  $0 \leq i < N$ ,  $C(\alpha)$  is sampled to have constant chord length. This approach minimizes distortions due to the not perfectly circular shape of the contours while maintaining an accurate mapping of angles to the short axis.

Given a point in Cartesian space in the volumetric bull's eye plot, its parameterized form can be computed using simple geometry. This parameterized form can then be directly interpreted as being in the parameterized space of the myocardium. Finally, the point in Cartesian space of the late enhancement scan can be found by using  $h$  to determine the slice the point is on,  $r$  to determine whether the point is on the endocardium or the epicardium, and  $\varphi$  as an offset in the contour corresponding to that position. Since all parameters are continuous, an interpolation scheme is required to combine multiple neighboring contours. Here Catmull-Rom interpolation is applied for  $\varphi$  and  $h$ , while linear interpolation is applied for  $r$ . To minimize sampling errors, this unfolding of the myocardium is performed on-the-fly.

The on-the-fly unfolding of the myocardium is realized by computing two two-dimensional transformation maps; one for the endocardium and one for the epicardium. Each transformation map contains at each location the coordinates of the corresponding point in unfolded space. Using

transformation maps does not require the volume data to be resampled into an unfolded representation, but still provides high performance. Apart from being more memory efficient, using transformation maps does not introduce resampling artifacts.

The two transformation maps define functions  $f_{\text{endo}} : \mathbb{R}^2 \rightarrow \mathbb{R}^3$  and  $f_{\text{epi}} : \mathbb{R}^2 \rightarrow \mathbb{R}^3$  from parameterized space to Cartesian space of the late enhancement scan. These two functions can be combined using the assumption of linearity to define a function  $f : \mathbb{R}^3 \rightarrow \mathbb{R}^3$  given a point  $\vec{x}_{\text{parm}} = (\varphi, h, r)$  as follows.

$$f(\vec{x}_{\text{parm}}) = (1 - r) \cdot f_{\text{endo}}(\varphi, h) + r \cdot f_{\text{epi}}(\varphi, h)$$

Each transformation map is implemented as a two-dimensional texture, storing the value of  $f_{\text{endo}}(x, y)$  and  $f_{\text{epi}}(x, y)$ , respectively, at location  $(x, y)$ . The required resolution of these textures depends on the resolution of the late enhancement scan. Note that since each side of the cylinder of the volumetric bull's eye plot is circular and textures are square, the respective functions are not defined for each point on of the texture.

Linearity is assumed between the endo- and epicardial layers, as the circles, to which the contours of these layers are mapped in the volumetric bull's eye plot, only differ in displacement along the primary axis of the cylinder. Due to this assumption of linearity, only two two-dimensional transformation maps are required instead of a full three-dimensional map. While it may seem better to unfold along the normal direction of the center surface (in between the endo- and epicardial layers), the approach presented here preserves the relation between the distance to the center in the volumetric bull's eye plot and the distance to the apex along the long axis in the three-dimensional case. In other words, all points on a concentric cylinder in the volumetric bull's eye plot lie in a plane orthogonal to the long axis. This is expressed by the gray circles on the ventricle and the volumetric bull's eye plot in Figure 2.4. This is an important and intuitive relation, which is also present in the bull's eye plot.

### 2.3.2 Overall Distribution of Scar

When the cylinder that is the result of the volumetric bull's eye plot unfolding is viewed from the bottom, it gives a similar global overview as a bull's eye plot. This can be seen by comparing Figures 2.3a and 2.3b. The volumetric nature of this cylinder requires an algorithm that projects the three-dimensional volume onto a two-dimensional images. In this work both direct volume rendering [46] and maximum intensity projection [87] are applied. In Figure 2.3b a direct volume rendering strategy is applied. A linear gradient of two visually distinct colors is used to color-code the degree of scar according to the scar classification. In

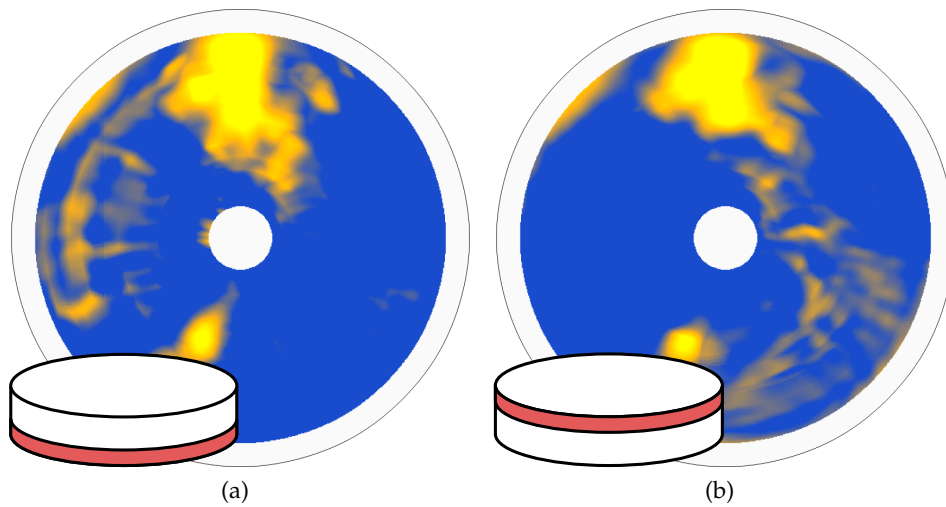


Figure 2.5: Two volumetric bull's eye plots that show only a slab of the cylinder; (a) shows only viability information near the epicardial layer and (b) only near the endocardial layer.

Figure 2.3 blue and yellow represent healthy tissue and scar, respectively. More colors provide little advantage and may cause visual clutter, an overly complex appearance that hampers effective interpretation, especially when additional annotations are added.

In Figure 2.3b, all the data from the myocardial segmentation are used, similar to the bull's eye plot. The volumetric aspect of the volumetric bull's eye plot can be used to control the amount of data visualized by selecting a slab of the cylinder. This concept is demonstrated in Figure 2.5. By varying the slab of the cylinder that represents the selection, the viability information either near the epicardial surface (see Figure 2.5a), the endocardial surface (see Figure 2.5b), or in the center can be visualized separately. This functionality is useful for assessing the severity and the transmural extent of local scar.

### 2.3.3 Transmurality of Scar

The main advantage of the volumetric bull's eye plot is its volumetric nature preserves information on the transmural extent of scar, i.e. the extent of scar tissue into the left ventricular wall. This is demonstrated in Figure 2.6, where the volumetric bull's eye plot is shown from the side with a wedge cut-out. Along the edge of the cut-out, the transmural extent can be observed. However, only a small part of Figure 2.6 actually shows the transmural extent of the region of interest. The cylindrical shape of the volumetric bull's eye

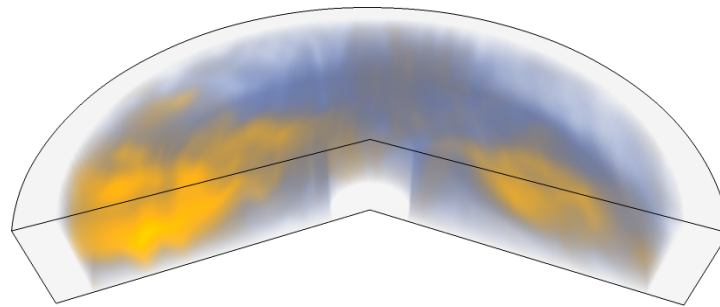


Figure 2.6: A volumetric bull's eye plot with a wedge cut-out, exposing the transmural scar.

plot also makes it difficult to assess the transmural scar of a larger region of interest.

Therefore a second unfolding of the myocardium is introduced specifically intended for exploring the transmural scar of a region of interest. For this unfolding, called the rectangular unfolding, the myocardium is first cut open along the long axis and is then unfolded and reformatted to a cuboid. This is illustrated in Figure 2.7. Proportions inside the myocardium are better preserved in the rectangular unfolding than in the volumetric bull's eye plot since less stretching is involved during the reformatting. The rectangular unfolding is implemented similarly to the volumetric bull's eye plot unfolding. The main difference is that the two transformation maps have a rectangular shape instead of circular one. When the rectangularly unfolded myocardium is viewed from the side, the transmural scar can be perceived easily.

The motivation behind constructing this rectangular unfolding is as follows. On the volumetric bull's eye plot the user can select a pie-shaped area of interest (see Figure 2.9a), for which a visualization of the transmural scar is desired. The key observation is that this pie-shaped area in the volumetric bull's eye plot corresponds to a rectangular slab in the rectangular unfolding. By visualizing only this slab and viewing it from the side, the transmural scar of the region of interest can be observed (see Figure 2.9b). When the pie-shaped section would be viewed from the side, distortions would appear due to variations in thickness along the viewing direction and due to its cylindrical shape. These distortions are no longer present in the side projection of the rectangular slab.

Similar to the volumetric bull's eye plot, this approach yields a three-dimensional object and thus requires a projection algorithm. Figure 2.9b demonstrates both a direct volume rendering and a maximum intensity projection scheme. Since the transmural scar varies throughout the ventricle, it varies along the viewing direction of the slab. To obtain an accurate visualization of the transmural scar, the slab should remain thin. Thus the

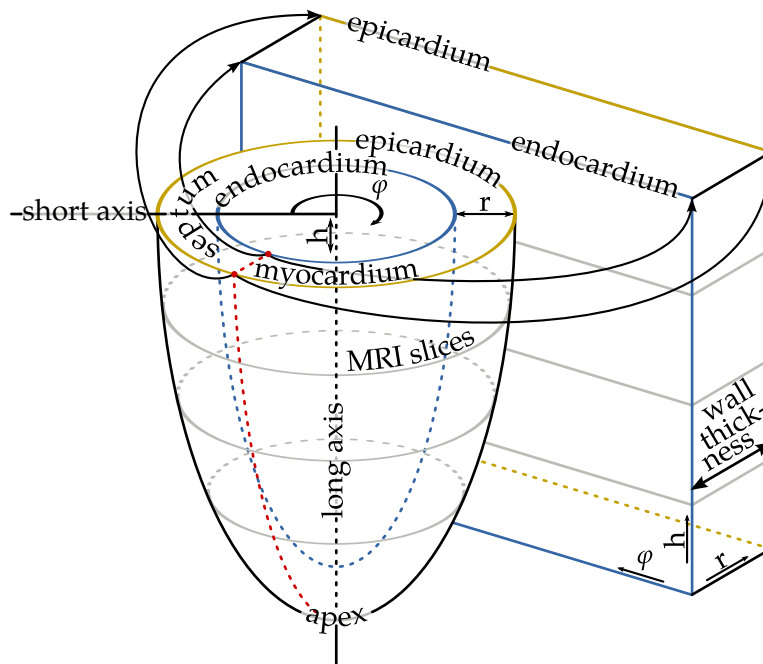


Figure 2.7: The rectangular unfolding is constructed by cutting open the myocardium along a line parallel to the long axis and unfolding it to a cuboid.

pie-shaped area on the volumetric bull's eye plot should not be too big, as this may reduce the visibility of the variations in transmural intensity inside that area. For example, with a direct volume rendering scheme only the transmural intensity of the front part would be visible, while with a maximum intensity projection scheme only the maximum transmural intensity of the slab is visualized.

### 2.3.4 Preservation of Wall Thickness

In the volumetric bull's eye plot the three-dimensional nature of the left ventricular wall is preserved. In Figure 2.4 the wall thickness was reformatted to be uniform. The absolute wall thickness information can also be preserved. This would cause the height to vary throughout the volumetric bull's eye plot, as is demonstrated in Figure 2.8. Figure 2.8a shows a volumetric bull's eye plot with uniform thickness. In Figure 2.8b the height of the cylinder is proportional to the difference between the values of  $r$  of endo- and epicardial contours in the parameterization at each point. Although this approach also exposes the transmural intensity of scar, the rectangular unfolding captures phenomena inside the ventricle wall in a better way.

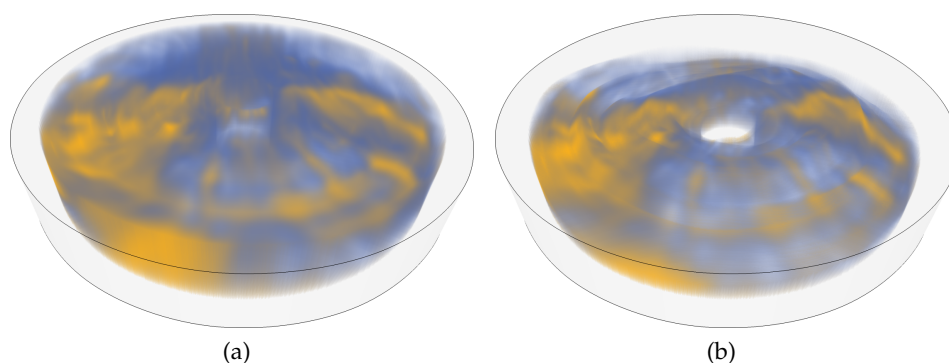


Figure 2.8: Wall thickness preservation in the volumetric bull's eye plot; (a) uniform wall thickness; (b) absolute wall thickness preserved.

When the myocardium is reformatted to have uniform thickness, this allows for the perception of *relative* transmuralty (%). When absolute wall thickness information is preserved, it allows for perception of *absolute* transmuralty (mm). This distinction is relevant during diagnosis, as the absolute thickness of remaining healthy tissue is relevant for the estimation of improved functionality if the patient would undergo revascularization. On the other hand, relative transmuralty gives a more uniform visualization of the overall distribution of scar, not distorted by the varying wall thickness.

The absolute wall thickness information is of most value when assessing the transmuralty of scar. While top or bottom projection of the volumetric bull's eye plot gives an overview of the distribution of scar, absolute wall thickness information and transmuralty are best visible in the rectangular unfolding. Wall thickness is preserved in the rectangular unfolding in an identical way as for the volumetric bull's eye plot. Figure 2.9b shows an example of a transmuralty visualization both with uniform and with absolute wall thickness information. The wall thickness is visualized by adjusting the distance of the endocardial contour to the epicardial contour. This keeps the epicardial side flat and eases comparison of wall thickness throughout the slab.

The wall thickness may vary throughout the slab along the viewing direction. This variation is visualized using lines indicating the minimum and maximum wall thicknesses. These lines can be used to detect large variations in wall thickness in the slab. If the two lines are far apart, variations in wall thickness are causing an inaccurate visualization of transmuralty and a thinner slab should be selected. This is similar to the phenomenon that a too thick slab occludes transmuralty due to the accumulation scheme as discussed in Section 2.3.3.

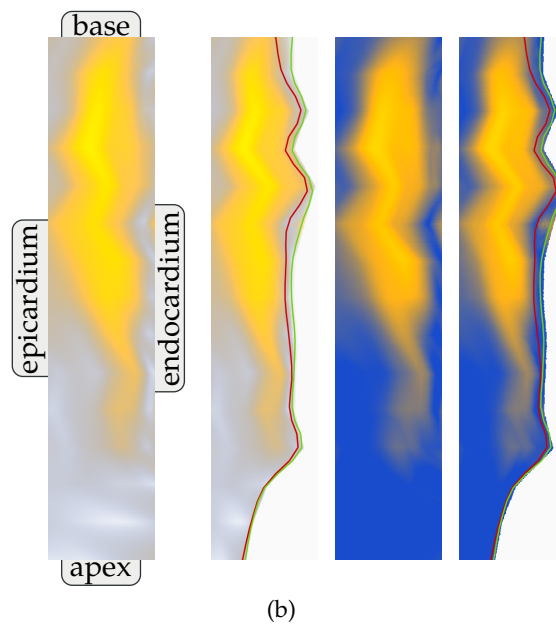
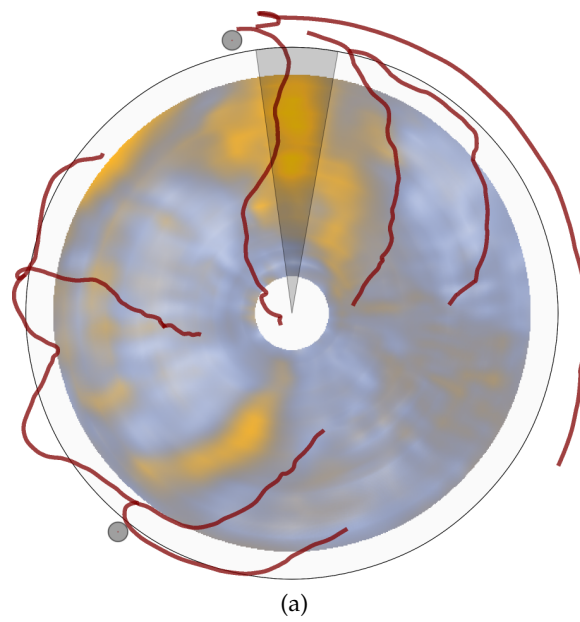


Figure 2.9: Visualizing transmuralty using the volumetric bull's eye plot: (a) a volumetric bull's eye plot with a region of interest highlighted and (b) a direct volume rendering (left two) and maximum intensity projection (right two) of the region of interest viewed from the side, exposing the transmuralty of the scar, both without (left) and with (right) absolute wall thickness information. The red and green lines correspond to the minimum and maximum wall thicknesses of the region of interest, respectively.

### 2.3.5 Overlaying Coronary Arteries

As additional context information, the coronary arteries can be mapped to the epicardial surface of the volumetric bull's eye plot. First each vessel centerline is projected onto the epicardial surface. Next these centerlines are mapped to the volumetric bull's eye plot using the same unfolding process as used for the myocardium. The projection is necessary since the unfolding transformation is only defined within the volume of the late enhancement contours. It can generally be assumed that each part of the myocardium is fed by the closest coronary artery. The mapping of the coronary arteries to the epicardial surface has no significant impact on the relation between the myocardial tissue and its closest coronary artery. It is therefore an acceptable solution. Parts of the coronary arteries that have a distance to the epicardial layer greater than a predefined threshold, e.g. coronary arteries feeding the right ventricle, are not mapped to the volumetric bull's eye plot.

An example of a volumetric bull's eye plot with the coronary arteries mapped on the epicardial surface is given in Figure 2.3b. The coronary arteries act as additional context information only and no diameter information is available. They are rendered as lines with a single color and without shading information to avoid visual clutter as much as possible.

### 2.3.6 Implementation Details

The presented techniques have been implemented using OpenGL 2.0. They take advantage of the capabilities of current graphics hardware to offer interactively explorable visualizations. The implementation was tested on a NVIDIA GeForce 7950 GX2 which provided more than 20 frames per second for all presented visualizations. All late enhancement scans used in these tests consisted of 20 short-axis slices of 512 by 512 voxels, where the myocardium covered approximately 100 by 100 voxels in each slice.

## 2.4 Summary and Conclusions

This chapter introduced the volumetric bull's eye plot, a novel visualization technique based on the bull's eye plot, which is an existing, clinically accepted visualization concept. The volumetric bull's eye plot preserves transmural information and does not include discontinuities. Additionally anatomical context is provided by annotating it with the centerlines of the coronary arteries. The transmural scar is visualized in a rectangular unfolding of the myocardium, which is closely related to the volumetric bull's eye plot. Preserving wall thickness allows both for the assessment of relative transmural, as well as the assessment of the absolute amount



of remaining healthy tissue. By mapping the coronary arteries to the volumetric bulls eye plot, scar can be related to these coronary arteries.

Due to the advantages of the volumetric bull's eye plot over the bull's eye plot, it can be hypothesized that this technique may lead to a more accurate and efficient diagnosis of patients with coronary artery disease. Although a thorough medical evaluation has yet to be performed, this work has been developed in tight cooperation with medical partners. Company experts in close contact with medical heart specialists provided the required specifications and steering feedback to accommodate the needs of the domain experts.



Seeing, contrary to popular wisdom, isn't believing. It's where belief stops, because it isn't needed any more.

---

Terry Pratchett

# 3

## Viability in an Anatomical Context

During the assessment of viability a relation between scar and the coronary arteries is often hard to make, because the coronary arteries are often not visible in a late enhancement scan. The volumetric bull's eye plot introduced in the previous chapter improves on this by mapping the coronary arteries onto an abstract representation of the left ventricle. This chapter presents a visualization framework that visualizes viability with detailed anatomical context extracted from a whole heart scan in three dimensions. It combines multiple MRI scans (whole heart anatomical data, late enhancement data) and multiple segmentations (polygonal heart model, late enhancement contours, coronary artery tree). By selectively combining different rendering techniques, comprehensive yet intuitive visualizations of the various data sources are obtained.

### 3.1 Introduction

**V**IABILITY INFORMATION is commonly assessed by analyzing the original slice data and bull's eye plots of a late enhancement MRI scan. Since anatomical details, including the coronary arteries, are not well visible in a late enhancement scan, most relations to anatomy have to be made mentally. Anatomical context is lost even further in the more abstract representation of a bull's eye plot, although the volumetric bull's eye plot introduced in Chapter 2 partially solves this problem. During analysis, the shape, location, and size of the scar are all important properties that are hard to estimate based on slices and bull's eye plots.

This chapter presents a three-dimensional visualization of scar in an anatomical context that clearly shows the shape, size, and location of

the scar in relation to the myocardial anatomy and the coronary arteries. This view is annotated with various visualizations of the anatomy of the coronary arteries, to relate scar to arteries that may be responsible for supplying the infarcted area. Due to the three-dimensional nature of the visualization, there are no deformations of the scar. Therefore shape and size compared to the rest of the heart are easily perceived. Linking this visualization to a volumetric bull's eye plot enables the user to navigate through the data examining both myocardial and coronary anatomy and scar shape, location, and transmuralty in a comprehensive way.

### 3.2 Related Work

In earlier work the desire for a three-dimensional visualization accompanying a bull's eye plot was already acknowledged. Noble *et al.* [59] presented late enhancement data using both bull's eye plots and a mapping of those bull's eye plots on a three-dimensional mesh of the left ventricle. Oeltze *et al.* [62] presented a framework that combines bull's eye plots showing analysis results on perfusion data with a three-dimensional model showing the coronary arteries.

In general medical visualization techniques can greatly benefit from segmentation information. Recently fully automatic segmentation of whole heart MRI data has become possible. The approach presented by Ecabert *et al.* [20] uses a geometric heart model that can be adjusted to each patient without user interaction. Similar approaches have been developed simultaneously [51]. Whole heart segmentations allow a more robust approach to selective visualization, where irrelevant parts of the data can be left out. They also provide excellent anatomical context for advanced three-dimensional visualization techniques that combine various data sources.

### 3.3 Overview of the Framework

The visualization approach of this chapter is implemented in a framework called CoViCAD, which is short for comprehensive visualization of coronary artery disease. The presented techniques are intended for the combined analysis of late enhancement and whole heart MRI data, supplying tissue viability and anatomical information, respectively. The framework combines the volumetric bull's eye plot from Chapter 2 with a comprehensive three-dimensional visualization providing anatomical context. The framework establishes an intuitive relation between the volumetric bull's eye plot and the three-dimensional visualization through interactive exploration facilities.

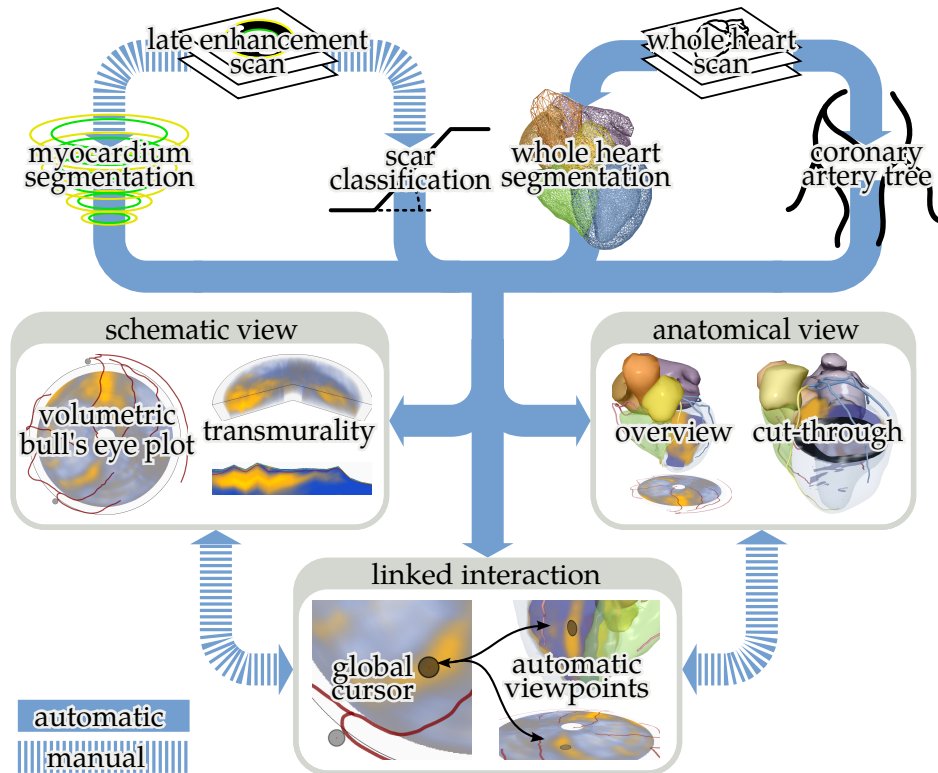


Figure 3.1: Overview of the CoViCAD framework showing the relation between the MRI scans, data derived from these scans, and the visualization modules.

The relations between the various data sources and the relation to the analysis system are depicted in Figure 3.1. The CoViCAD framework can be divided into two visualization components. The first component provides a schematic view of the late enhancement data using the volumetric bull's eye plot. It abstracts from the anatomy to give a clear, global overview of the distribution of scar. The second component is the anatomical view. It is a three-dimensional view of the heart, visualizing scar tissue in an anatomical context. These two components are coupled by an interaction module that provides an intuitive relation between the two views. The schematic view is intended for the visualization of the overall distribution and transmuralities of scar, while the anatomical view is intended for visualizing the size and location of scar in an anatomical context.

While similar approaches of visualizing viability information in an anatomical context have been presented before [59, 62], the approach presented here differs in that it combines multiple data sources with multiple visualization techniques. This approach has been shown to be useful before [28]. Detailed anatomical information is extracted from a

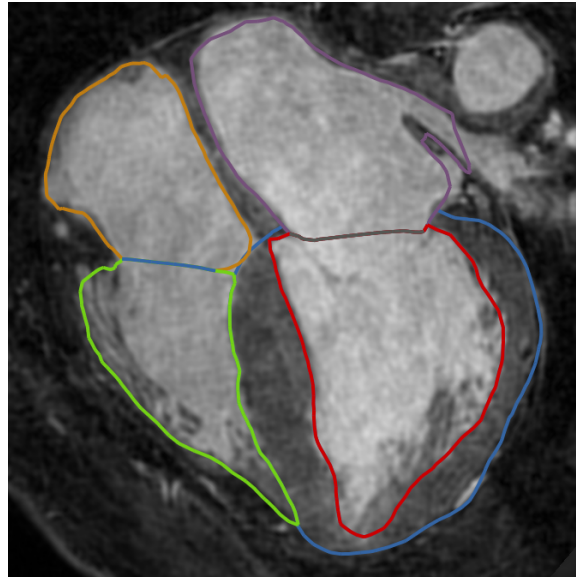


Figure 3.2: A four-chamber long-axis view of a whole heart scan annotated with the intersection of the segmented heart model.

whole heart scan as a geometric heart model. A volume rendering of a late enhancement scan is combined with this geometric heart model. Additionally the coronary artery tree is rendered in a representation of choice, including a set of solid tubes, a maximum intensity projection [70], and a curved planar reformation [39] of the neighborhood of the vessel centerline. This makes it possible to relate scar to a coronary artery branch.

The approach of visualizing scar tissue presented in this chapter relies on segmentations of both the whole heart and late enhancement scans. A technique presented by Ecabert *et al.* [20] extracts a geometric heart model from the whole heart scan without user interaction. The whole heart scans used in this work were acquired using steady-state free precession and consisted of approximately 160 slices of 512 by 512 voxels per slice. The heart model is a polygonal mesh consisting of 11 parts. It includes the four chambers, the four valves, the aorta, the pulmonary artery, and a point indicating the apex. The long and short axes are extracted from the heart model. These two axes are more commonly used for image acquisition than the standard patient axes. In this work they are used for automatic viewpoint configuration and as interaction guides for cutting planes. Figure 3.2 shows a reformatted four-chamber long-axis view of a whole heart scan with the intersection of the segmented heart model as an overlay. The short-axis late enhancement scan typically consists of 20 slices covering the left ventricle with 512 by 512 voxels per slice. It is segmented using the same manual contouring approach as discussed in Chapter 2.

### 3.4 Viability in an Anatomical Context

The schematic view produced by the CoViCAD framework, driven by the volumetric bull's eye plot, has more anatomical context than a standard bull's eye plot, but it still is an abstraction from the actual anatomy. The anatomical view on the other hand preserves the shape and proportions of the structures in the heart. This makes the anatomical view especially suitable for the observation of location and size of scar.

An example of the anatomical view is shown in Figure 3.3. The different parts of the geometric heart model are rendered in different colors. A feature-preserving mesh smoothing algorithm [37] is applied to the heart model to remove high frequency noise in the mesh. This noise is caused by the nature of MRI rather than the underlying anatomy. The segmented late enhancement data are rendered using direct volume rendering [46]. All late enhancement data are rendered using a single constant color, only the opacity varies based upon the degree of scar. The same approach for classifying scar is used as in Chapter 2. In Figure 3.3 scar is visible as the orange areas in the wall of the left ventricle. The epicardial wall is rendered semi-transparently to prevent occlusion of the late enhancement data. The endocardial wall is rendered in semi-transparent blue—yet less transparent than the epicardium—so that mostly scar at the front of the heart is visible. Rendering the endocardium semi-transparently also visualizes scar at the back, but too much transparency will interfere with perceiving whether a patch of scar is at the front or back of the ventricle.

Only the late enhancement data inside a closed polygonal mesh constructed from the manually drawn contours segmenting the myocardium are rendered. Creating a volume rendering of only this part of late enhancement data is non-trivial, since the shape of mesh segmenting the myocardium is typically concave. An approximating solutions that assume this mesh is convex either do not render areas of scar from some viewpoints or include structures outside the myocardium in the rendering. The myocardium is surrounded by other bright structures that could easily be misinterpreted as scar. To solve this problem, depth peeling [22, 76] is used to extract depth layers of the polygonal mesh segmenting the myocardium. These depth layers are used to determine which part of each viewing ray intersects the myocardium, which can subsequently be used to render only the myocardium. Using four depth layers typically gives satisfactory results, as experiments have shown that using more layers does not increase image quality in practical cases.

Anatomical context is provided using polygonal meshes of the myocardial and coronary anatomy. For contextual purposes these segmentations provide sufficient detail and the visualization could become cluttered from adding the original MRI data with for example direct volume rendering. The original MRI data should however still be accessible to the user. This

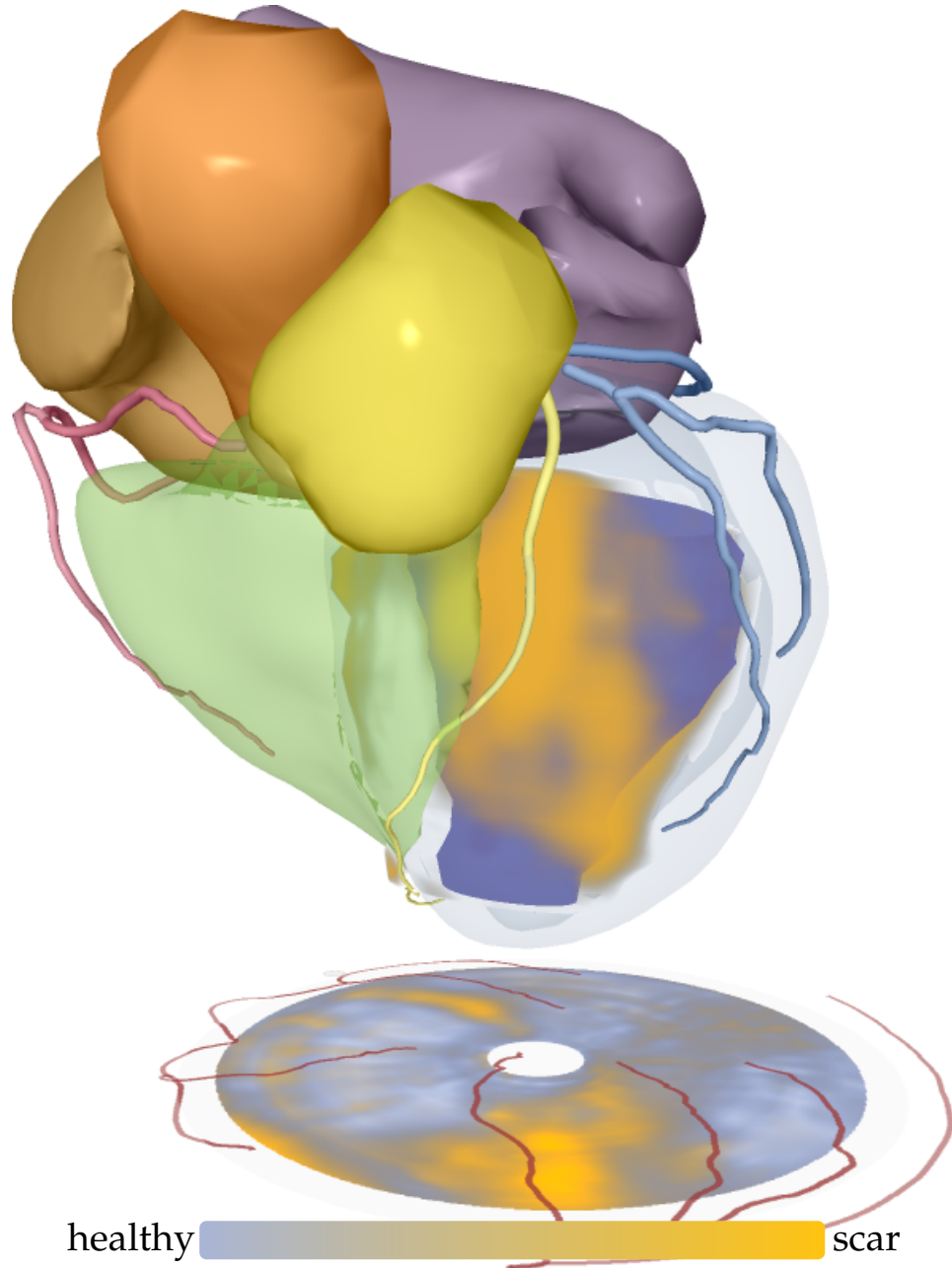


Figure 3.3: View showing the anatomy of the individual parts of the heart, the anatomy of the coronary artery tree, and scar tissue in semi-transparent orange inside the left ventricular myocardium.



is accomplished by the cutting planes that show the late enhancement data inside the myocardium and the different representations of the coronary arteries showing the whole heart data. The individual parts of the heart model are rendered in perceptually distinct colors to make them visually clearly separable. The same strategy is applied to the coronary artery tree. Shading is applied using the Phong shading model for increased perception of shape. For navigational purposes a volumetric bull's eye plot of the late enhancement data is projected on the ground plane. It serves as a map of the late enhancement data and gives a better perception of the orientation of the heart.

### 3.4.1 Visualization of Coronary Arteries

The addition of the coronary arteries is of great diagnostic value. Once a region of scar is identified, it can be related to a coronary artery near that area. The segmentation used only provides the centerline of the vessels. Current MRI technology does not provide enough resolution to extract absolute diameter information for the coronary arteries [41]. This also means that surface rendering techniques may not provide accurate results. The image data can however provide an indication of a possible stenosis, which can then be further investigated using other technologies including coronary angiography.

To facilitate the detection of a possible stenosis, three different visualizations of the coronary arteries are offered, each depicted in Figure 3.4. For each vessel, a polygonal tube around its centerline is constructed. These tubes have a radius proportional to the distance to the apex. The first visualization of the arteries renders these tubes in visually distinct colors (see Figure 3.4a). The tubes are constructed with a relatively small radius, to avoid the false impression of giving vessel diameter information and to cause minimal occlusion. The relation between the radius and the distance to the apex provides a navigational aid. This representation allows scar to be related to a particular coronary artery, without providing information on the artery itself.

The second visualization is a maximum intensity projection [70] of the whole heart data inside a tube of constant radius (see Figure 3.4b). This approach requires a larger diameter of the tubes than in the first visualization, since the lumen of the vessel should be clearly distinguishable from the background. The localized maximum intensity projection allows perception of the vessel diameter and detection of a possible stenosis. Using a maximum intensity projection preserves the three-dimensional nature of the vessels and is thus an intuitive representation. A downside is that when the radius of the tube is chosen too large, neighboring structures might be included in the rendering and may occlude the vessel.

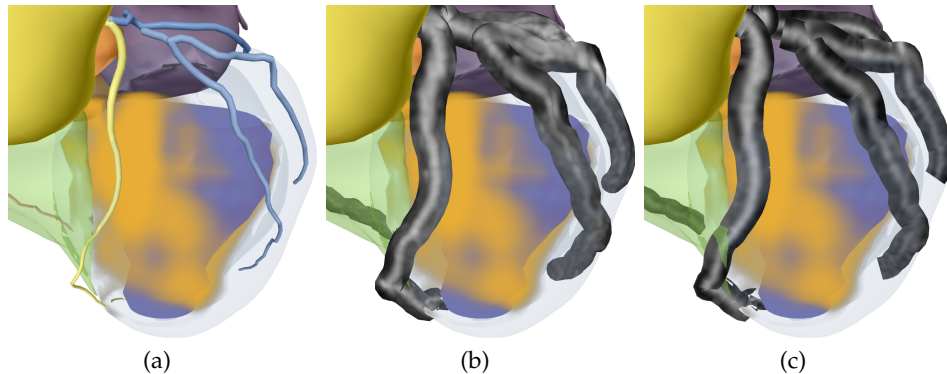


Figure 3.4: The coronary arteries rendered (a) as polygonal tubes around the vessel centerline; (b) as a maximum intensity projection of the whole heart data inside the tubes, and (c) as a curved planar reformation of a surface through the vessel centerlines.

The third representation of the coronary arteries does not suffer from the drawback of occluding the vessel lumen. It uses a curved planar reformation [39] along a surface through the centerline of the vessel (see Figure 3.4c). The combination of volume rendering with curved planar reformation has been presented before [74]. An initial orientation of the surface used for the curved planar reformation is computed using the long axis extracted from the heart model. The vector from a point on the vessel centerline to the corresponding closest point on the long axis is taken as the normal vector of the curved planar reformation surface through that point. This causes the surface to be approximately tangential to the epicardial surface near the vessel. The user can specify an offset angle that controls the rotation around the centerline of the vessel.

A different surface is used for displaying the reformation to ensure that the curved planar reformation is always well visible. This display surface is similar to the reformation surface, except that it is always oriented towards the viewer. This has the advantage that changing the viewpoint does not change the curved planar reformation representation of the coronary arteries. While the curved planar reformation has the advantage that the vessel lumen is always visible, it does not give a three-dimensional view on the vessel neighborhood, contrary to the maximum intensity projection rendering.

### 3.4.2 Resolving Occlusion of Scar

To prevent occlusion of the late enhancement data by the coronary arteries, the opacity of the coronary arteries can be locally controlled by the opacity of the late enhancement data it is occluding. This approach is hereafter

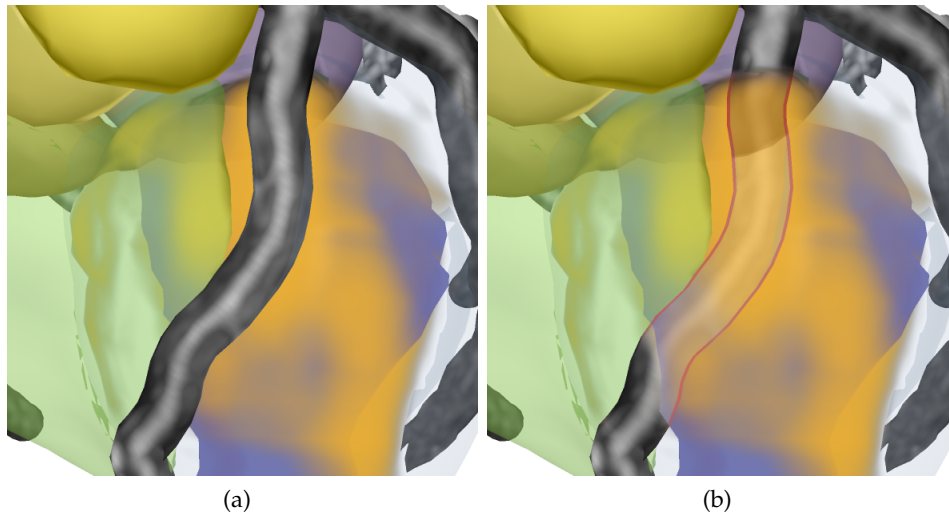


Figure 3.5: Solving occlusion due to the coronary arteries: (a) coronary artery occluding scar; (b) coronary artery rendered semi-transparently with its outline highlighted.

called coronary ghosting. Figure 3.5 demonstrates this concept. The degree of transparency is determined by the amount of scar that is visible beneath the artery. Coronary arteries occluding areas that contain no scar are rendered fully opaque. Areas that contain a lot of scar, such that it shows up completely opaque in the volume rendering, cause the coronary arteries to be rendered with a very low opacity. To ensure that the contours of the arteries are always visible, the edges of the coronary arteries are emphasized around parts that are rendered with low opacity.

Apart from occlusions caused by the coronary arteries, the individual parts of the heart can also cause occlusions. This is most obvious with the right ventricle, which completely occludes the septum, as is shown in Figure 3.6a. The septum is not directly fed by the coronary arteries. Therefore infarction occurs more easily in this area. Since most parts of the polygonal heart model, including the right ventricle, offer only context information, simple visibility reduction techniques are sufficient. Figure 3.6b illustrates a rendering with a reduced opacity for the right ventricle, causing the scar in the septum to become visible.

### 3.4.3 Visualizing Slice Data

The CoViCAD framework also allows for the exploration of the MRI slice data of both the late enhancement and whole heart scans. This is achieved by adding a cutting plane to the anatomical view and visualizing the image data on this plane. Figure 3.7 demonstrates this concept. The part

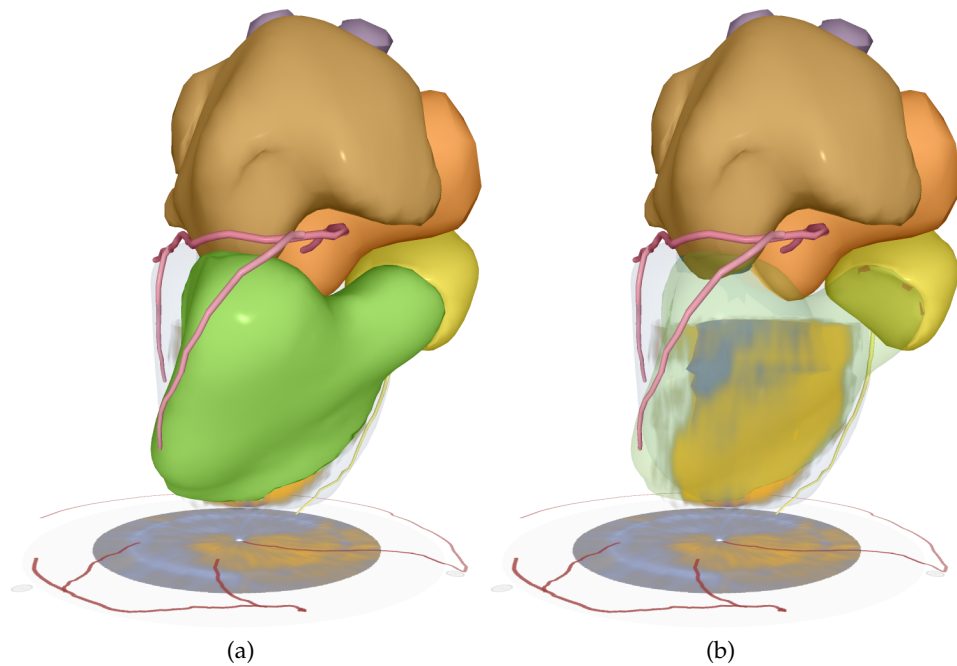


Figure 3.6: Solving occlusion due to the right ventricle: (a) right ventricle occluding scar in the septum and (b) revealing the septum by making the right ventricle semi-transparent.

of the heart model and the late enhancement data that are in front of the cutting plane are clipped. Along the portion of the cutting plane inside the left ventricular myocardium either the whole heart or late enhancement data are reformatted. This allows for the observation of the slice data in the myocardium without occlusions, while the rest of the heart model still provides anatomical context. The late enhancement data are rendered behind the cutting plane. Depending on the viewpoint and orientation of the cutting plane, this can still provide information on the distribution of scar.

To a certain degree, the use of a cutting plane also enables the visualization of the transmuralty of scar. However, an area exhibiting scar is commonly first identified in the anatomical view without using a cutting plane. Using the anatomical view to visualize the transmuralty of that particular area of scar requires a different viewpoint. Manually positioning the cutting plane and adjusting the viewpoint can be a time-consuming and complex task.

To simplify the specification of the location and orientation of the cutting plane, two basic orientations are offered. The first orientation, shown in Figure 3.7a, starts with the typical four-chamber view of the

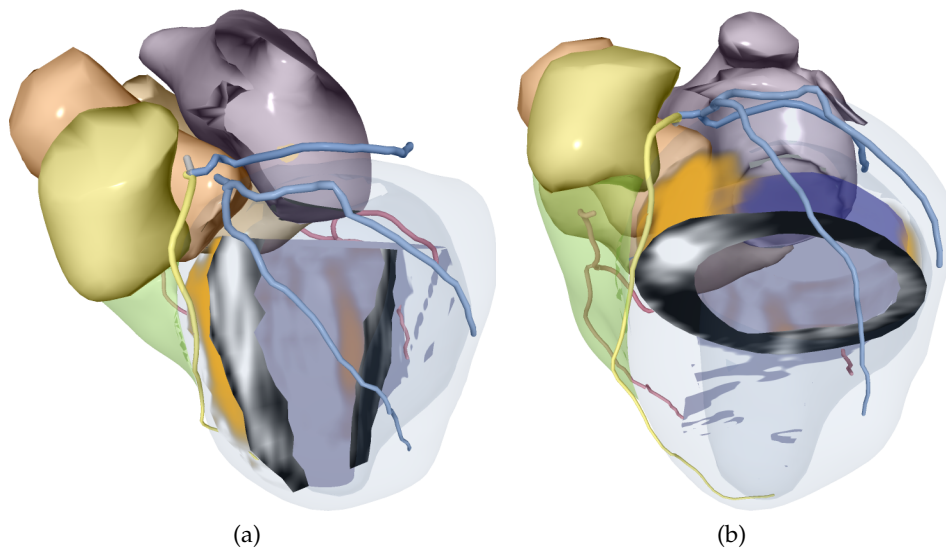


Figure 3.7: Cutting plane in (a) long-axis orientation and (b) short-axis orientation both with late enhancement data reformatted along the plane. The white spots represent scar.

heart. Here the plane is parallel to both the short and long axes. In this orientation the plane can only be rotated around the long axis. A preset rotation offset is offered that also gives a two-chamber view. The second orientation, shown in Figure 3.7b, corresponds to the standard short-axis view, where the plane is orthogonal to the long axis. Interaction is restricted to translating the plane along the long axis. These restrictions make specifying the location and orientation of the cutting plane much simpler and more intuitive.

#### 3.4.4 Integration of Diverse Rendering Techniques

The heart model is rendered as a polygonal mesh, the late enhancement data are rendered using direct volume rendering and the coronary artery tree is rendered either as a set of solid tubes, as a maximum intensity projection, or as a curved planar reformation. Due to the difference in rendering methods, these components are first all rendered to individual images, while depth information is preserved. For volume rendering techniques such as direct volume rendering and maximum intensity projection where depth is not clearly defined, the depth is used of the sample that causes the accumulated opacity to exceed a predefined threshold. This threshold is typically set to 0.2. This proves to be an acceptable solution in practice. To construct the final anatomical view, these images are blended together. The depth information of each image is taken into account to preserve correct

depth relations. The coronary ghosting takes advantage of this approach. It is implemented by controlling the opacity of the layer of the coronary artery rendering with the opacity in the layer of the late enhancement rendering. For the ghosting the edges of the coronary arteries are rendered using an edge detection operator on the depth information.

The framework has been implemented using OpenGL 2.0 to take full advantage of the capabilities of modern graphics hardware. The development machine contained an Intel Xeon 3 GHz processor and a NVIDIA GeForce 7950 GX2 graphics card. On this machine, all configurations of both the volumetric bull's eye and the anatomical view can be rendered at more than 20 frames per second, which is sufficient for interactively exploring the visualizations.

### **3.5 Interactive Exploration with Linked Views**

An important requirement of a clinical software application is that it should be intuitive, comprehensive, and time-efficient. With most current systems, a lot of time-consuming interaction is required. The CoViCAD system aims to reduce the required amount of interaction to a minimum. The various views on the data present in this system are intended to be used together. This helps maintain a relation between the different views and the properties expressed.

#### **3.5.1 Standard Views**

A number of standard views on the heart is used in clinical practice. The most common are the short-axis, two-chamber long-axis, and four-chamber long-axis views. The corresponding imaging planes are often used for data acquisition. The long and short axes provide a more natural coordinate system for the heart than the standard patient axes.

This knowledge is applied to the viewpoint control of the anatomical view. The four-chamber long-axis view as seen in Figure 3.3 provides a good starting viewpoint for the heart. An advantage of using standard views as an initial viewpoint estimation is that it can compensate for the differences in orientation of the heart between patients. Due to occlusion issues the other standard views are more useful in combination with a cutting plane. The standard views are in fact originally intended for the exploration of the inner parts of the heart. As mentioned in Section 3.4.3, the orientation and interaction possibilities of the cutting plane according to these standard views are also restricted. This makes interacting with the cutting plane more intuitive and time-efficient.

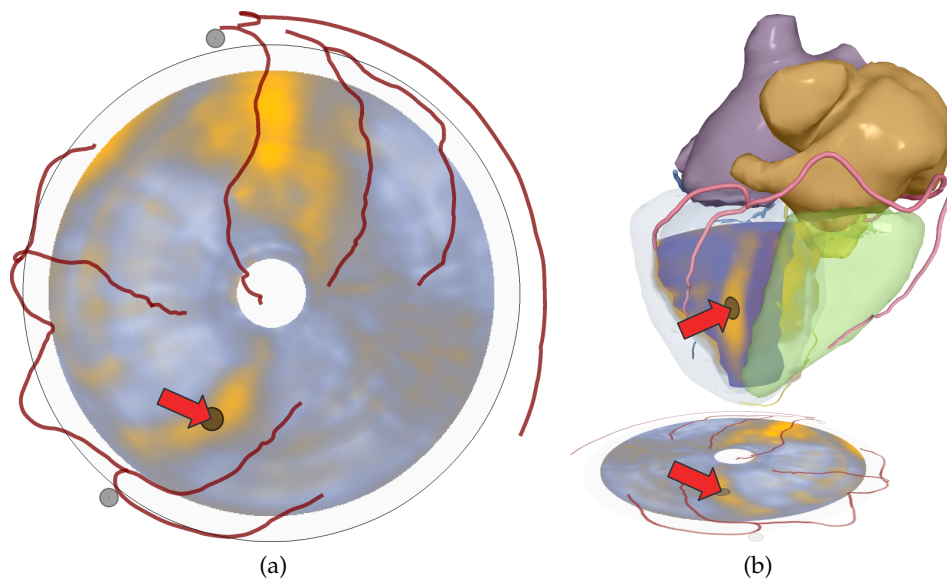


Figure 3.8: Global cursor for linking two views: (a) shows a volumetric bull's eye plot with the global cursor (indicated by the red arrow) highlighting an area of scar; (b) shows the same region highlighted in the anatomical view. The viewpoint of the anatomical view is controlled by the position of the cursor.

### 3.5.2 Interactive Navigation

The volumetric bull's eye plot serves well for visualizing the overall distribution of scar. Due to the deformations introduced by the unfolding, proportions are however not optimally preserved. Therefore the size of scar is better perceived in the anatomical view. The latter also provides a more detailed, three-dimensional anatomical context. To easily relate a region of interest between these two views the user is provided with a navigation cursor. It can be used to specify a region of interest on the volumetric bull's eye plot. The corresponding region in the anatomical view is subsequently highlighted. This is demonstrated in Figure 3.8. It provides a simple but effective linked navigation between the two views.

### 3.5.3 Automatic Viewpoint Control

Interactive specification of orientation in three-dimensional visualizations is a time-consuming task and one of the reasons most such visualizations still lack medical acceptance. Therefore the presented framework provides an automatic computation of the orientation of the anatomical view. Once a region of interest is specified on the volumetric bull's eye plot in a similar way to the navigation cursor, the corresponding region on the

epicardium is calculated. The viewing direction of the anatomical view is then configured such that it corresponds to the vector from the center of the region and a point located on the long axis, in the middle between the aortic valve and the apex. The latter point acts as the rotation center of the model. This approach is similar to the work of Viola *et al.* [85], although it employs a more restrictive and much simpler viewpoint specification.

One step further would be to automatically create case-specific views without the specification of a region of interest. Using the scar classification specified by the user, regions in the volumetric bull's eye plot that exhibit scar can automatically be calculated. For each of these areas, an accompanying anatomical view can be generated. In this case the regions of interest are automatically identified. In a typical work-flow scenario a clinician would step through the automatically generated anatomical views, discarding those where the tissue in focus was falsely classified as scar. This could prove to reduce the required amount of interaction and the duration of the analysis. The full potential of this approach has however not yet been explored.

### 3.6 Summary and Conclusions

This chapter presented CoViCAD; a comprehensive medical visualization framework for the diagnosis of patients with coronary artery disease using segmented whole heart and late enhancement MRI data. The framework presents the data both in a schematic way and in a three-dimensional view with anatomical context. The former presentation mainly visualizes the overall distribution and transmuralities of scar, while the latter serves for the assessment of size and location of scar with relation to the myocardial and coronary anatomy.

The three-dimensional visualization of scar in an anatomical context provided by the anatomical view of the framework restores the relation to the myocardial and coronary anatomy. Regions of scar can be related to coronary arteries, which can be examined for a possible stenosis using various representations. This allows the clinician to relate the cause (stenosis) to the result (scar). The essential part of this approach is that it offers a *visual examination* of the coronary anatomy in relation to scar. Currently the resolution of the coronary arteries in whole heart MRI scans is not sufficient for accurate diameter measurements. Moreover a stenosis can even be hard to find through visual inspection. A visualization in relation to scar therefore helps to find a stenosis by focusing on particular parts of the coronary tree. The volumetric bull's eye plot also facilitates relating scar to coronary arteries. Due to these advantages, combined with the increased accuracy and additional information on transmuralities of the volumetric bull's eye plot compared to the bull's eye plot, it is expected



that this framework will lead to a more accurate and efficient diagnosis of patients with coronary artery disease.

The visualization of scar in an anatomical context is also applicable to patients that suffer from an electrical disorder that causes part of their heart to beat asynchronously. These patients may be treated with cardiac resynchronization therapy, a procedure in which a pacemaker with multiple wires is implanted into the patient. It is important that none of these wires are placed on areas of scar, since scar has a reduced conductivity and thus would void their functionality. A three-dimensional visualization is in this case better understandable than a series of two-dimensional images. It relates better to the anatomy visible during surgery. This is most likely also the reason that there is an increasing demand from medical partners, especially from cardiologists, for three-dimensional visualizations like the anatomical view presented here.

The integration of multiple data sources and rendering techniques in the anatomical view is more comprehensive than has been presented up to now. Much thought has been spent on the interaction between the different views in order to keep the amount of required interaction as low as possible. The result is an intuitive and comprehensive analysis tool for diagnosing patients with coronary artery disease.



Clouds are not spheres,  
mountains are not cones,  
coastlines are not circles, and  
bark is not smooth, nor does  
lightning travel in a straight line.

---

Benoît Mandelbrot

# 4

## Patient-Specific Coronary Territories

The segmentation of the myocardium based on the 17-segment model as recommended by the American Heart Association is widely used in medical practice. The patient-specific coronary anatomy does not play a role in this model. Due to large variations in coronary anatomy among patients, this can result in an inaccurate mapping between myocardial segments and coronary arteries. This chapter presents two approaches to include the patient-specific coronary anatomy in this mapping. The first approach adapts the 17-segment model to fit the patient. The second approach generates a less constrained mapping that does not necessarily conform to this model. Both approaches are based on a Voronoi diagram computation of the primary coronary arteries using geodesic distances along the epicardium in three-dimensional space. Both approaches are demonstrated with several patients and show how the first approach can also be used to fit volume data to the 17-segment model. The technique presented in this chapter gives detailed insight into the coronary anatomy in a single diagram. The feedback provided by clinical experts indicates that it has the potential to provide a more accurate relation between deficiencies in the myocardium and the supplying coronary arteries.

### 4.1 Introduction

**I**N THE CONTEXT of cardiac tomography, the American Heart Association (AHA) has published a set of recommendations to standardize part of the clinical routine [14]. These recommendations concern the segmentation of the left ventricular myocardium. They also include a standardized nomenclature for the coronary arteries. One of these recommendations is

the use of a 17-segment model for the segmentation of the myocardium. This model defines a mapping of each of the segments to the coronary arteries that supply that region. The relation between the myocardium and its supplying coronary arteries is important during diagnosis.

The individual paths of the coronary arteries and the way they supply the myocardium varies greatly among different patients. This causes the standardized mapping between myocardial segments and coronary arteries to be of varying accuracy across different patients. This issue is acknowledged by the American Heart Association, with the note that the suggested model is based upon the methods available at that time [14].

With current MRI technology it is possible to segment the three major coronary arteries in a whole heart scan [88]. The three primary coronary arteries are the left anterior descending (LAD), the left circumflex (LCX), and the right coronary artery (RCA). While there are still cases where a complete segmentation is not feasible, these issues will most likely be resolved in the near future.

The patient-specific coronary anatomy can be used to improve the relation between the myocardium and the supplying coronary arteries. This chapter explores two possible approaches. In the first approach the 17-segment model as defined by the AHA is adapted to fit to the coronary anatomy of the patient in question. In other words, a number of constraints is set to force the mapping between the myocardium and the areas the coronary arteries are supplying to correspond to the 17-segment model. In the second approach no constraints are set, which allows for arbitrary mappings between the coronary arteries and the myocardium. Both approaches are based on Voronoi diagrams of the coronary arteries using geodesic distances along the epicardium, the outer part of the myocardium. The resulting relation divides the myocardium into several coronary territories, regions of the myocardium supplied by the coronary artery that corresponds to that territory. These territories, along with the coronary arteries themselves, are finally mapped onto a two-dimensional bull's eye plot.

Both approaches result in customized diagrams that better reflect the actual relation between myocardial tissue and supplying coronary arteries. The approach of adapting the 17-segment model is less sensitive to incomplete segmentations of the coronary anatomy. On the other hand, unconstrained coronary territories may be more accurate for patients that do not correspond well to the 17-segment model.

This chapter is structured as follows. First an overview of related work on the 17-segment model from the American Heart Association and patient-specific coronary territories is given in Section 4.2. Section 4.3 discusses the computation of the coronary territories and the mapping on a bull's eye plot. Section 4.4 discusses both approaches of computing patient-specific coronary territories. Section 4.5 describes the results of an

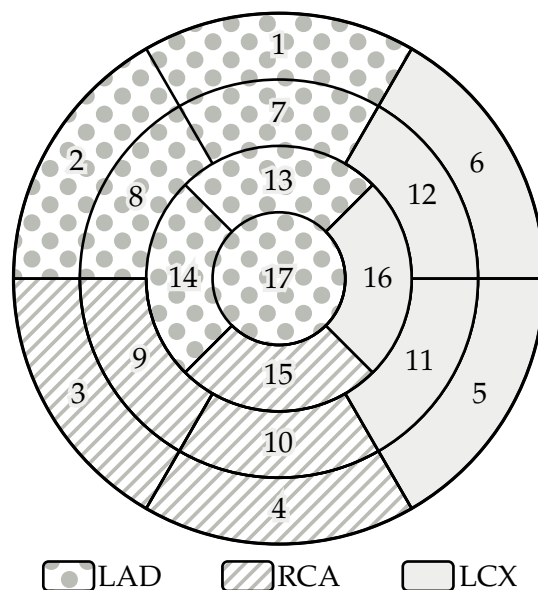


Figure 4.1: The 17-segment model for the segmentation of the left ventricle as presented by the American Heart Association [14]. The patterns indicate the mapping of the segments to coronary territories.

evaluation experiment and provides a use case of the presented techniques with viability data. Section 4.6 discusses the medical applications and issues of the presented approach. Finally, Section 4.7 summarizes and concludes this chapter.

## 4.2 Related Work

The American Heart Association (AHA) published a set of recommendations to standardize the segmentation of the left ventricular myocardium [14]. This includes a division of the myocardium into 17 parts accompanied by a mapping of each of the segments to coronary territories. As a reference this 17-segment model is depicted in Figure 4.1. It shows the myocardium in a bull's eye plot, a two-dimensional representation of the left ventricle. Since its introduction, the 17-segment model has become widely accepted in clinical practice and it has replaced previous models. In the area of SPECT, for example, a 20-segment model [3] was more common prior to the introduction of the 17-segment model.

A medical study performed by Pereztol-Valdés *et al.* [65] using myocardial perfusion nuclear imaging gives a more precise relation between each of the 17 segments and the supplying coronary arteries. It shows that contrary to the model of the AHA, only nine segments are commonly

supplied by one coronary artery; the remaining segments are supplied by multiple coronary arteries. It also verifies that there is great variability among patients, especially in the apical area of the left ventricle. Based on the outcome of this study, the authors presented a revised mapping of segments to coronary territories, where some segments are assigned to multiple territories. Recently a similar study was published by Ortiz-Pérez *et al.* [64] using contrast-enhanced MRI. Their work also confirmed the variability in coronary anatomy and the need for a better model to more accurately attribute perfusion defects in segments to coronary arteries.

Beliveau *et al.* [5, 6] previously presented the idea of computing patient-specific coronary territories. In their work coronary arteries are segmented from a whole heart CT scan and projected on the segmented epicardial surface. The patient-specific coronary territories are computed using a Voronoi diagram of the projected arteries. While their work is in several ways similar to ours, there are several key differences. Besides a different implementation approach and a different method to map the territories onto a bull's eye plot, no explicit relation between the 17-segment model and the coronary territories is made, although the 17-segment model is mentioned in their work. Their approach is thus not capable of forcing correspondence to this model. Section 4.5.2 demonstrates how this can be used to regularize a bull's eye plot of viability data, while their approach is limited to showing an overlay. In other work, Voronoi diagrams are also being used for the analysis of modeled and segmented artery trees [40].

Oeltze *et al.* presented several novel visualization techniques for the analysis of perfusion data [62]. Their redefined bull's eye plot shows myocardial perfusion data of both rest and stress states in a single bull's eye plot based on the 17-segment model. They also presented an interactive bull's eye plot that is linked to a three-dimensional visualization showing coronary artery branches. Picking a segment on the bull's eye plot automatically adjusts the view of the three-dimensional view to show the corresponding artery.

### 4.3 Computation of Coronary Territories

A coronary territory defines the region of the myocardium supplied by a specific coronary artery. Determining which part of the myocardium a coronary artery is supplying is a complex and yet unsolved problem. This can be resolved by assuming that each part of the myocardium is supplied by its closest coronary artery. This approximation suffices for the purposes of this work. To further reduce complexity, all computations are performed on the epicardial surface, instead of taking the three-dimensional nature of the myocardium into account.

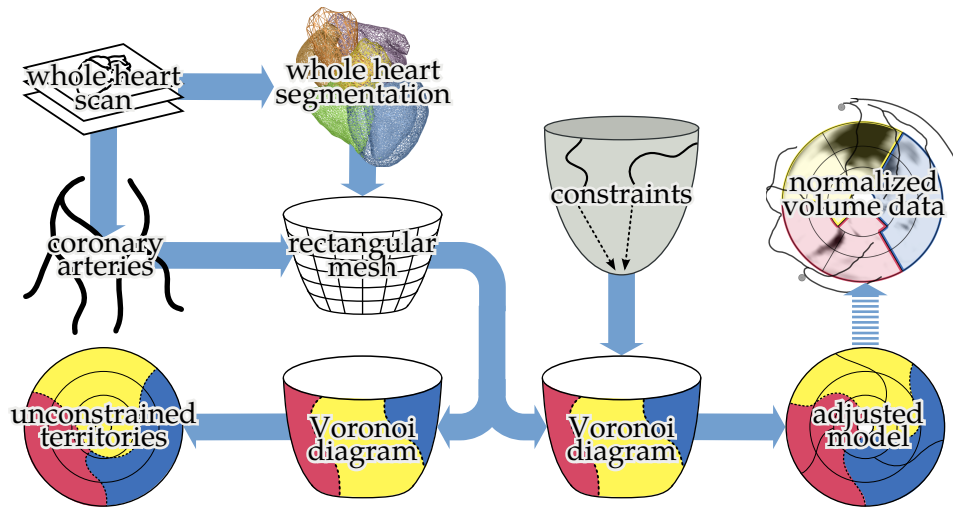


Figure 4.2: Overview of the presented approach towards patient-specific coronary territories.

An overview of the presented approach is shown in Figure 4.2. A whole heart segmentation is extracted from a whole heart MRI scan using an approach by Ecabert *et al.* [20]. The left ventricular epicardium part of this segmentation is used to create a rectangular mesh of the epicardium to gain more control over the resolution and uniformity of the mesh. The same whole heart scan provides the centerlines of the three primary coronary arteries. They are segmented using a semi-automatic vessel tracking method [50] and projected onto the mesh of the epicardium. Subsequently a Voronoi diagram of these projected arteries is computed. This diagram is finally mapped onto a bull's eye plot.

Prior to computing the Voronoi diagram, a number of constraints can be set which force the resulting division of the epicardium into coronary territories to correspond to the 17-segment model. In this case the borders and middle lines of the coronary territories can be used to adapt the 17-segment model to the patient. The deviation between the original and the adapted models can then also be used to deform data from a different scan of the same patient to fit to the original 17-segment model. Without setting any constraints, the resulting coronary territories can have arbitrary shapes and need not correspond to the 17-segment model. Both these approaches are discussed in more detail in Section 4.4.

### 4.3.1 Mesh of the Epicardium

The automatic segmentation algorithm gives a segmentation of the left ventricular epicardium in the form of an unstructured polygonal mesh. In

order to guarantee sufficient accuracy throughout the mesh during the Voronoi diagram computation a rectangular mesh is generated instead. The unstructured mesh is intersected with two sets of planes. One set consists of evenly spaced planes orthogonal to the long axis, the other set consists of planes through the long axis at evenly spaced angular offsets to the short axis. The points at the intersections of a plane from each set and the unstructured mesh form control points for a set of interpolating Catmull-Rom spline patches. Tessellating each patch at the desired accuracy gives the final rectangular mesh.

### 4.3.2 Projection of the Coronary Arteries

After the computation of a proper mesh of the epicardium, the coronary arteries are projected onto this mesh. A discrete representation of the coronary artery tree is computed by generating a set of points spaced approximately one millimeter apart along each coronary artery. For each of the points along each coronary artery, the closest vertex of the mesh is computed. The index of the artery and the Euclidean distance to that artery is stored at that vertex.

### 4.3.3 Computation of the Voronoi Diagram

The first step towards computing the Voronoi diagram of the arteries on the epicardial mesh is to compute the closest coronary artery and the distance to that artery for all vertices of the mesh. This is achieved by propagating the information in the vertices encountered during the projection of the arteries in the previous step. Starting with an active set consisting of only those vertices, the distances to all neighboring vertices are propagated using an 8-neighborhood approach. In other words, each vertex has eight neighbors to which distances are propagated, except at the border of the mesh (see Figure 4.3). Distances and indices to arteries are only updated if the distance is shorter than the one already present in the vertex, if any. Once the algorithm terminates, each vertex contains an index of and distance to its closest coronary artery.

The closest coronary artery for a vertex is defined as the artery for which the distance along the epicardium to a projection of that coronary artery is minimal. This definition approaches reality better than using Euclidean distances in space, as the curved nature of the ventricle wall is taken into account. Due to the use of a discrete mesh of the epicardium, the distance is an approximate geodesic distance along this mesh. In order to obtain a good approximation of the true geodesic distance, the distance propagation requires a sufficiently fine-grained mesh. In the experiments for this chapter a mesh with 80 contours between the apex and the base of the left ventricle was constructed and the contours were divided into



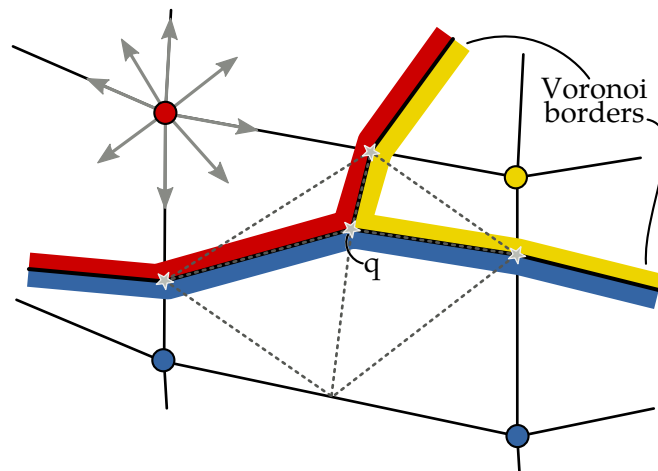


Figure 4.3: The distances to the closest coronary artery are propagated to all neighbors of a vertex along the edges and diagonals of each quadrilateral it is part of. Each quadrilateral can be divided in up to four territories. The gray lines indicate the triangularization of this particular case. Note that the presented approach, opposed to the traditional marching squares algorithm, generates a vertex in the middle of the quadrilateral.

128 vertices. Experiments using finer grained meshes indicate that the maximum error due to interpolation between vertices is less than one millimeter.

The Voronoi diagram is given by the lines passing through edges whose vertices have different closest coronary arteries. These lines are extracted using an approach based on marching squares, as all faces of the mesh are quadrilaterals. The marching squares algorithm is the two-dimensional equivalent of marching cubes [49]. The difference with traditional marching squares is that each quadrilateral can be divided in up to four parts. Figure 4.3 shows a case where the four vertices of a quadrilateral belong to three different coronary territories, dividing the quadrilateral into three parts. The division of the quadrilateral has been generalized to cover the cases where it needs to be divided into three or four parts. The intersection points on the edges of the quadrilateral are computed first. To ensure the quality of the dividing lines, intersection positions are computed using linear interpolation. Next, the average of these points is computed, giving a point  $q$  inside the quadrilateral. For edges that have no intersection point, the point on the middle of these edges is computed. The quadrilateral can then be divided into four regions where each region is given by one corner point, the two intersection points or middle points of the edges connected to the corner, and point  $q$ . Note that all of these four regions are always convex, as point  $q$  is inside or

on the rhombus spanned by the four intersection or middle points. The four regions can then be triangulated independently using at most two triangles, as is shown in Figure 4.3 by the gray dashed lines. The number of triangles used for parts consisting of multiple regions can be reduced. The blue part in Figure 4.3, consisting of two regions of the quadrilateral, can for example also be triangulated using three triangles. The edges of the Voronoi diagram are given by the edges of the triangles that belong to different parts.

#### 4.3.4 Projection onto a Bull's Eye Plot

Once a complete Voronoi diagram on the epicardial surface has been computed, it is mapped onto a two-dimensional bull's eye plot. The mapping is based on a parameterization of the left ventricle, which is illustrated in Figure 4.4. Each point in the left ventricular myocardium can be specified using a 3-tuple  $(\varphi, h, r)$ . In this tuple  $\varphi$  represents the angle with the short axis in a plane orthogonal to the long axis,  $h$  the distance to the apex along the long axis, and  $r$  the distance to the long axis. The mapping of the Voronoi edges is constructed by computing the parameters of all vertices and directly interpreting  $(\varphi, h)$  as polar coordinates. The coronary arteries are mapped onto the bull's eye plot using the same approach.

An example result of the coronary territory computation is shown in Figure 4.5. Note the hole in the mapped diagram due to the missing segment number 17 of the apex, which is not part of the mesh of the epicardium.

### 4.4 Patient-Specific Coronary Territories

In the 17-segment model there is no variation in shape among patients of the three coronary territories. Although this eases interpretation and comparison, it does not give any details about the patient-specific coronary anatomy.

Using the method of computing patient-specific coronary territories described above, the 17-segment model can be improved upon in two different ways. The first approach is to alter the 17-segment model by fitting the model's edges to the patient-specific coronary territories and is discussed in Section 4.4.1. The second approach is to compute the coronary territories without taking a model into account to allow arbitrarily shaped coronary territories and is discussed in Section 4.4.2.

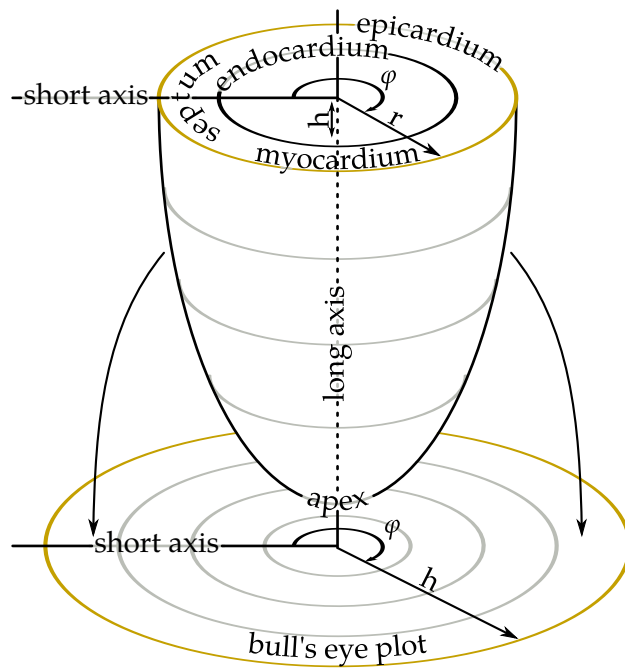


Figure 4.4: Parameterization of the left ventricle and its mapping onto a bull's eye plot.

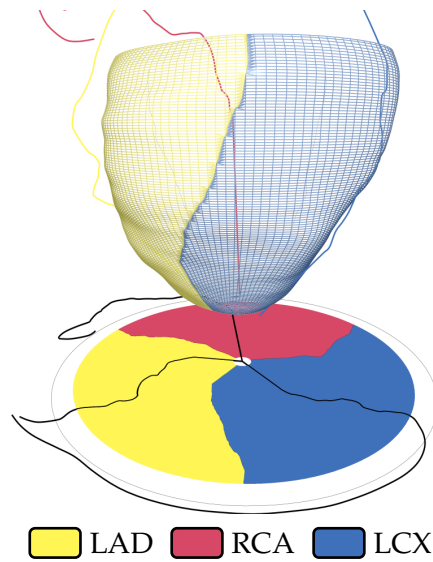


Figure 4.5: An example of a rectangular mesh of the left ventricle and the coronary artery centerlines. The mesh surface is colored based on the Voronoi diagram.

#### 4.4.1 A Patient-Specific 17-Segment Model

In order to fit the 17-segment model to the patient-specific anatomy, the morphology of the coronary territories should match that of the 17-segment model. The first 16 segments of the 17-segment model divide the left ventricle into three parts: a basal part, a mid-cavity part, and an apical part. Each of these parts correspond to one of the rings in the model shown in Figure 4.1. Each of the primary coronary arteries supplies part of each of these three parts.

The segmentation of the coronary arteries in a whole heart MRI scan is a difficult task. As the coronary arteries become thinner towards the end, segmentation of the complete branch is rarely possible due to the resolution of current whole heart MRI scans. This often results in incomplete segmentations of the coronary arteries, which in turn causes the morphology of the coronary territories based on these segmentations to rarely match that of the 17-segment model. A correspondence can be forced by artificially completing the segmentation of the coronary arteries by connecting the endpoint of each artery to the apex. This approach is a compromise between a solely segmentation-driven approach, like the approach discussed in Section 4.4.2, and a solely model-driven approach, like the 17-segment model.

When adapting the 17-segment model, the borders of the coronary territories in the model are fit to the corresponding borders in the Voronoi diagram. The edges of segments indicating the center of each territory are mapped to lines equidistant to the borders of that coronary territory. Both these mappings require that each coronary territory has two borders, i.e. it has a “left” and a “right” side. This means that each coronary territory should run from the apex to the base and should be connected, just as is the case in the 17-segment model.

The basal, mid-cavity, and apical segments of the 17-segment model are equal thirds of the heart along the long axis. This means that any differences between the original and an adapted 17-segment model are strictly *angular* differences. The relation of the distance to the apex along the long axis is also preserved in the 17-segment model; adapting the model thus does not affect  $h$ . It follows that a function  $f$  exists such that for any point  $(\varphi, h)$  in a bull’s eye plot of the 17-segment model,  $(f(\varphi), h)$  gives the corresponding point in a bull’s eye plot of an adapted 17-segment model.

Figure 4.6 gives an overview of the implementation of function  $f$ . Given a tuple  $(\varphi, h)$  in a coronary territory (the red dot), the two angular differences between the borders of the coronary territory according to the 17-segment model and the Voronoi diagram respectively are computed (the gray arcs), at distance  $h$  from the apex along the long axis. Linear interpolation is applied between these two angular differences to find the

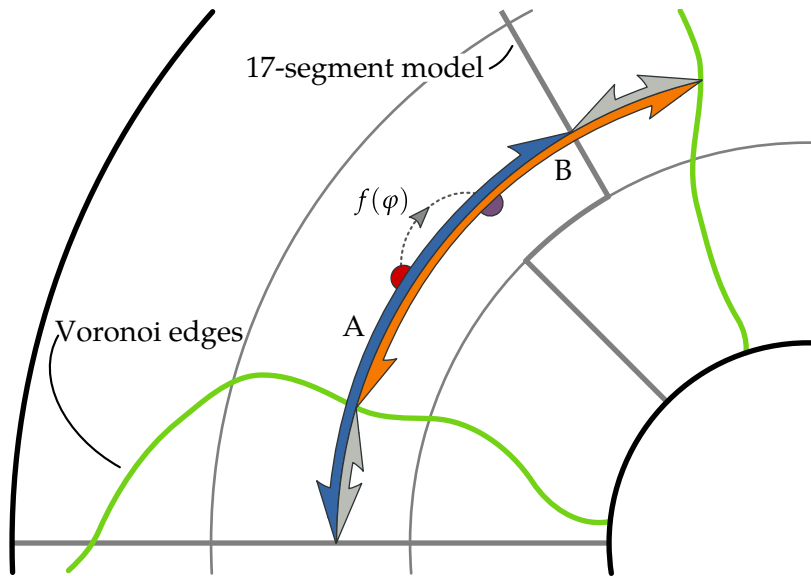


Figure 4.6: Function  $f$  transforms the query point (red dot) from the 17-segment model to the adapted model. The angular differences (gray arcs) are used to transform the blue arc A into the orange arc B.

angular difference for the specified value of  $\varphi$  (the arc marked  $f(\varphi)$ ). This approach essentially transforms the blue arc A into the orange arc B using an angular scaling and translation. Note that function  $f$  is in fact defined for every point inside the myocardium, even though it is only applied to the edges of the segments for computing the adapted 17-segment model. In Section 4.5.2 this property is used to adapt volume data to the 17-segment model instead, using the inverse of  $f$ .

Figure 4.7 shows a comparison between a standard 17-segment model (Figure 4.7a) and the same model adapted to the patient-specific coronary anatomy (Figure 4.7b). The coronary arteries are also mapped on top of the bull's eye plots. Note that the Voronoi diagram is computed using geodesic distances in three-dimensional space, so in the bull's eye plot the borders of the coronary territories generally are not equidistant to the coronary arteries between them. Also, part of the RCA wraps around the right ventricle. Since the distance to the long axis is lost in the bull's eye plot, this is no longer visible in the mapping of the RCA. For this specific patient, the divergence from the model is not particularly big. This is not too uncommon, as the 17-segment model is based on an average of the population.

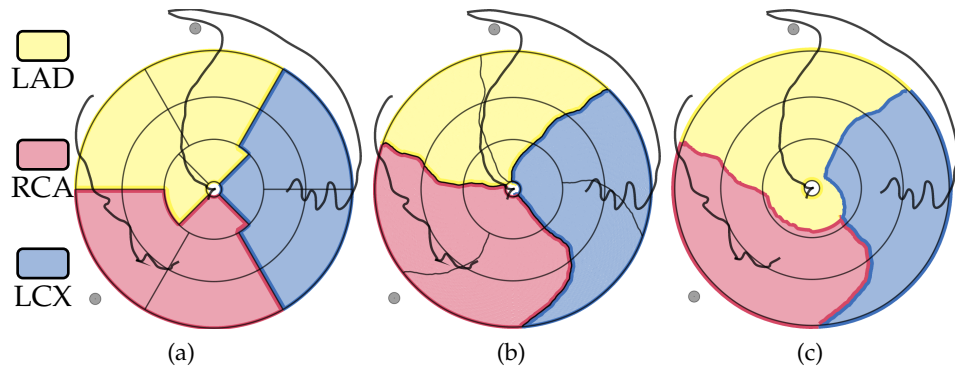


Figure 4.7: A comparison of (a) the 17-segment model; (b) the 17-segment model adapted using the patient-specific coronary anatomy; and (c) unconstrained coronary territories. The three coronary arteries are shown as black lines. All three bull's eye plots correspond to the same patient.

#### 4.4.2 Unconstrained Coronary Territories

The previously discussed approach artificially completes the segmentation of the coronary arteries by connecting the end points to the apex. This process can also be omitted and the coronary anatomy can instead be used directly. However, the resulting division of the myocardium into coronary territories does not necessarily correspond to the 17-segment model. Experiments show that there is no perfect correspondence for most patients. In most of the cases this is due to the varying way the apex is supplied. This is confirmed by earlier studies [65, 64]. Also the fact that the LAD becomes too thin to be successfully segmented well before it has reached the apex often plays a role.

Figure 4.7c shows the coronary territories computed without artificially completing the coronary artery segmentation. In this particular case, the divergence from the 17-segment model is rather minor and correspondence is only lost in the apical segment of the model, corresponding to the inner ring. Since no constraints are set, the divergence may be arbitrarily large. In fact, the territories may even be disjoint, although this rarely occurs in practice. While this approach imposes less constraints on the coronary territories, it is also more sensitive to incomplete segmentations of the coronary arteries.

### 4.5 Medical Expert Evaluation

An informal evaluation of the presented approach has been performed by selecting five patients who underwent a whole-heart cardiac MRI scan and by generating four bull's eye plots for each patient. The first bull's eye

Case	Method 1	Method 2	Method 3
Patient 1	5	5	5
Patient 2	4	4	4
Patient 3	2	2	4/5
Patient 4	1	N/A	4/5
Patient 5	1	2	4/5
Overall	3	3	4

Table 4.1: Results of the evaluation experiment. Method 1 corresponds to the original 17-segment model, method 2 corresponds to the 17-segment model adapted using the patient-specific coronary anatomy, and method 3 corresponds to using unconstrained coronary territories. The scale ranges from one (very bad) to five (very good).

plot contained only a mapping of the three primary coronary arteries. The second, third, and fourth bull's eye plots contained the original 17-segment model, adapted 17-segment model, and unconstrained coronary territories, respectively. Figure 4.7 gives the latter three bull's eye plots for patient 2 used in this experiment. For patient 4 an adapted 17-segment model could not be generated. This issue is further discussed in Section 4.6. The complete questionnaire is listed in Appendix A.

An experienced cardiologist first manually drew the coronary territories on the first bull's eye plot for each patient. The next task was to rate the correspondence between the mapped coronary arteries and the coronary territories as produced by each of the three approaches on a scale from one (very bad) to five (very good). The results of this evaluation are listed in Table 4.1.

Finally the expert provided an overall rating for each approach of determining coronary artery territories. The manual approach was given a score of 4, both the original and the adapted 17-model were rated 3, and using unconstrained coronary territories was rated 4. Note that this overall score is not an average of the scores assigned to the individual cases. Other factors, including intuitiveness, were also taken into account for this score.

The expert expressed that it was difficult to get a feeling for the concept of forcing the coronary territories to correspond to the 17-segment model. The continuous bull's eye plot mapping also created some confusion. It was not clear whether strong variations within one ring, such as in the lower right part of Figure 4.7c, corresponded to epicardial and endocardial territories or whether the diagram should be interpreted as having infinitely many rings. The latter of these two interpretations would be the correct one. Finally, a suggestion was made to restrict the segmentation of the LAD in the inferior wall, as current segmentations often led to an overestimation

of the LAD territory. This is also the reason why it was not possible to compute constrained coronary territories for patient 4.

In the manually drawn territories the inner ring was entirely allocated to the LAD in all patients except the first. Since this does not correspond to the original 17-segment model, this was only reflected by the unconstrained coronary territories. This is clearly visible in the scores given in Table 4.1 and is also the primary reason this method is preferred. In summary, the expert was positive about the presented work, especially the unconstrained coronary territories. The evaluation indicates that this approach can compete with a manual approach.

#### 4.5.1 Application to CT Data

The technique has also been applied to a whole heart CT scan. The same segmentation techniques can be used as for the MRI scans. Due to the better spatial resolution of CT, a more detailed coronary artery tree can be extracted. Figure 4.8 shows the unconstrained coronary territories of a test dataset. The hue encodes which primary coronary artery a territory belongs to and the lightness distinguishes territories from subbranches. This visualizes the hierarchy in the coronary artery tree. The example also demonstrates that the presented approach is capable of generating an arbitrarily large number of territories. Due to the more fine-grained segmentation of the coronary artery tree, there is little difference when the end points of the coronary arteries are connected to the apex. For the same reason as before, forcing correspondence to the 17-segment model was not feasible for this patient.

#### 4.5.2 Application to Late Enhancement Data

The primary advantage of patient-specific information on the coronary territories is that it allows to establish a more accurate relation between a functional defect and the coronary arteries. This involves including other types of data, such as cine, late enhancement, and perfusion data. Here an example is given of how the presented approach can be combined with viability information from a late enhancement scan. A late enhancement scan shows areas where a contrast agent has accumulated, typically indicating dead tissue called scar. It is demonstrated that the patient-specific coronary territories can lead to a better understanding of which coronary arteries are related to areas of scar.

Figure 4.9 shows two bull's eye plots that each depict both the coronary territories and viability data. The darker areas in the bull's eye plots correspond to areas of scar. The top bull's eye plot shows the coronary territories as an adapted 17-segment model. In the bottom bull's eye plot, the volume data are adapted to fit the original 17-segment model using



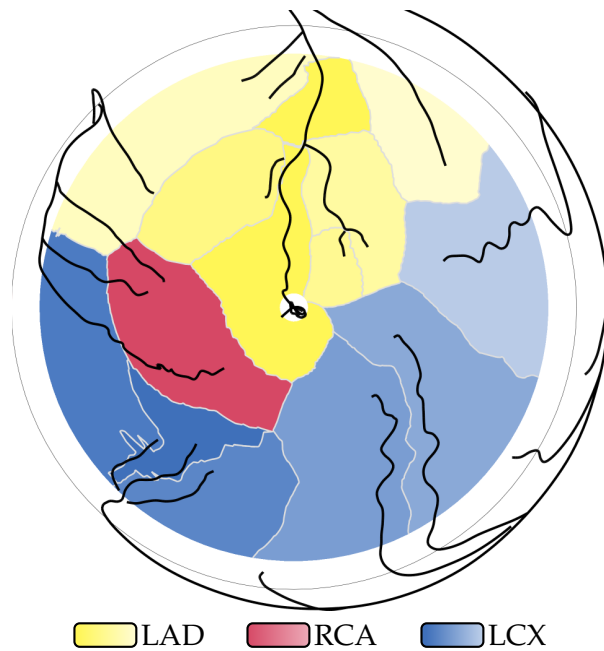


Figure 4.8: Unconstrained coronary territories computed from a detailed coronary artery tree extracted from a CT scan. The hue of each territory encodes its primary coronary artery, while the lightness is used to distinguish territories from subbranches.

the inverse of function  $f$  discussed in Section 4.4.1. This is implemented using on-the-fly resampling of the volume data. In other words, function  $f^{-1}$  is evaluated for every pixel during the rendering of the bull's eye plot. In this case the scar on the top side of the bull's eye plot is stretched to fill the entire segment.

On the right of Figure 4.9 a three-dimensional view is shown to relate the scar to the three-dimensional coronary and cardiac anatomy. The coronary territories are projected on the epicardial surface, using the adapted 17-segment model approach. To establish a strong correspondence between the bull's eye plot and the three-dimensional view, a cursor is shown on both views, indicated by the red arrows in Figure 4.9. To facilitate easy navigation, the viewpoint can be controlled by the position of the cursor. The user can then explore the three-dimensional view by moving the cursor on the bull's eye plot.

## 4.6 Discussion

For some patients, the coronary anatomy is too different from what the 17-segment model assumes. As was verified by Pereztol-Valdés *et al.* [65]

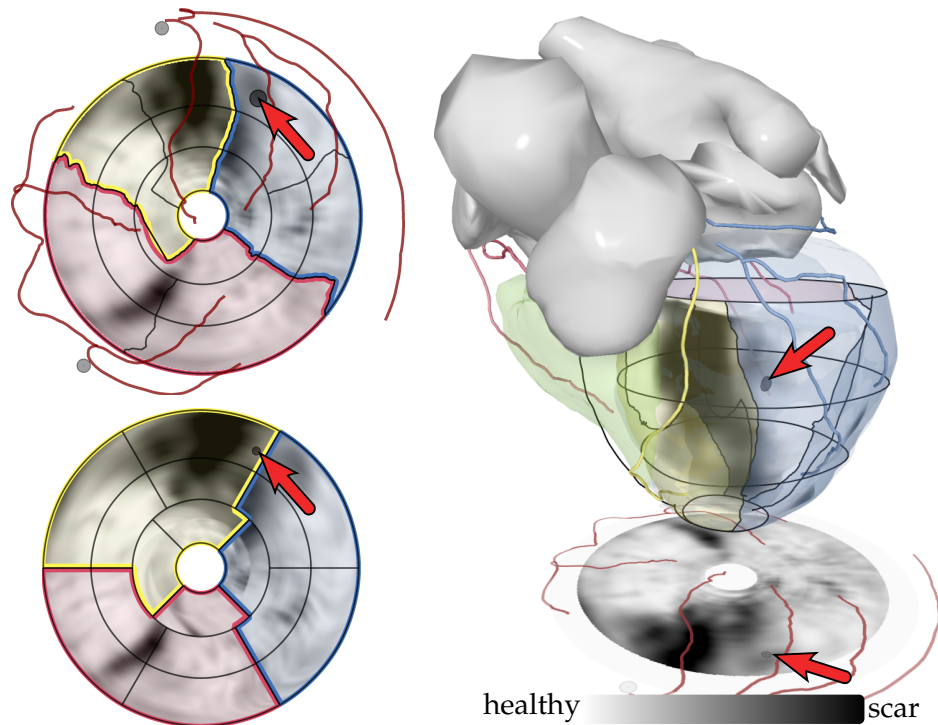


Figure 4.9: Combined visualization of coronary territories and viability information. The darker areas in the bull's eye plots and the three-dimensional view correspond to areas of scar. A cursor (red arrows) shows corresponding points on both bull's eye plots and the three-dimensional view. The 17-segment model is shown in the three-dimensional view as a set of black lines around the epicardium.

and Ortiz-Pérez *et al.* [64], especially in the apical region there is a lot of variance among patients. Figure 4.10a shows the unconstrained coronary territories of one of the patients used in the evaluation. The territory of the LAD is relatively large because the LAD covers both the anterior and inferior left ventricular walls in the apical area. Moreover, the part of the RCA that was visible in the whole heart MRI scan did not extend toward the apical region. For this patient, the approach of adapting the 17-segment model fails since a correspondence cannot be forced due to the dominant LAD. If an adapted 17-segment model is desired, the segmentation of the LAD could be restricted in the apical area. Analyzing the unconstrained coronary territories as shown in Figure 4.10a is in fact especially useful for patients with a coronary anatomy that considerably diverges from the average.

There are also patients that correspond very well to the 17-segment model. Figure 4.10b shows a comparison of an adapted 17-segment model

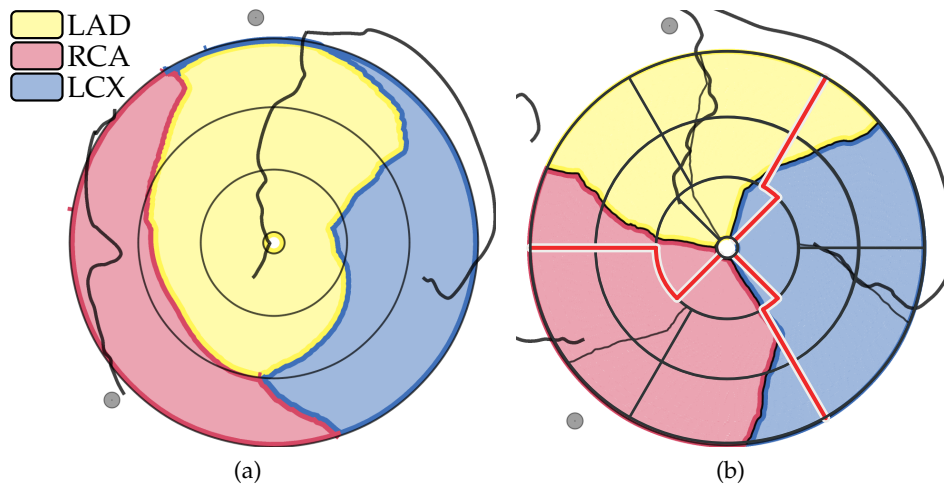


Figure 4.10: Varying correspondence to the 17-segment model: (a) a case where adapting the model fails; (b) a case with relatively little difference to the model.

and the standard 17-segment model in red and black lines, respectively. For this particular patient, the edges of the coronary territories map fairly well to what the 17-segment model predicts. It should be noted however that the model of each part of the myocardium being exclusively perfused by a single artery is especially inaccurate near these borders of the coronary territories. Another aspect that is visible in Figure 4.10b is that due to the circular nature of the bull's eye plot, differences near the apex result in smaller visual differences in the diagram.

Segment number 17, corresponding to the apex, was not included in the experiments. This segment forms a special case compared to the other 16 segments. It is connected to all other territories and only has one border. A special approach is required to assign it to a coronary territory, since there is no clear mapping between this segment and the Voronoi diagram on the epicardial mesh. Thus when adapting the 17-segment model, it would only have to be decided to which coronary territory this segment should be assigned, but no edges need to be adjusted.

In the experiments meshes of the epicardium consisting of approximately  $10^4$  quadrilaterals were used. The entire preprocessing phase, including the mesh computation, coronary artery mapping, Voronoi diagram computation, and computing the adapted 17-segment models typically takes less than one second on a modern workstation (Intel Xeon 3 Ghz, 2 GiB RAM, NVIDIA GeForce 8800 GTX).

## 4.7 Summary and Conclusions

This chapter introduced two approaches for establishing a relation between the patient-specific coronary anatomy and the myocardium. In the first approach the borders of the segments of the 17-segment model as defined by the American Heart Association are adapted to fit to the patient-specific anatomy. In the second approach the coronary territories are computed without taking any model into account. Both approaches are based on a Voronoi diagram computation of the coronary arteries projected onto a quadrilateral mesh of the epicardium.

Both approaches provide detailed insight into the patient-specific coronary anatomy. Adapting the 17-segment model forces a correspondence between the coronary territories and the 17-segment model by connecting the end points of the primary coronary artery branches to the apex. This approach forms a compromise between using a model-based approach and a segmentation-based approach. The second approach does not pose any constraints and thus allows for arbitrarily shaped coronary territories. It is therefore also more sensitive to incomplete segmentations of the coronary arteries. While the uniform appearance of the 17-segment model is lost, the additional patient-specific information on the coronary territories allows for a better understanding on the relation between the coronary arteries and the myocardium.

An application of using patient-specific coronary territories with visualizing viability information from a late enhancement scan was presented. Instead of altering the 17-segment model to correspond to the coronary anatomy, it was shown that it is also possible to fit the underlying volume data to the original 17-segment model. This approach creates uniformly looking bull's eye plots, regardless of the coronary anatomy of the patient.

Feedback obtained through an evaluation experiment with a cardiologist gave a clear signal that this work has clinical relevance. Results indicated that there is a preference towards using unconstrained coronary territories. The latter method produced territories that best matched those indicated manually by a cardiologist and are considered to have a greater correspondence than those that the original 17-segment model suggests.

Do not worry about your  
difficulties in mathematics. I can  
assure you mine are still greater.

---

Albert Einstein

# 5

## Visualization of Simulated Myocardial Perfusion

Visually assessing the effect of the coronary artery anatomy on the perfusion of the heart muscle in patients with coronary artery disease remains a challenging task. This chapter explores the feasibility of visualizing this effect on perfusion using a numerical approach. A computational simulation of the way blood is perfused throughout the myocardium is performed purely based on information from a three-dimensional anatomical tomographic scan. The results are subsequently visualized using both three-dimensional visualizations and bull's eye plots, partially inspired by approaches currently common in medical practice. The approach results in a comprehensive visualization of the coronary anatomy that compares well to visualizations commonly used for other scanning technologies. Techniques are demonstrated giving detailed insight in blood supply, coronary territories, and feeding coronary arteries of a selected region. The advantages of the approach are demonstrated through visualizations that show information which commonly cannot be directly observed in scanning data, such as a separate visualization of the supply from each coronary artery. It is thus shown that the results of a computational simulation can be effectively visualized and facilitate visually correlating these results to for example perfusion data.

### 5.1 Introduction

**C**ORONARY ARTERY DISEASE may change the way blood perfuses throughout the myocardium, which in turn may cause decreased motion of the heart muscle. A whole heart MRI or CT scan images the

anatomical defect directly, while scanning protocols such as cine, perfusion, and late enhancement image the effect of this defect on the functioning of the heart. The reason these latter scanning protocols are used is that it is very difficult to estimate the relevance of a stenosis based on the coronary artery anatomy. Due to its higher resolution, CT can image the coronary arteries with more detail than cardiac MRI. Although perfusion and functional scans are possible with CT, they are rarely used in practice due to a range of issues, including heart beat limitations, a lower scanning speed, and harmful radiation.

This chapter presents an indirect approach to visualize the coronary anatomy through the combination of a computational simulation and a set of comprehensive visualization methods. From a whole heart scan the myocardial surface of both the left and the right ventricle is segmented. The main coronary arteries are segmented including diameter information. These segmentations form the input for a computational simulation, that computes the perfusion of the myocardium based on the patient-specific coronary anatomy. Finally comprehensive visualization methods are applied on the results of this simulation. This provides detailed information on the effects of defects in the coronary anatomy on the distribution of blood throughout the myocardium.

The main contribution is the demonstration that information from such a computational simulation can be effectively visualized. It is shown that it can provide a more comprehensive visualization of the information contained within a whole heart scan compared to common methods that render the anatomical data directly. The visualization methods provided are visually similar to those often used for the analysis of data from different scanning protocols. This simplifies the task of finding correlations between various sources of data.

The structure of this chapter is as follows. Section 5.2 discusses previous work used by or related to the presented approach. Section 5.3 provides details on the computational simulation used to compute the flow of blood throughout the myocardium. Section 5.4 presents methods for visualizing the results from the computations. Section 5.5 demonstrates the effectiveness of the approach by comparing a healthy case to one with an artificial stenosis. Section 5.6 discusses feedback from an expert clinician and the limitations of the presented approach. Finally, Section 5.7 summarizes and concludes this chapter.

## 5.2 Related Work

The anatomy of the coronary arteries varies greatly among individuals. A set of recommendations published by the American Heart Association (AHA) on the segmentation of the myocardium included a standardized

mapping of myocardial segments to supplying coronary arteries [14]. It was presented with the remark that there is indeed tremendous variability in the coronary artery blood supply. The variation among patients was later verified in clinical studies that evaluated the correspondence between the 17 segments of the recommended model and the coronary arteries [65, 64]. This great variability calls for using a patient-specific approach towards assessing the coronary arteries and their relation to the myocardium. Beliveau *et al.* [5, 6] proposed a method of creating a patient-specific mapping between myocardial segments and coronary arteries using tomographic scans to determine the closest coronary arteries for each segment.

There has been extensive research in the area of simulating blood flow in the coronary arteries, or the arterial system in general. Several studies have been performed on the correlation between flow simulations and quantitative measurements of the flow in vessel trees. Good correlations between the two have been reported [7, 45, 24, 10]. The majority of these studies focus on the numerical results and the correlation to flow measurements. They do not provide effective and intuitive visualization methods.

In the area of cardiac medicine, a commonly recurring visualization primitive applied to various types of data is the bull's eye plot. Although several variations of the same idea are in use, their common purpose is to provide a two-dimensional overview of the left ventricle. The recommendations of the AHA also included a proposal how to arrange the 17 segments in a bull's eye plot [14]. These types of bull's eye plots are often applied when the resolution of the data is fairly low, for example in the visualizations of Hennemuth *et al.* [30] of perfusion data. Occasionally the right ventricle is included as well [18]. Oeltze *et al.* [60] show that perfusion data can also be efficiently analyzed using a more statistical approach. When more precision is available, a bull's eye plot with a higher resolution can be constructed. This is demonstrated in the work of Noble *et al.* on combining late enhancement and cine data [59]. In their work the bull's eye plot visualization is combined with a mapping of the results on the three-dimensional left ventricular surface. Termeer *et al.* [79] introduced the volumetric bull's eye plot which uses a continuous transformation of the volume data to obtain a diagram similar to the bull's eye plot, yet preserving continuity and wall thickness.

The most common approach to examine the anatomy of the coronary arteries is to directly inspect the three-dimensional tomographic data, although methods exist to simplify this process. A typical approach is demonstrated in the work of Kuehnel *et al.* [43], where a segmentation of the coronary artery centerlines is used to provide cross-sectional views of the volume data. Curved planar reformations [39] are popular for examining coronary arteries. Since these methods only visualize the

coronary anatomy, they do not facilitate a correlation to data from other sources.

When additional data are available, these can be simultaneously visualized to allow a correlation between the data and the coronary anatomy. Oeltze *et al.* [62] visualize perfusion data and use an anatomical model of the coronary arteries to relate the two. Here the great variance of coronary anatomy could cause problems, as is noted by the authors. Nakaura *et al.* [57] apply fused volume rendering to visualize the coronary anatomy from a CT scan and relate it to SPECT data.

This chapter presents an approach to visualize the relative distribution of blood throughout the myocardium using a computational simulation of the perfusion of the myocardium. The simulation uses patient-specific segmentations of the coronary and myocardial anatomy. Figure 5.1 gives a schematic overview of the presented approach. An automatic whole heart segmentation algorithm [20] is applied to obtain segmentations of the left and right ventricle, both represented as unstructured polygonal meshes. A semi-automatic vessel tracking algorithm [50] provides segmentations of the main coronary arteries, represented by their centerlines and a set of diameter measurements along those centerlines. This approach involves manually indicating seed points at the beginning and end of each coronary artery branch. All information is extracted from a single whole heart scan. These patient-specific segmentations are the input for a computational simulation, which is discussed in Section 5.3. The results of these computations are subsequently visualized, which is elaborated on in Section 5.4. The visualizations provide insight into the overall distribution of blood supply and the areas each coronary artery is supplying. A method to query the relative supply from each coronary artery to a region of interest is presented.

### 5.3 Computation of Coronary Flow

Since the prime task is a visualization feasibility study, a simulation was developed which is sufficient for this purpose, but may prove to be too simplistic for clinical applications. The approach does not take the dynamic nature of cardiac flow into account. Furthermore all the computations are performed on the epicardium, the outer surface of the myocardium, rather than on a true three-dimensional representation such as a tetrahedral mesh. The additional complexity of a more advanced computational model would make it harder to integrate such an approach. Therefore the use of a simpler method was chosen at first.



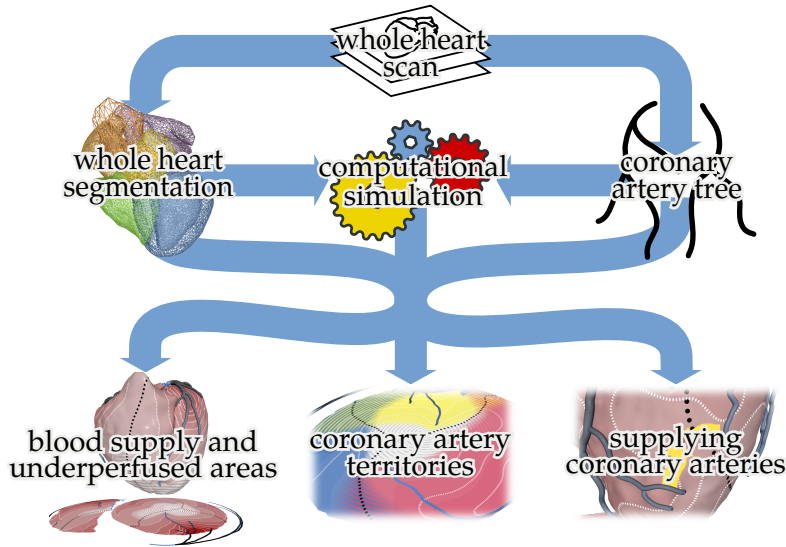


Figure 5.1: Overview of the approach presented in this chapter.

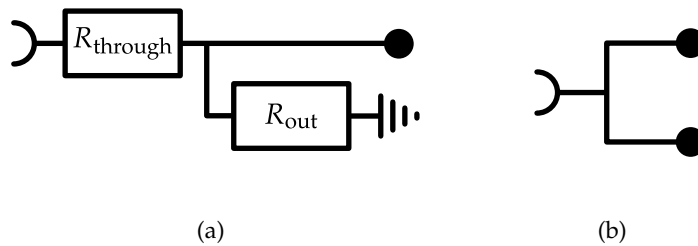


Figure 5.2: The two building blocks used to construct a network of resistors representing the coronary artery tree. The block in (a) represents a linear segment of an artery while the block in (b) represents a bifurcation.

### 5.3.1 Perfusion through the Coronary Arteries

The amount of blood that can flow through a coronary artery is limited by the radius of that artery. The radius of each coronary artery varies along its path. Coronary arteries typically are thinner towards the end, near the apex, than they are at their origin near the base of the left ventricle. Also a stenosis can be a source of a varying diameter. The amount of blood flowing through a point in an artery also determines the amount that can flow out of the artery at that point and out of the remainder of the artery.

The influence of the diameter of the vessel on the amount of blood that can flow through it is modeled by representing the coronary artery tree as a network of resistors. The entire coronary artery tree is constructed using two simple building blocks depicted in Figure 5.2. Using a discrete

representation of the centerline of a coronary artery, the artery is modeled by a connected chain of building blocks as depicted in Figure 5.2a. The resistor labeled  $R_{\text{through}}$  controls the flow through the artery while the resistor label  $R_{\text{out}}$  controls the flow out of the artery at that point. The actual values of  $R_{\text{through}}$  are based on the diameter of the artery at that point using Poiseuille's law, which states that the resistance is inversely proportional to the radius of the artery to the fourth power [25].

For the value of  $R_{\text{out}}$  a predefined constant is used. This does not mean that an equal amount of blood flows out of an artery at each point. The blood volume present at a point is dependent on the radius at that point and the previous part of the artery. This constant is typically several orders of magnitude larger than the average value of  $R_{\text{through}}$  to prevent all blood from flowing out at the beginning of an artery. If it is set too high however, the effect of the variance of  $R_{\text{through}}$  due to a varying artery diameter is reduced.

Once all arteries are represented as chains, the final tree can be constructed by inserting building blocks as depicted in Figure 5.2b at the bifurcations. Note that no additional resistors are necessary. The split of the flow is automatically taken care of by the parallel circuit created and the resistors following a bifurcation, which represent the diameters of the two branches.

Once the tree is complete, the relative amount of flow out of the artery is computed at each point along the artery. By applying the laws for series (Equation 5.1) and parallel (Equation 5.2) circuits, the total equivalent resistance ( $R_{\text{total}}$ ) of a network of resistors, with resistor  $n$  having resistance  $R_n$ , can be computed. This facilitates computing the total equivalent resistance of the remainder of the coronary artery tree at any point. Using Ohm's law we find that, as shown in Equation 5.3, the ratio between the flow through ( $I_{\text{through}}$ ) and the flow out ( $I_{\text{out}}$ ) of the artery is inversely proportional to the ratio between  $R_{\text{through}}$  and  $R_{\text{out}}$ .

$$R_{\text{total}} = \sum_n R_n \quad (5.1)$$

$$\frac{1}{R_{\text{total}}} = \sum_n \frac{1}{R_n} \quad (5.2)$$

$$\frac{I_{\text{through}}}{I_{\text{out}}} = \frac{R_{\text{out}}}{R_{\text{through}}} \quad (5.3)$$

The end of each artery is treated as closed, meaning that all incoming flow has to leave the artery through the set of  $R_{\text{out}}$  resistors. This is a valid assumption, as all the blood has to leave the coronary arteries in order to be lead back into the coronary veins.

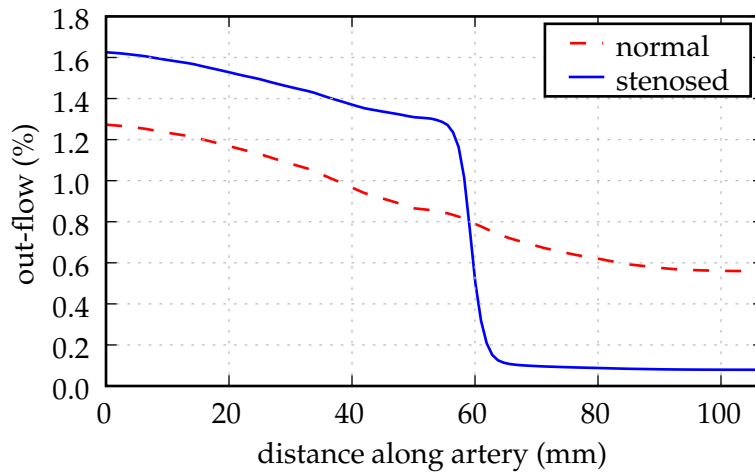


Figure 5.3: Plot showing the relative flow out of a healthy artery and the same artery with a simulated stenosis.

### 5.3.2 Modeling of a Stenosis

With the methods described above, a stenosis can easily be modeled by modifying the radius of an artery at a location of choice. In Figure 5.3 the dashed red line shows the relative out-flow, the flow of blood out of the artery, at each point along an artery without stenosis. Note that there is less flow out of the artery towards the end, as the artery narrows along its path.

Around the middle of the artery a stenosis has subsequently been simulated by narrowing the artery by 70%. This causes the values of  $R_{\text{through}}$  near the stenosis to increase, which affects the ratio between  $I_{\text{through}}$  and  $I_{\text{out}}$  (Equation 5.3) in the area preceding the stenosis. The relative out-flow is shown by the solid blue line. The relative out-flow after the stenosis severely decreases, as can be expected. Since relative flows are being computed, the out-flow before the stenosis increases. This does not necessarily mean that the absolute flow out of the artery has also increased in that segment, since the overall resistance of the artery has also increased. A stenosis in one artery can thus lead to a global change in the distribution of blood throughout the entire coronary artery tree.

### 5.3.3 Diffusion of Flow

Once the flow out of the coronary artery tree is determined, it needs to be diffused throughout the myocardium. The myocardium is approximated by the surface of the epicardium, represented as an unstructured triangle

mesh. This mesh is extracted from a whole heart scan using an automatic segmentation algorithm based on an approach by Ecabert *et al.* [20].

The diffusion process consists of three parts. First, blood from the coronary artery tree is diffused onto the myocardial surface. Second, blood on the myocardial surface itself is diffused. Finally, blood on the myocardial surface is absorbed. The last step simulates the flow of oxygen-depleted blood out of the myocardium through a network of veins.

Both the diffusion from the coronary arteries and the diffusion on the myocardial surface are implemented as iterative convolutions with a Gaussian kernel. All computations are performed on the unstructured triangle mesh of the epicardium. To obtain the desired accuracy during the diffusion process, a subdivision scheme is applied to the epicardial mesh to ensure the area of each triangle is below a predefined threshold. This subdivision scheme guarantees that the kernels used for the convolution process are approximately isotropic. An approach loosely based on Loop's subdivision scheme [48] is employed. Instead of subdividing all triangles in each iteration, only those triangles with an area exceeding the threshold are subdivided. Neighboring triangles are split if necessary to avoid T-junctions. Experiments indicated that the smoothing step proposed by Loop may introduce undesired modifications of the mesh near sharp edges. Therefore it was decided not to smooth new vertices. Also the smoothness of the surface is of less importance for the accuracy of the simulation. The subdivision is applied iteratively until all triangles have an area below the specified threshold. The dynamic subdivision approach, compared to Loop's original subdivision scheme, significantly reduces the number of triangles in the resulting mesh, which gives better performance during the diffusion process.

Given the subdivided triangle mesh, a diffusion neighborhood is computed for each node of the coronary artery tree. This neighborhood forms the kernel for the convolution process. It consists of a set of vertices of the epicardial mesh and a diffusion weight for each vertex. The diffusion weight is the Gaussian function applied to the Euclidean distance of the node to that particular vertex. This is shown in Equation 5.4, where  $w(d)$  denotes the diffusion weight,  $d$  denotes the Euclidean distance between the node and the vertex,  $\sigma$  is a parameter of the diffusion process and  $\epsilon$  denotes the minimum diffusion weight of vertices to include in the diffusion neighborhood.

$$w(d) = \begin{cases} e^{-\frac{d^2}{2\sigma}} & \text{if } d^2 \leq -2\sigma \ln(\epsilon) \\ 0 & \text{otherwise} \end{cases} \quad (5.4)$$

A similar neighborhood is computed for each vertex of the epicardial mesh, except that here between vertices geodesic distances along the epicardial surface are used to compute the diffusion weights. The average size of

the diffusion neighborhoods is significantly decreased by removing vertices that have a very small diffusion weight, controlled by  $\epsilon$  in Equation 5.4. The weights of each neighborhood are normalized to ensure that the total amount of blood remains equal.

An absorption ratio is also computed for each vertex of the mesh. The demand for oxygenated blood at a certain point is related to the amount of myocardial tissue near that point. This is incorporated in the simulation by relating the absorption coefficient at a vertex to the area of the myocardium on a slice perpendicular to the long axis of the heart and intersecting the corresponding vertex. While some degree of absorption is necessary to prevent the continuous accumulation of blood, experiments indicated that the distribution of the absorption coefficients is not a significant factor in the outcome of the computational simulation.

After the above values are precomputed, a constant flow of blood is set into the root node of the coronary artery tree. The three phases of the diffusion process are then iteratively executed, i.e., the diffusion from the coronary artery tree to the myocardial surface, the diffusion within the myocardial surface, and the absorption. The absorption phase consists of decreasing the amount of supply at each vertex of the myocardial surface by the absorption coefficient of that vertex. After a sufficient number of iterations, this process will converge to a stable state. The iterative process is then stopped. The amount of blood at each point in the myocardium in this stable state represents the amount of supply to that point. To retrieve additional information on which coronary artery is supplying which area, the entire diffusion process is performed separately for each of the three primary coronary arteries. This information can easily be combined to obtain global supply information. In the following part it is demonstrated how these quantities can be effectively visualized.

## 5.4 Visualization of Coronary Flow

The previously discussed model is simple, but sufficiently effective for the purposes of the approach presented here. This section demonstrates that the results of the computational simulation can be effectively visualized. The term effective here refers to being able to assess the effect of the coronary anatomy on the perfusion of the heart. This should be possible without detailed technical knowledge or understanding of the computational simulation. The latter requirement is essential for the viability of these techniques in clinical practice.

This section presents visualization methods that directly use the three-dimensional segmentation data to portray the results of the computational simulation as well as two-dimensional projections of these segmentations. First it is discussed how these projections are constructed. Second, the

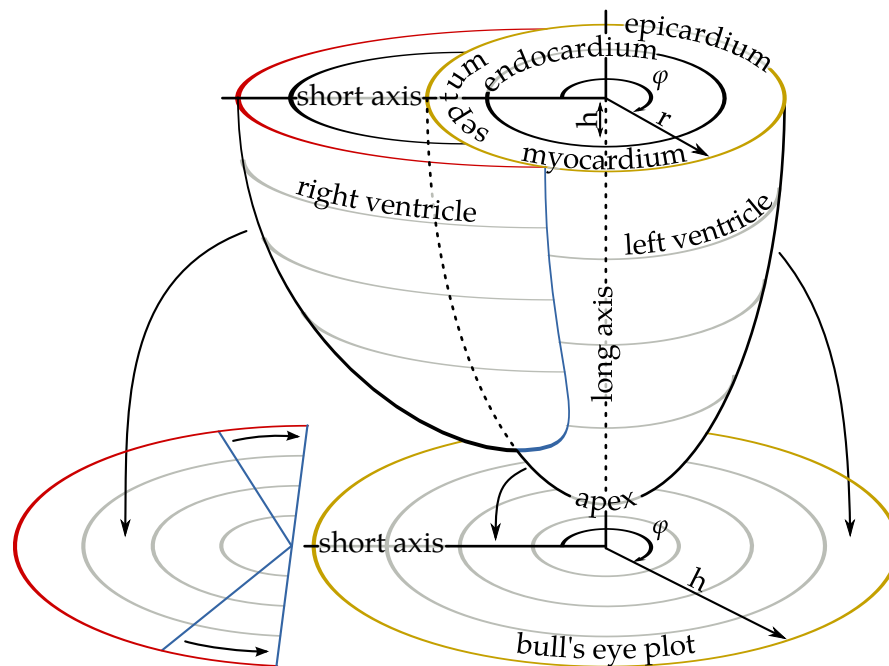


Figure 5.4: The parameterization of the left and right ventricle and the mapping to a bull's eye plot.

direct visualization of supply and underperfused regions using color, isocontours, and textures is demonstrated. Third, it is shown how the area each coronary artery is supplying can be visualized by using borders of the coronary artery territories. The supply area of each coronary artery can also be visualized separately. Finally the inverse of the latter is shown, i.e., finding the supplying coronary arteries of a region of interest.

### 5.4.1 Bull's Eye Plot Representation

The bull's eye plot is a visualization primitive that is commonly used in cardiac imaging. Its main goal is to provide a two-dimensional overview of the left ventricle and optionally the right ventricle. The classical approach to generate a bull's eye plot is to segment the myocardium in a stack of short-axis slices and map these segments to a set of concentric rings.

Here however a bull's eye plot is constructed as a continuous unfolding of the left ventricle along the long axis. The segmentation of the heart used is an unstructured grid of vertices along the epicardium. Each of these vertices can be represented by three parameters: the angle  $\varphi$  with the short axis on a plane perpendicular to the long axis, the distance  $h$  to the apex along the long axis, and the distance  $r$  to the long axis. This is illustrated in Figure 5.4. Any point can then be projected onto a cylinder

by interpreting this triplet as cylindrical coordinates. Since the surface will be projected onto a plane, it is not necessary to maintain the information provided by  $r$ . Therefore only  $\varphi$  and  $h$  are used as polar coordinates to form a circle.

The segmentation covers the entire left and right ventricles, including the top areas, near the bigger arteries and valves. These areas do not correspond to contracting myocardium and are not commonly part of a bull's eye plot. The small variation in  $h$  in these areas would also cause a cluttered projection. Therefore these top areas are not included in the bull's eye plot. The maximum value of  $h$  in the septum, the myocardial wall shared by the left and right ventricle, is used as a cut-off value. Any part of the heart with a larger distance to the apex than this threshold is not included in the projection.

Since the right ventricle is also part of the simulation, it should also be depicted in the bull's eye plot. While several approaches to visualize the right ventricle in a two-dimensional manner exist, the most common method is to represent it by a half circle. This approach is based on the idea that the right ventricle is essentially half of a left ventricle in shape. This representation is common in clinical practice [18].

To realize a half-circle unfolding, first the same parameterization is applied to the right ventricle as is done to the left ventricle. In the bull's eye plot the right ventricle is translated along the short axis to prevent overlap with the projection of the left ventricle. Next  $\varphi$  is normalized to the range  $[-\frac{1}{2}\pi; \frac{1}{2}\pi]$  to form a half circle. This step also eliminates any inter-patient shape variations of the right ventricle.

The orientation of the bull's eye plot that is used in clinical practice would correspond to a viewpoint from below the diagram looking upwards. This orientation is used whenever a separate bull's eye plot is shown. Compared to the projection below a three-dimensional view of the heart this orientation is vertically mirrored.

### 5.4.2 Blood Supply Area and Underperfused Regions

The primary outcome of the computational simulation is the blood supply present at each point in the myocardium. This is directly visualized using color coding, as can be seen in Figure 5.5. To avoid visual clutter due to too many colors, a light gray to dark red discrete color gradient is used. For additional insight in the structure of the supplying regions, isocontours are added as white dashed lines. These contours delineate borders where the supply of blood is equal. Finally a striped pattern is applied to the underperfused regions, i.e., regions where the supply is below a user-specified threshold.

Due to the simplicity of the computational simulation, the absolute values obtained may not correspond closely to reality. Currently it is

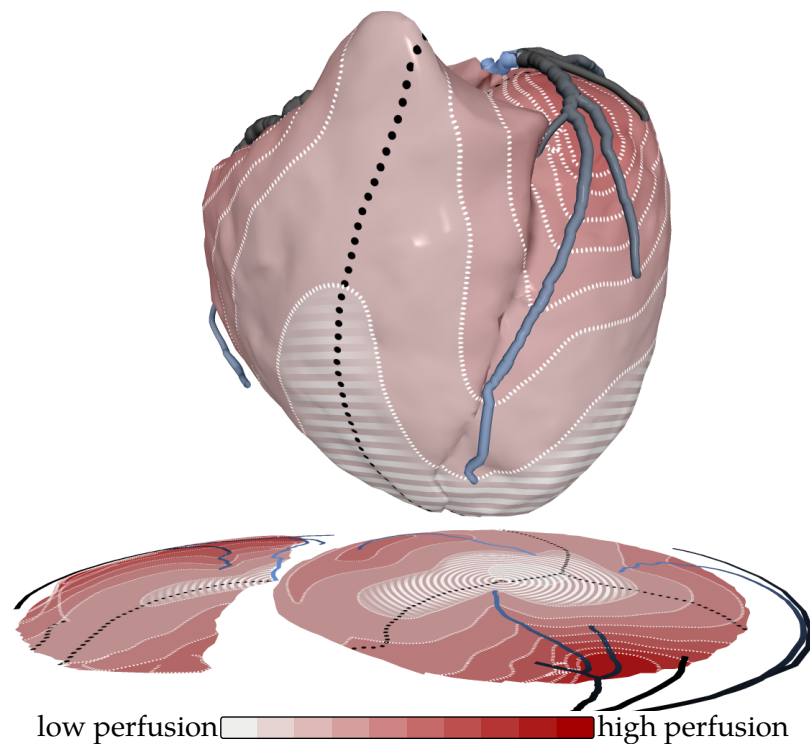


Figure 5.5: Visualization of coronary artery blood supply. The supply of blood is shown using color coding. Isocontours delineate regions of equal supply as white dashed lines. Lines indicating equal supply from multiple coronary arteries are shown as black dotted lines. Underperfused regions are represented by a striped pattern. Below the mesh, a two-dimensional projection shows the same data.

therefore not possible to define intervals that correspond to a healthy supply. This is solved by showing relative supply instead, which is based on the maximum supply in the simulation under analysis. In order to perceive both large and small differences in the distribution of blood throughout the myocardium, the data are logarithmically scaled prior to applying color coding and computing the isocontours. This eases the interpretation of the shape of regions with near-equal supply. The striped pattern provides a way of marking underperfused areas, i.e., areas where the supply of blood is below a predefined threshold. The borders of the pattern are made fuzzy, to indicate an area of uncertainty.

The striped pattern is implemented using  $h$ , the distance to the apex along the long axis. All parts where the fractional part of  $\delta \cdot h$  is larger than  $\frac{1}{2}$  are made opaque, the others transparent. The factor  $\delta$  controls the thickness of the stripes. This gives stripes perpendicular to the long axis in the three-dimensional view, and circles or arcs in the two-dimensional



projection. An advantage of this pattern is that it is rotation invariant. The orientation of the pattern is perceived equally throughout the entire mesh and the two-dimensional projection.

The coronary arteries are displayed in the three-dimensional view as well as on the bull's eye plot. In the three-dimensional view the coronary arteries are displayed as tubes with radii corresponding to the actual artery radii. In order to prevent intersections of the coronary arteries with the myocardium, parts of the coronary arteries are modified. These modifications are done only for visualization purposes. The computational simulation uses the original, unmodified coronary arteries. The coronary arteries are first projected onto the myocardium and subsequently translated a constant distance along the surface normal. This causes each coronary artery to have a constant distance to the myocardium. A black (high) to blue (low) color coding is applied to show the relative outflow at each point in the coronary artery tree.

The coronary arteries are also mapped onto the bull's eye plot using the same projection technique as described in Section 5.4.1. Whether a point along an artery should be mapped on the projection of the left or right ventricle is based on which ventricle it is closest to. The same color coding is applied showing relative outflow on the mapped coronary arteries.

### 5.4.3 Coronary Artery Territories

To gain insight which region each coronary artery is supplying, the coronary artery territories are visualized. The coronary arteries are divided into three groups: left anterior descending (LAD), left circumflex (LCX), and right coronary artery (RCA). This division is common in clinical practice and is also recommended by the AHA [14]. In the direct visualization of blood supply, the coronary territories are visualized by drawing black dotted lines along which the supply from two or more coronary arteries is equal according to the simulation. This is illustrated in Figure 5.5.

While visualizing the equi-perfusion lines already gives a good basic insight into the area each coronary artery group is supplying, these areas are not separated by discrete borders. Although there is generally little overlap in the coronary territories in practice, the simulation suggests that areas near the borders are supplied by multiple coronary artery groups. This is due to the diffusion approach. All details of how the coronary arteries supply the myocardium are not yet fully understood. We can thus also interpret the overlap generated by the simulation as an uncertainty of coronary territories. As is depicted in Figure 5.6, this is visualized by showing the full territory each coronary artery group is supplying in separate colors. Where these regions overlap, a striped two-color pattern is applied to indicate an uncertainty on which coronary artery groups are supplying this region. This striped pattern is implemented using the same

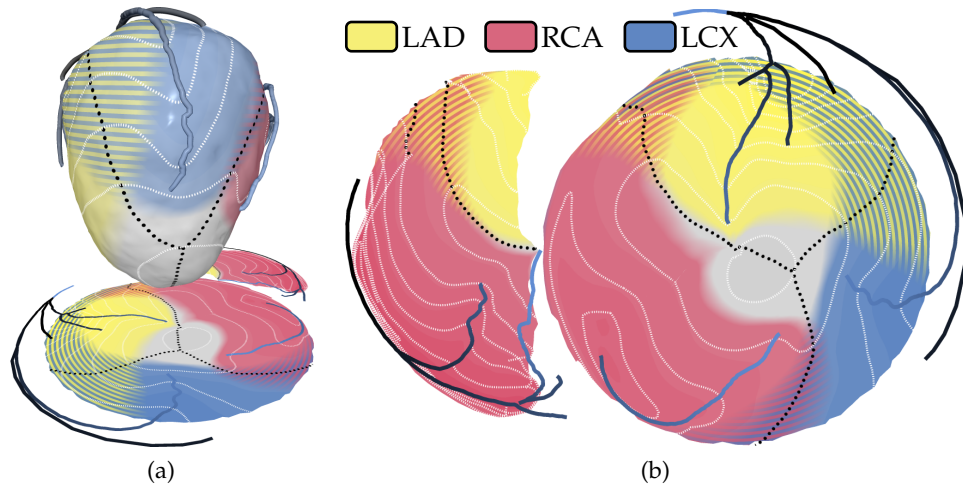


Figure 5.6: Individual coronary territories visualized using separate colors. A striped pattern with fuzzy borders is used in regions of uncertainty where the exact territory is unknown. Underperfused regions are not colored. The yellow territory corresponds to the LAD, the red territory corresponds to the RCA and the blue territory corresponds to the LCX.

approach as for the striped pattern to visualize underperfused regions. The border of the pattern is made fuzzy, to further emphasize an area of uncertainty.

The boundaries of each coronary territory are controlled by a user-specified threshold. If the supply from a coronary artery group in a certain location is above this threshold, that location is considered to be part of the respective coronary territory. Figure 5.6 shows that using this approach, the regions each coronary artery group is supplying as well as areas of uncertainty can be clearly identified.

#### 5.4.4 Separate Coronary Artery Territories

The computational simulation provides separate information on the supply for each coronary artery group. This allows for separate visualization of the blood supply by each group. It gives a focused view on the area a particular group is supplying.

Figure 5.7 shows an example of the separate visualization of coronary artery groups by showing four bull's eye plots. Figure 5.7a shows the supply of all three coronary artery groups combined, while Figures 5.7b, 5.7c and 5.7d show the supply of the LAD, LCX, and RCA, respectively. Due to the separation, more detailed visualization techniques can be applied than when visualizing the coronary territories in a combined fashion, as proposed in Section 5.4.3. A combined visualization of the coronary

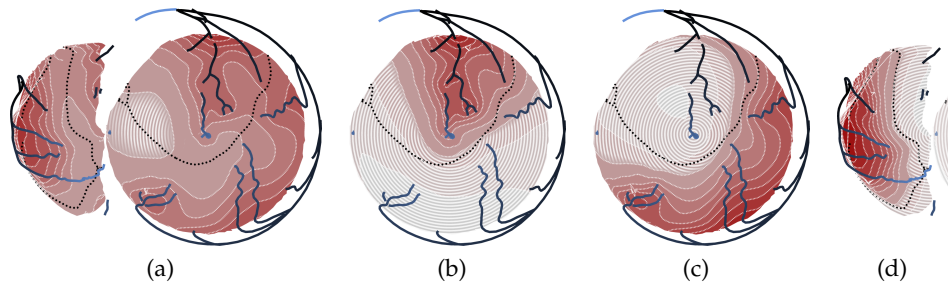


Figure 5.7: Separate visualization of the supply by each coronary territory group in two-dimensional bull's eye plots. Figure (a) shows the supply of the three groups combined; (b) shows the supply of the LAD; (c) shows the supply of the LCX; and (d) the supply of the RCA. Only the relevant ventricles are depicted.

territories allows for assessing the relation between them, while separate visualization allows for a more comprehensive analysis of a particular group.

Showing supply from coronary arteries separately benefits from the two-dimensional projection, as this allows for a quick comparison of the regions each coronary artery group is supplying. The ease of comparison argument holds for the bull's eye plot in general. Comparisons cannot be as easily performed using different viewpoints of the three-dimensional view. In the bull's eye plot the relation to the three-dimensional anatomy is however partially lost.

#### 5.4.5 Querying Supplying Coronary Arteries

The previously discussed techniques visualize the region each coronary artery group is supplying. The inverse can also be done, i.e., to visualize the coronary artery group that a region of interest is supplied by. This approach is demonstrated in Figure 5.8. The user indicates a region of interest by specifying a location on either the three-dimensional mesh or the bull's eye plot and a radius to determine the size of the region. Then the relative supply from each of the three coronary artery groups is computed. Again taking into consideration that there is minimal overlap between coronary territories in practice, this can be interpreted as the *likelihood* that the region is supplied by one or more arteries. Arrows are drawn from the closest point of each coronary artery group to the specified location of interest. The start and end point of each arrow are projected on a cylinder with the long axis as cylinder axis. Next the shortest path on the cylinder between these two points is projected back onto the myocardium. On the bull's eye plot a straight path is drawn between the two projected

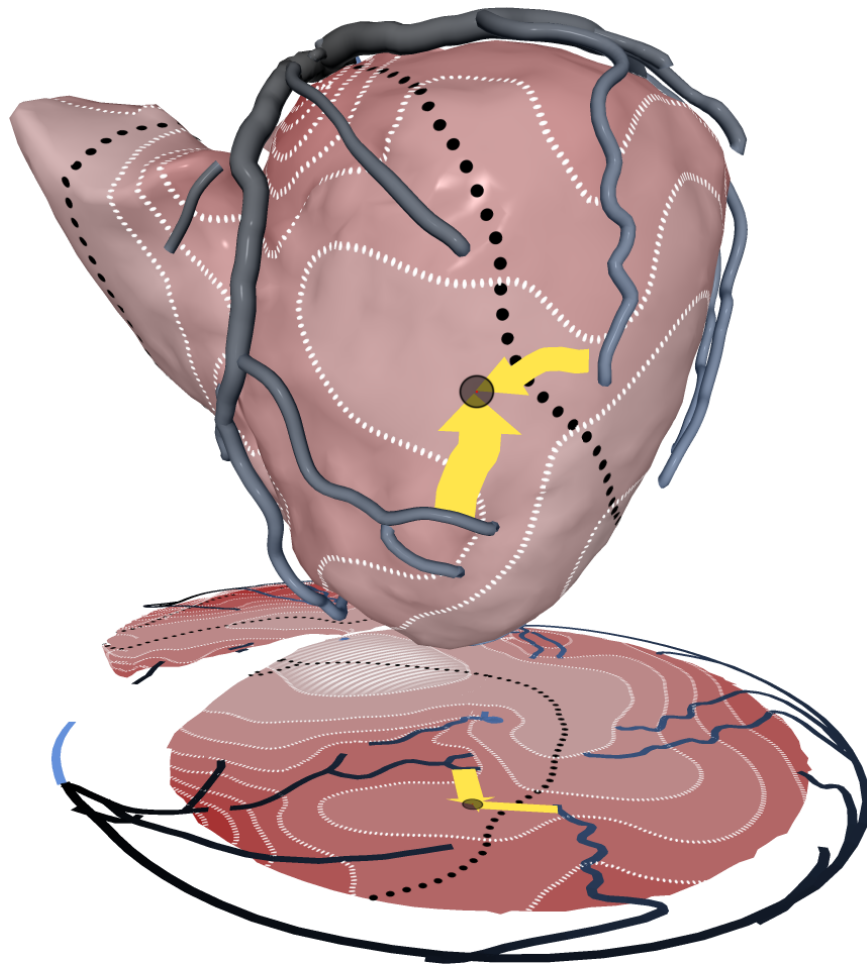


Figure 5.8: For a selected region arrows indicate the relative supply by, or likelihood of being supplied by, each of the three coronary artery groups. The relative supply is encoded in the width of the arrows.

points. The relative supply by each group is expressed in the width of each arrow.

This approach allows for a quick identification of the supplying coronary arteries in a visualization where this may not be directly apparent. An example is to query the supplying coronary arteries of an underperfused region in visualizations as discussed in Section 5.4.2.

## 5.5 Simulation and Visualization of a Stenosis

In order to evaluate the effectiveness of the previously described visualization techniques, an experiment was performed. Starting out with a

scan of a healthy subject, the coronary anatomy was visualized using the computational simulation and the proposed visualization techniques. Next a stenosis was artificially induced in one or more of the coronary arteries. Afterwards the change in the visualization of the coronary perfusion was observed.

The presented approach requires a whole heart scan of sufficient accuracy to allow a detailed segmentation of the coronary arteries with diameter measurements. CT currently provides better resolution than MRI, so the use of CT scans was chosen for the experiment. When MRI has advanced sufficiently to allow accurate segmentation of the coronary arteries, using MRI may be preferable over CT. MRI allows for the acquisition of additional data that show the functioning of the heart, which can lead to a more comprehensive diagnosis.

### 5.5.1 Supply and Underperfused Regions

A stenosis often causes a perfusion defect in the area normally supplied by the coronary artery that contains the stenosis. When simulating a stenosis, we would expect to observe this perfusion defect in the resulting visualizations. Figure 5.9 shows a comparison of a healthy case (Figure 5.9a) and the same case with an artificially induced stenosis blocking part of the upper LAD by approximately 70% (Figure 5.9b). This means that the cross-sectional area of the vessel has been locally decreased by 70%. Conforming to expectations, Figure 5.9b shows an increased underperfused region near the lower segment of the LAD. The shape of the isocontours also expresses the change in supply in the affected area. Note that Figure 5.9a shows an underperfused region in the basal septal wall, which is commonly not regarded as an indicator of CAD.

### 5.5.2 Coronary Artery Territories

A stenosis is also expected to change the shape of the territory of the respective coronary artery. Figure 5.10 compares the coronary artery territories of a normal case and the same case with an artificially induced stenosis in the RCA. In Figure 5.10b the severe reduction in size of the RCA territory can clearly be observed. Especially the posterior and septal parts of the left ventricle are affected. Note that the isocontours, representing the overall supply, have also somewhat changed in the other territories.

### 5.5.3 Querying Supplying Coronary Arteries

Finally, the effect of a stenosis can also be observed in the visualization of the supplying coronary arteries of a region of interest. Figure 5.11 compares a region of interest in a healthy case and a case with an artificially induced

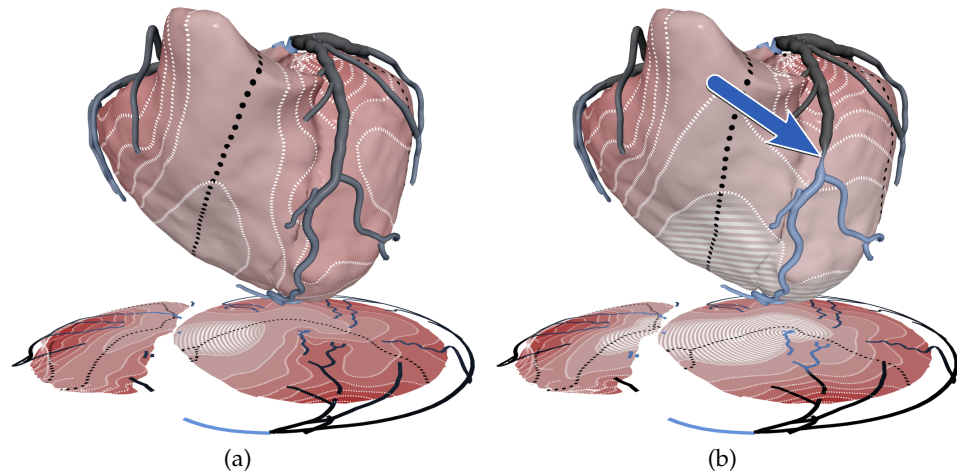


Figure 5.9: Comparison of supply between (a) a healthy case and (b) the same case with an artificially induced stenosis in the upper segments of the LAD indicated by the arrow.

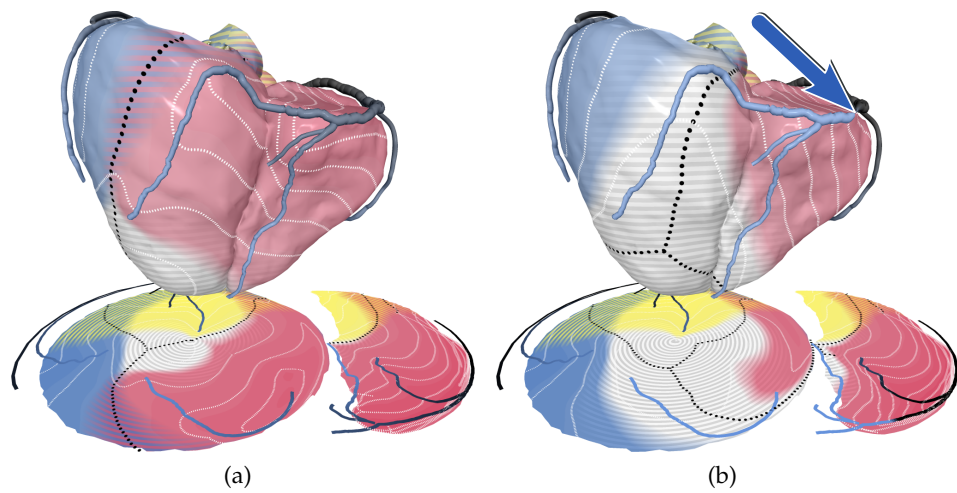


Figure 5.10: Comparison of the coronary territories between (a) a healthy case and (b) the same case with an artificially induced stenosis in the RCA indicated by the arrow.

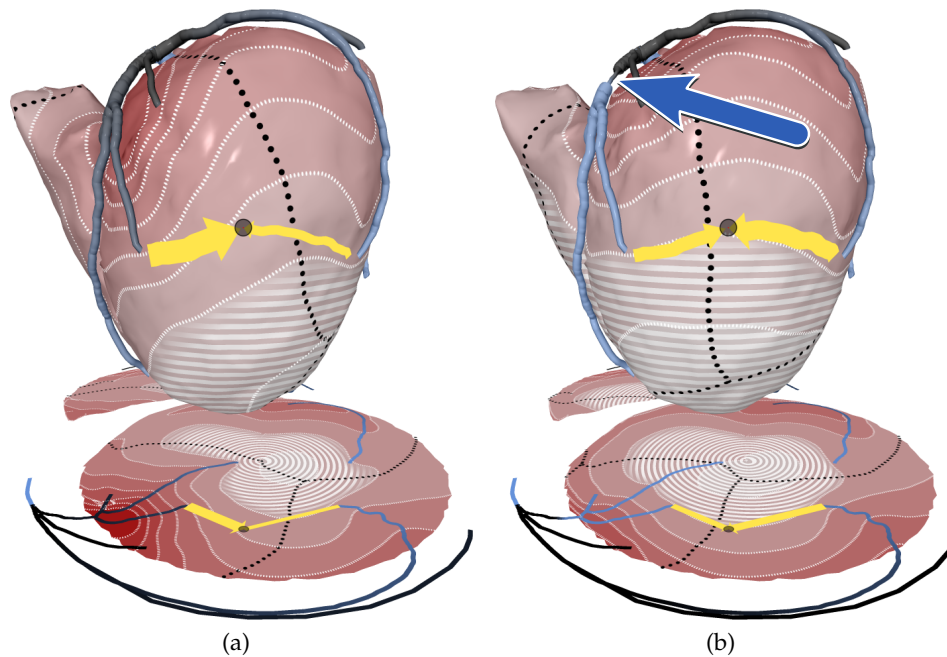


Figure 5.11: Comparison of supplying coronary arteries between (a) a healthy case (b) and the same case with an artificially induced stenosis in the LAD indicated by the arrow. The relative supply is encoded in the thickness of the arrows.

stenosis in the LAD. The region is primarily supplied by the LAD in the healthy case. It is primarily supplied by the LCX and lies at the border of an underperfused region in the stenosed case. Note that because the arrows encode *relative* supply, the thicker arrow from the LCX does not necessarily indicate an increase in supply.

## 5.6 Discussion

In current clinical practice the 17-segment model from the AHA is used as a reference for the relation between the coronary arteries and the myocardium. This model is not based on patient-specific information. In this work this model has been extended by including such information. Applying a computational simulation, a more detailed relation between the coronary arteries and the myocardium is obtained. While the presented simulation is primitive, it gives more detailed information than is currently available in medical practice. This approach can be seen as a top-down approach. There are more advanced approaches to compute myocardial



perfusion based on computational fluid dynamics which can be seen as a bottom-up approach.

In clinical practice a more advanced perfusion simulation is probably preferable. The presented simulation only uses a two-dimensional surface of the myocardium, does not take the dynamic nature of the heart cycle into account, and the perfusion method may not correspond close to reality. This can hamper correlating results to for example perfusion imaging, although the basic functionality is captured by this approach. In the experiments CT data was used since the approach requires a detailed coronary artery tree segmentation. When MRI advances enough to allow for more detailed imaging of the coronary arteries, additional scanning protocols can be used to provide a more comprehensive visualization of the patient.

### 5.6.1 Feedback from Expert Clinicians

In a discussion with two expert radiologists the clinical relevance of the various aspects of the visualizations was evaluated. Very positive feedback was received on the visualization of supply and underperfused regions. It displays the relevant data in a clear way. The black dotted lines give a good indication of the coronary territories, but could perhaps be annotated with uncertainty information and colored in case the relations to arteries are not obvious.

The detailed visualization of the coronary territories may be good for assessing the area at risk in more detail, but gives a less comprehensive view than the direct visualization of supply. One expert believes that for many cases this level of detail is not necessary. It may thus be worthwhile to integrate more of the coronary territory information in the visualization of supply such that a separate visualization thereof may no longer be necessary. The separate visualization of a single coronary territory provides a more focussed view, but similarly it may not be necessary for all patients. In Figure 5.7d it was not immediately obvious that a bull's eye plot of the right ventricle was shown instead of part of a left ventricular plot.

One expert was critical towards the approach of querying the supplying coronary arteries. He questions whether the cost of having to interact with a three-dimensional visualization would outweigh the limited additional information it provides. In summary, although both experts commented that the simulation may not be sufficiently realistic, positive feedback was received on the presented visualizations. One expert noted that they may also have potential for communication between doctor and patient.



### 5.6.2 Implementation Details

Both the left and right coronary arteries branch off from the aorta. The aorta is not part of the segmentation of the coronary artery tree, which is therefore not connected. In order to construct a tree with a single root node, the two subtrees of the left and right coronary arteries are connected with a building block from Figure 5.2b. No additional resistors are required in this area, as no significant flow out of the arteries takes place in the corresponding segments. Since typically also no flow out of the left main artery occurs, also this artery is modelled only using building blocks from Figure 5.2b at the bifurcations.

In the computational simulation only the two types of resistors  $R_{\text{through}}$  and  $R_{\text{out}}$  determine the distribution of blood throughout the coronary artery tree. The value of  $R_{\text{through}}$  is based on the local artery radius. For the value of  $R_{\text{out}}$  a manually specified constant is used instead of basing it on physical properties. This causes the supply in a region to be partially related to the amount of close-by vessels.

Practice showed perfusion defects near the apex in some cases. This is probably caused by an incomplete segmentation of the coronary arteries, mainly near the apex. The diameter of the coronary arteries decreases towards the apex, making segmentation in that area more difficult. The segmentations thus may contain shorter coronary arteries near the apex as compared to reality, which manifests itself as a perfusion defect in the simulations. Perfusion defects also tend to show up between two vessels, where the true perfusion situation, both in reality and in the simulation, is not fully understood.

In the experiments the triangle mesh of the myocardial surface was subdivided such that all triangles have an area of at most  $1\text{mm}^2$ . The resulting surface consists of about 35,000 triangles. The diffusion neighborhoods for the coronary artery tree and the myocardial surface are computed using a  $\sigma$  of 5 and 7, respectively. A kd-tree is used to compute the neighborhoods efficiently. For both diffusion processes an  $\epsilon$  of  $10^{-2}$  is used. Elements with a diffusion weight below this threshold are not included in the diffusion neighborhood. A value of  $R_{\text{out}}$  of  $10^3$  is used. The radius-based values of  $R_{\text{through}}$  typically vary between 0.1 and 4.5. With these parameters the diffusion process stabilizes after approximately 500 iterations.

All visualizations are implemented using OpenGL 2.0. All of the images were generated on a desktop PC (Intel Xeon 3 Ghz, 2 GiB RAM, NVIDIA GeForce 8800 GTX). The precomputation phase of the computational simulation takes approximately two seconds. Performing sufficient iterations until a stable state is obtained typically takes 15 to 20 seconds. All visualizations can be computed at interactive rates.

## 5.7 Summary and Conclusions

This chapter presented a computational simulation for the perfusion of blood throughout the myocardium and a set of visualization methods for the visual assessment of the results of these computations. The computational simulation computes the flow of blood through the coronary arteries using a network of resistors, while the successive distribution of blood is implemented using iterative convolution with a Gaussian kernel. This computational simulation advances on current clinical practice by including patient-specific information. It establishes a more advanced mapping between the myocardium and the coronary arteries based on perfusion. In contrast current approaches assume that each area is supplied by its closest coronary artery. The presented simulation produces sufficiently accurate results to demonstrate the effectiveness of the visualizations.

Comprehensive visualizations of the computed myocardial perfusion were presented. A direct visualization of blood supply was presented. Furthermore the coronary artery territories and the supplying coronary arteries of a region of interest were visualized. The computational simulation gives separate information on the supply from each coronary artery group. This demonstrates the advantages of a simulation approach, as this information is not commonly available from scanning technology. An example how these techniques visualize a stenosis was discussed by artificially inducing one.

Some of the presented techniques extend visualization primitives currently common in clinical practice, including the bull's eye plot. This approach simplifies the process of visually correlating the anatomical data to information from other imaging modalities and should ease clinical adoption. The work has been discussed with radiologists and the feedback received was overall very positive. The combination of two- and three-dimensional approaches provides a good blend between a clear overview and a detailed relation to the three-dimensional anatomy.

The only way to discover the limits of the possible is to go beyond them into the impossible.

---

Arthur C. Clarke

# 6

## Comprehensive Cardiac MRI Visualization

Coronary artery disease is often diagnosed using several different scanning protocols, including late enhancement, functional, and perfusion imaging, that each provide different information on the heart. Clinical workstations can provide a quantitative analysis of these data. In current clinical practice these data are analyzed sequentially or side-by-side, requiring them to be combined mentally. This chapter explores combining data from late enhancement, functional, and perfusion scans into a single visualization. One explicit example with specific techniques for each data type is discussed in detail. The types of scans made as well as the structure of the diagnostic process depend on the condition of the patient. How this information may be incorporated is briefly discussed. Several issues on how and when combined visualization should be applied are identified.

### 6.1 Introduction

**A**N MRI EXAM of a patient with suspected coronary artery disease often contains scans from different protocols that allow a quantitative analysis. During the diagnosis a clinician examines these scans sequentially, gradually expanding the amount of information known about the patient. Finally, all information is combined to form the final diagnosis. The fact that in the final diagnosis the quantitative data have to be combined seems to justify that the clinician should also be presented with a visualization where these data are combined. Due to the high concentration of information such a visualization may not be suitable for

acting as the primary representation of the quantitative data. It can however be of assistance by providing an overview of the previously analyzed data. The visualization can for example be gradually expanded during the diagnosis, adding information each time a scan has been analyzed. This approach supplies the clinician with an overview of the patient throughout the analysis process.

The protocols used in an MRI exam of a patient with suspected coronary artery disease depend on whether that patient is suspected to suffer from ischemia, acute infarction, chronic infarction, or heart failure. Once the scans are available, the order in which they are analyzed and what decisions they facilitate may differ. The latter process can be captured in a decision tree: a graph that holds a question in each node based on one type of scan and links to either decisions or follow-up questions. A visualization that aims to combine multiple scans should be aware of the diagnostic process and is therefore dependent on the disease type and accompanying decision trees. Previous chapters presented visualization techniques for only one type of quantitative data, optionally combined with anatomical information. This chapter explores the concept of combining multiple types of quantitative data in a single visualization.

This chapter is structured as follows. Section 6.2 provides an overview of typical scanning strategies and accompanying decision trees based on the type of disease a patient has. Section 6.3 discusses an example of how multiple types of quantitative data can be visualized in a combined fashion. Section 6.4 briefly discusses decision trees and how they could affect a combined visualization approach. Finally, Section 6.5 summarizes and concludes this chapter.

## 6.2 Medical Background

Coronary artery disease refers to a collection of diseases of the heart caused by a malfunctioning in the coronary artery circulatory system. The effect of such a malfunctioning can manifest itself in various ways. The following lists cases that are commonly distinguished and briefly mentions typical approaches to imaging them. Note that imaging approaches may vary due to the preference of the clinician, the history of the patient, or new developments in scanning technology.

**Ischemia** is a condition where part of the myocardium is not supplied by sufficient oxygenated blood to perform its function, but is still perfused well enough to remain viable. Often the symptoms of hampered function show up only under stress conditions, i.e., when the patient's heart rate is increased by pharmaceutical means.

Ischemia is primarily diagnosed through functional and perfusion scans. A functional scan of three to five short-axis slices at four to five different stress levels is made to assess the behavior of wall thickening as a function of stress. A perfusion scan of the same three to five short-axis slices at two stress levels (rest and stress) is used to compute the myocardial perfusion reserve index (MPRI). A single functional scan of 10 to 15 short-axis slices and a two- and four-chamber view of a single slice each at rest is used to compute the ejection fraction (EF), cardiac output (CO), and wall thickening (WT). Finally, a whole-heart scan visualizes the coronary arteries and is used to construct a whole-heart model.

**Acute infarction**, also called heart attack, refers to a sudden blockage of a coronary artery, resulting in part of the myocardium no longer receiving oxygenated blood and dying. This region is the area of infarction and the necrotic tissue is often called scar.

During diagnosis the location and size of the infarction is of primary concern, both of which can be observed in a late enhancement scan. Such a scan consists of 15 to 20 short-axis slices. Another important element during diagnosis is to assess the “area at risk,” regions that are not yet infarcted but are threatened by a lack of oxygen. This is often measured by a  $T_2$ -weighted scan. A similar functional scan as for ischemia provides information on the effect of the infarct on the functioning of the heart. Finally, a whole-heart scan shows the relation between the position of the coronary arteries and the infarcted area. Optionally, a perfusion scan can be made.

**Chronic infarction** refers to long-term presence of scar that has a significant effect on the functioning of the heart, but has since stabilized. This means that there typically is no “area at risk” to monitor, but only the development of the infarcted region itself is of interest. The amount of remaining viable tissue is also of importance. It is diagnosed with similar functional, late enhancement, and whole-heart scans as for acute infarction. A perfusion scan is normally not taken.

**Heart failure** is a collective term for a range of conditions including some that can be the end result of coronary artery disease or the long-term effects of an infarct. It is primarily diagnosed through a functional scan of 15 to 20 short-axis slices. Besides ejection fraction and cardiac output, also the synchronicity of the wall motion is of importance in analyzing this scan. A late enhancement scan provides information on the location and size of any remaining scar. The coronary arteries are of lesser importance, as the coronary artery branches previously involved in the infarct are commonly already known. A whole-heart

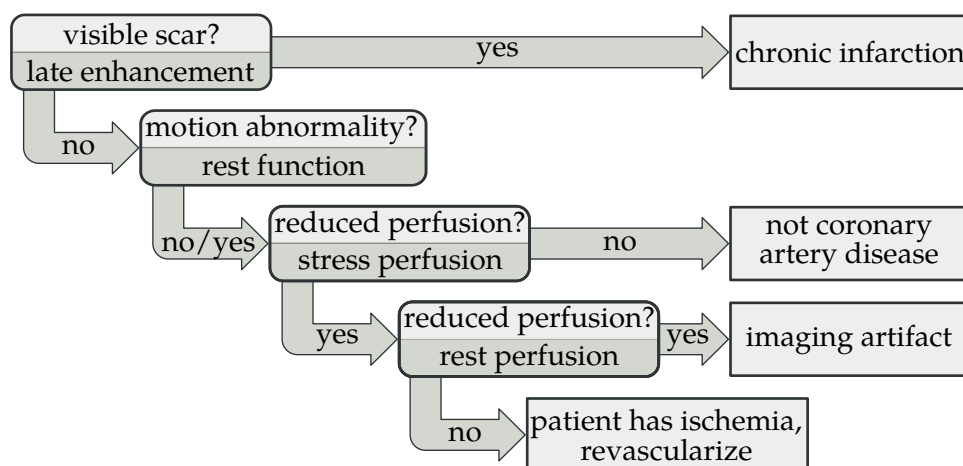


Figure 6.1: An example decision tree for a patient suspected to suffer from ischemia.

scan with contrast agent can visualize the coronary veins, which is useful for planning the placement of wires of a pacemaker.

Which scans physicians will make and in which order they will process them largely depends on the information already known about the condition of the patient. For example, when a patient has a known history of having one or more infarctions, that patient will be diagnosed as a chronic infarction case. There are however many cases in practice where the situation is unclear and the scanning approach used will depend on the experience of the clinician.

Closely related to the scanning protocols used for a particular patient are the decisions taken during the diagnosis based on these scans and the order in which these decisions are taken. A clinician in general answers a set of questions based on each piece of information to confirm respectively rule out a hypothesis. This set of questions contains a graph structure and can be grouped into a decision tree. Figure 6.1 gives an example of a decision tree for the case of ischemia. Many cases will however not fit perfectly to such a scheme, nor will the questions always lead to a binary decision. For the sake of simplicity the remainder of this chapter will ignore the latter issue and explore how data from multiple quantitative analyses can be effectively combined, incorporating knowledge of the decision tree.

### 6.3 Simultaneous Visualization of Multiple Quantitative Analyses

In order to provide a visualization intended to assist as an overview to the decision tree given in Figure 6.1, multiple quantities need to be visualized simultaneously. In previous work Oeltze *et al.* [61] visualize viability, functional, and perfusion data simultaneously. The perfusion data are visualized using glyphs that form an abstract representation of time-intensity curves. Scar is represented either as a colored surface inside a transparent myocardium or as isolines on the endocardium. Functional data are color-coded on the endocardium. While their visualization is three-dimensional, a viewing direction parallel to the long axis provides an image that looks similar to a bull's eye plot, at least concerning the perfusion data. Representing perfusion data as glyphs yields many possibilities, as several quantities can be extracted from the time-intensity curves. Oeltze *et al.* [63] previously explored this problem separately. Kuehnel *et al.* [43] integrated the analysis of coronary arteries and perfusion data, linking bull's eye plots and a three-dimensional visualization of the same data.

How viability, functional, and perfusion data should be combined for a particular disease type incorporating its associated decision tree is an interesting problem that has not yet been solved nor thoroughly explored. The remainder of this chapter presents one possible approach of combining these three types of data into a comprehensive visualization of a complete cardiac MRI exam of a patient. The presented approach uses texturing to represent scar, color coding to represent functional data, and glyphs to represent perfusion data. These data are mapped to both a three-dimensional mesh of the left ventricle and a bull's eye plot. The coronary arteries are rendered as polygonal tubes for additional anatomical context. An example result based on actual patient data is shown in Figure 6.2.

The visualization is built upon a segmentation of both the left and right ventricle extracted from a whole heart scan. These segmentations are part of the geometric heart model also presented in previous chapters. A non-iterative, feature-preserving mesh smoothing algorithm [37] is first applied to remove high frequency noise from the segmentation. The smoothed mesh is, besides being more aesthetic, less susceptible to cause distortions or occlusions when textures or glyphs are mapped to its surface.

In the following subsections the approach of adding information on viability, function, and perfusion to this visualization is discussed. As mentioned in Section 6.2, the various scanning protocols differ in resolution, some of which are too low to be considered continuous three-dimensional data. Furthermore, some quantitative analysis methods divide the myocardium in segments. In the visualization approaches discussed below an interpolation filter is applied to obtain continuous data. Interpolating

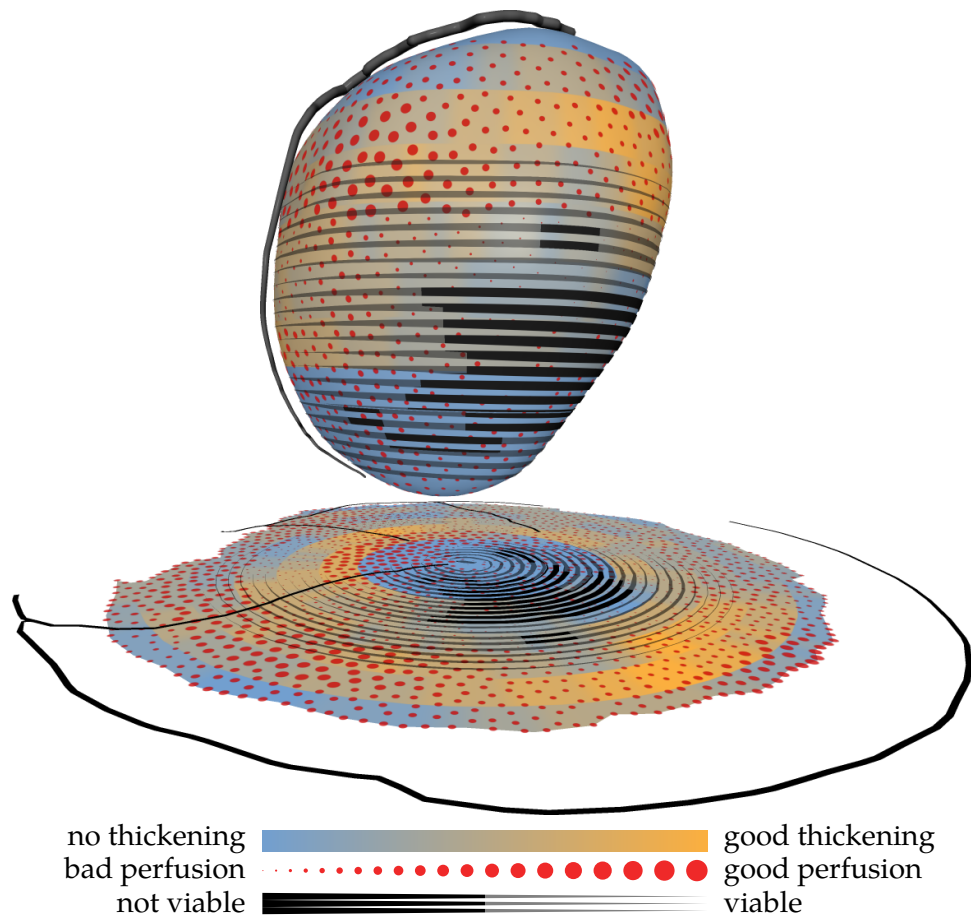


Figure 6.2: An example comprehensive cardiac MRI visualization showing three types of quantitative data simultaneously. Functional data (wall thickening) are shown as color coding, perfusion data (maximum upslope) are shown using glyphs of varying size, and scar is shown as a striped pattern overlay. The coronary artery centerlines are shown as polygonal tubes.



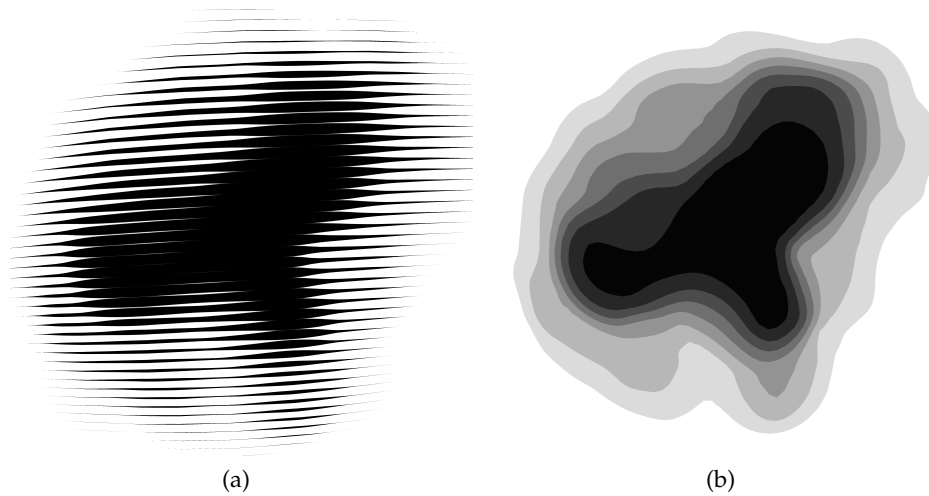


Figure 6.3: Scar represented by (a) a texture of stripes of varying thickness and (b) discrete color coding.

data between segments generally does not cause problems. Interpolating data between slices however conceals the resolution of the scan and the positions of the slices. Since this can be especially undesirable when a scan consists of very few slices, interpolation between slices is applied selectively.

### 6.3.1 Visualizing Viability using Textures

When analyzing viability data, the location, size, and transmuralty of scar are of importance. Scar is in essence dead tissue, so the functional and perfusion data of that area are of no importance since dead tissue does not contract nor is it perfused. Both the area directly surrounding scar as well as the healthy part of the myocardial wall in an area of non-transmural scar are however of great interest. These areas are common locations for hibernating myocardium, which may benefit from revascularization. The functional and perfusion data of those areas should thus not be occluded.

These observations lead to representing scar using a texture of black interleaving stripes, illustrated in Figure 6.3. The width of the stripes is based on the transmuralty of scar. This causes areas of transmural scar to be opaque black, occluding all other data. Areas with non-transmural scar are not fully occluded due to the screen-door effect of the texture. As opposed to using transparency, only part of the underlying data is exposed, but the colors of the visible areas are not influenced. Since in practice the underlying data have a lower resolution than the density of the stripes in the texture, no real information is occluded. Figures 6.3a and

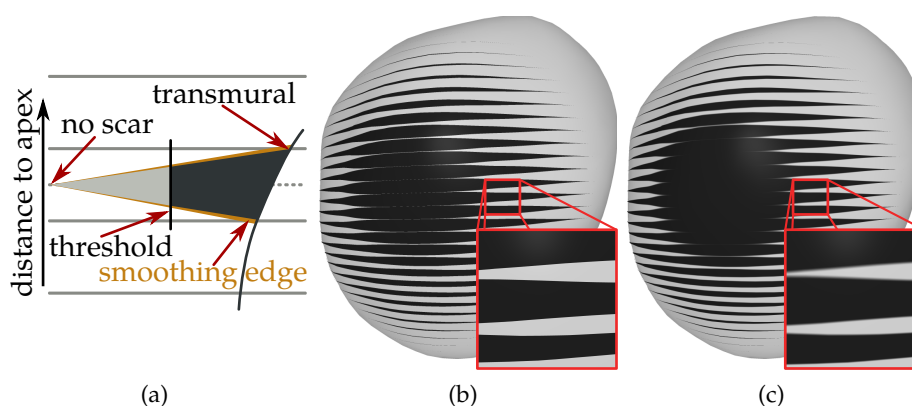


Figure 6.4: The width of the smoothing edge varies with the width of the edge itself. Parts of the texture where the width is below a threshold are rendered semi-transparently.

6.3b demonstrate the appearance of a patch of scar using the described texturing approach and color coding, respectively.

The edges of the stripes in the pattern are blurred to reduce the visibility of noise in areas of scar with a high transmurality. To avoid thickening stripes in areas where they are thin, the width of the blurred edge is proportional to the width of the stripe. This concept is demonstrated in Figure 6.4. This approach gives patches of transmural scar a more uniform appearance, while non-transmural areas feature less aliasing.

In clinical practice it is common to define a threshold for the percentage of scar, for example 50%, to make a distinction between still viable tissue and tissue that is considered dead. While the approach presented here provides a continuous visualization of scar, visualizing this threshold boundary provides a link to the traditional approach of classifying scar. It also improves quantitative perception possibilities of the visualization. The threshold is incorporated by reducing the transparency of the texture if the percentage of scar is below the predefined threshold. This is demonstrated in Figures 6.4 and 6.2 for a threshold of 50%.

### 6.3.2 Visualizing Function using Color Coding

The functional data are rendered on the epicardial surface using color coding. A color map consisting of two perceptually distinct colors is chosen to minimize visual clutter and avoid interference with the other data types. This color layer is rendered below the texture representing viability. To ensure that the visible color for a slice does not depend on the position of the stripes in the aforementioned texture, the function data are not interpolated between slices. The density of the stripes in the viability

texture are set higher than the density of slices in the functional scan. This ensures that the color coding of a particular slice is always visible behind an area of non-transmural scar.

### 6.3.3 Visualizing Perfusion using Glyphs

The perfusion data are visualized using glyphs. Since glyph-based visualizations can be difficult to understand, a simple two-dimensional glyph is chosen that is mapped onto the surface of the epicardium. The glyphs are rendered in a single, perceptually distinct color above the color coding of the functional data and below the texture pattern of the viability. A circle is used as the shape of the glyph, the area of which represents a single scalar value. The simplicity of the glyph comes at the price that only a single quantity can be expressed, while several quantities are typically extracted from the time-intensity curves of a perfusion scan. In the work of Oeltze *et al.* [61] an example of a more complex glyph is presented that captures more aspects of the time-intensity curves. In this work the glyph is not mapped onto the epicardial surface, but shown in rings around the myocardium. Meyer-Spradow *et al.* [53] presented a glyph-based visualization of SPECT data. They use torus-shaped glyphs on the surface of the myocardium. In the example shown in Figure 6.2 the maximum upslope parameter in the stress scan is mapped to the glyph area. Another suitable measure—that is often used in clinical practice—would be the myocardial perfusion reserve index, i.e., the ratio between the maximum upslope in the stress and rest scan.

The glyphs are evenly distributed throughout the surface, yet for aesthetic purposes not in a regular pattern. The desired number of glyphs is first randomly distributed on the centroids of the triangles of the epicardial mesh. A resulting distribution of glyphs after this phase is given in Figure 6.5a. Although this approach ensures a approximately uniform distribution of the glyphs throughout the surface, there is a high variance in the distance between the glyphs. This variation in distance largely depends on the shape of the triangle mesh.

To regularize the distance between glyphs, an iterative relaxation algorithm is applied similar to an approach presented by Turk [84]. For each glyph a repulsive force is defined that pushes away glyphs in a small neighborhood. The magnitude of the force between two glyphs decays proportionally to the distance between these glyphs to the third power. Figure 6.5b shows the result after 40 iterations of the relaxation algorithm, starting with the distribution of Figure 6.5a. The glyphs are clearly spaced more regularly.

The repulsive forces are based on the Euclidean distance between the edges of the glyphs. This results in a better distribution of glyphs of varying size, as demonstrated in Figure 6.5c. If the distance between the

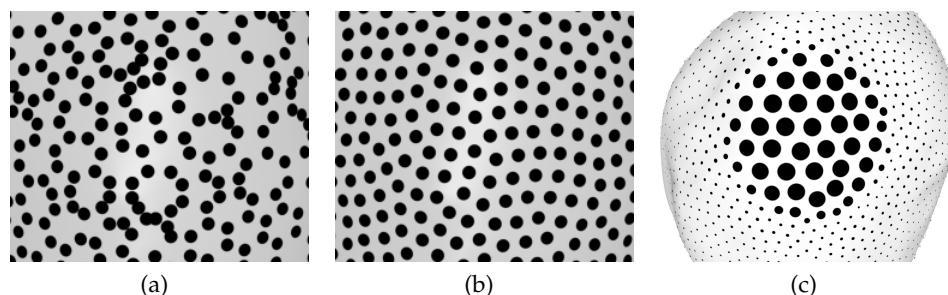


Figure 6.5: Glyph placement (a) randomly at the centroids of triangles and (b) after 40 iterations of a relaxation algorithm. (c) Glyphs are distributed so that the distances between the edges of the glyphs are equal.

centers of the glyphs were to be used, areas with small glyphs would either be covered more sparsely, or overlap would occur in areas with large glyphs. Since the neighborhoods used are relatively small, Euclidean distances suffice as an approximation of the geodesic distances.

## 6.4 Comprehensive Visualization using Decision Trees

The techniques discussed above can be used to construct a comprehensive visualization that shows viability, functional, and perfusion data simultaneously. Figure 6.2 gives an example of real patient data visualized using this approach. Late enhancement, functional, and perfusion scans were quantitatively analyzed using a Philips ViewForum clinical workstation. In this image the percentage of scar, wall thickening, and maximum upslope are chosen as parameters extracted from the late enhancement, functional, and perfusion scans, respectively.

How decision trees can be integrated into this approach has not yet been fully explored. When traversing a decision tree, the visualization could be gradually built up by adding additional information at each step. Each data type could also be visualized separately. An advantage of a combined visualization, as presented in Figure 6.2, is that it provides an improved and more intuitive spatial correlation between the data. Disadvantages compared to separate visualizations may include that the images are more difficult to interpret and may contain an overwhelming amount of information. Whether the advantages of a combined visualization outweigh its disadvantages is a question that has not yet been answered. Similarly it is not yet clear whether the same visualization primitives as in the combined visualization should be used in separate visualizations, if these two approaches were to be used simultaneously. Figure 6.6 provides a comparison of the visualization techniques used in this chapter to color

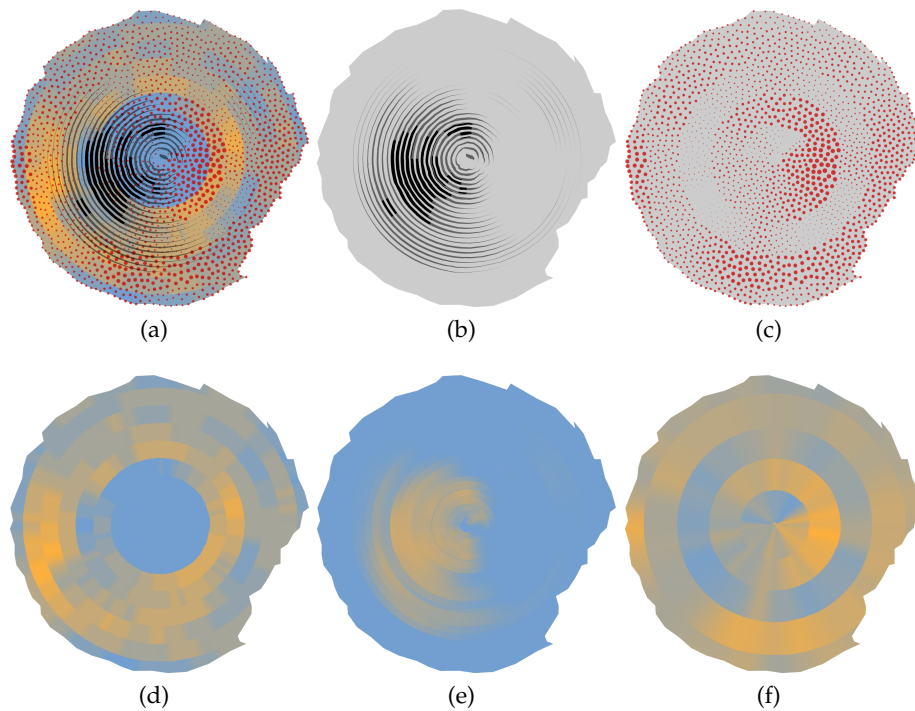


Figure 6.6: Comparison of combined and separately visualized parameters: (a) all data combined similar to Figure 6.2; (b) & (e) viability visualized using texture and color coding, respectively; (c) & (f) perfusion visualized using glyphs and color coding, respectively; (d) function visualized using color coding. The same legend applies as in Figure 6.2.

coding, both separately and combined. This is in turn related to the issue whether the quantitative perception properties of the chosen visualization primitives are adequate for the data they depict, for example the ability to judge whether some value is twice as high as another one. Concerning the integration of decision trees, it is interesting to know how sensitive the visualization is to changes in the decision trees. These issues have not yet been answered and are a suitable topic for future research in this area. Besides gaining insight in how different types of data should be combined, resolving these issues should also answer the more fundamental question whether it is at all desirable to present data in a combined fashion.

## 6.5 Summary and Remaining Challenges

This chapter presented an approach to visually integrate the results of a quantitative analysis of three different protocols of an MRI exam, specifically late enhancement, functional, and perfusion scans. An anatomical

model extracted from a whole heart scan is used to display viability, functional, and perfusion information simultaneously. While this visualization approach seems to provide a better spatial relation between the data, no evaluation of this approach has been performed yet.

The decision making process during a diagnosis was briefly described using decision trees. Incorporating decision trees into the visualization makes the visualization more applicable to cardiovascular diagnosis. By providing the clinician with visual feedback throughout the decision-making process, a better overview and correlation between the different data is provided. This awareness of the diagnostic process could eventually lead to a more efficient and more effective analysis. However, several questions remain open in the field how decision trees can be integrated in comprehensive visualizations as those presented in this chapter. Future research could address these issues, providing answers on how and when data should be combined visually.

I may not have gone where I intended to go, but I think I have ended up where I needed to be.

---

Douglas Adams



## Summary and Conclusions

CARDIAC MRI is a tomographic imaging technique suitable for the diagnosis of coronary artery disease [47, 19, 66, 69]. Its various scanning protocols can provide a comprehensive view of a patient's heart including information on anatomy, functioning, viability, and perfusion of the heart muscle tissue. This versatility, combined with its non-invasive nature and high resolution in both the spatial and temporal domains, make cardiac MRI an attractive alternative to other imaging modalities. The wealth of data supplied by cardiac MRI creates the need for efficient and effective analysis tools. Continuous advances in segmentation algorithms provide more accurate and less labour-intensive segmentations [20, 50, 29] that do not only facilitate a quantitative analysis of the data, but can also aid in constructing effective visualizations.

Visualization already plays an important role in analyzing the results of a cardiac MRI scan in clinical practice. The bull's eye plot is an example of a wide-spread visualization technique that can present the results of a quantitative analysis in a more approachable manner than for example a table with numbers. The graphical depiction of the results may allow for a faster assessment of the status of a patient. Due to the abstraction from the shape of the left ventricle, the relation to anatomy is lost, however. While bull's eye plots are used for late enhancement, functional, and perfusion scans, few visualization techniques are in use that draw relations between these scans.

In this thesis several novel visualization approaches were presented that build towards a comprehensive visualization of a patient that may assist in the diagnosis of coronary artery disease. Some common problems of current approaches were addressed, including the often limited relation

to the patient-specific anatomy and drawing relations between different scans. The comprehensive visualizations presented may also inspire the design of visualizations that are more suitable for patient briefing.

When assessing viability, the amount of scar, the transmurality of scar, and the amount of healthy remaining tissue are of importance. Common bull's eye plots depicting the percentage of scar or the transmurality of scar based on a late enhancement scan do not capture all of this information. The volumetric bull's eye plot addresses this issue with a novel concept to provide detailed information on the transmurality of scar, as well as the absolute amount of healthy remaining tissue. Furthermore continuity, three-dimensionality, and anatomical context are added. The additional information provides a more detailed view of the patients viability and may lead to a more accurate diagnosis. The familiarity with existing techniques should stimulate the clinical adoption of this technique.

A late enhancement scan measures an effect rather than the cause of coronary artery disease, yet a relation to the coronary arteries is often more difficult to make than it should be. This issue is addressed by the three-dimensional visualization of viability information in an anatomical context. It provides a better relation between scar and the coronary arteries. The three-dimensional myocardial anatomy provides information that is lost in abstract representations, including a bull's eye plot.

Coronary territories show the area of the myocardium that a branch of the coronary artery tree is supplying. They can provide a good relation between the coronary arteries and the myocardium in a bull's eye plot. While the use of coronary territories is common in clinical practice, most approaches are based on models relying on population averages. This issue was addressed by using the patient-specific coronary anatomy to compute the coronary territories. These territories can be superimposed on any bull's eye plot, not only those of viability data for which it has been demonstrated.

When the coronary arteries are imaged at a sufficiently high resolution to allow for segmentation with accurate diameter information, the visualization of simulated perfusion may provide an even more detailed relation between myocardium and coronary arteries. Ultimately, this data could be related to results of a real perfusion scan to increase confidence in the results of the simulation.

Late enhancement, function, and perfusion scans all provide information that has to be combined to form the final diagnosis. An example of how the results of a quantitative analysis of each of these scans can be combined in a single visualization was presented. While this visualization has the apparent advantage of a better spatial correlation between the data, the further implications of such comprehensive visualizations are not yet fully understood. This topic may therefore be suitable for future research.



Tell me what you need, and I'll  
tell you how to get along  
without it.

---

Dilbert



## Coronary Territory Questionnaire

### **Instructions for the participating medical expert**

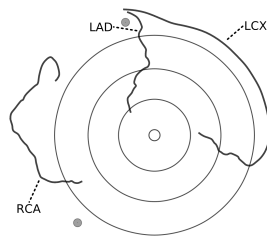
In each part of this questionnaire you are confronted with several bull's eye plots, each corresponding to a different patient. Two dots on the side of each bull's eye plot indicate the points where the right ventricle joins the left ventricle, which is generally on the left side of each bull's eye plot. The top of the bull's eye plot corresponds to the anterior part of the heart.

On each bull's eye plot, we have projected the paths of the three main coronary arteries and labeled them accordingly. The right coronary artery is labeled RCA, the left anterior descending artery is labeled LAD and the left circumflex artery is labeled LCX. Due to segmentation issues, the paths may not be complete.

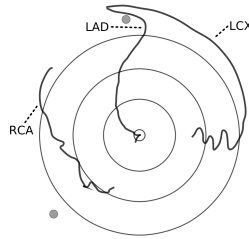
In the first part you will be asked to manually determine the coronary territories. In the second part the 17-segment model as defined by the American Heart Association is shown in each bull's eye plot. You are asked to judge the correspondence to the segmented coronary arteries on a scale from one (very bad) to five (very good). In the third part the 17-segment model is adapted using the patient-specific coronary anatomy and is subsequently shown in each bull's eye plot. You are again asked to give your opinion on the correspondence on a scale from one to five. In the fourth part the coronary territories are computed from the patient-specific coronary anatomy without forcing correspondence to the 17-segment model. You are again asked to give your opinion on the correspondence on a scale from one to five.

## A.1 Manually Defined Territories

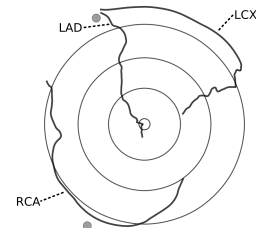
Below five blank bull's eye plots are shown with the three main coronary arteries projected on them. Each bull's eye plot corresponds to a different patient. Please divide each bull's eye plot into three parts by drawing the borders of the coronary territories. In other words, indicate the area that you expect to be supplied by each coronary artery.



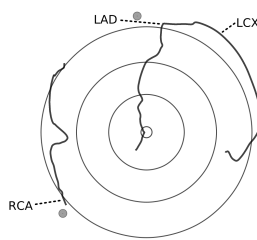
Patient 1



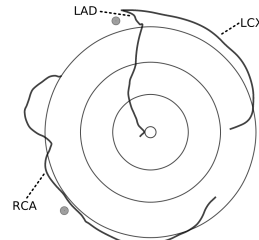
Patient 2



Patient 3



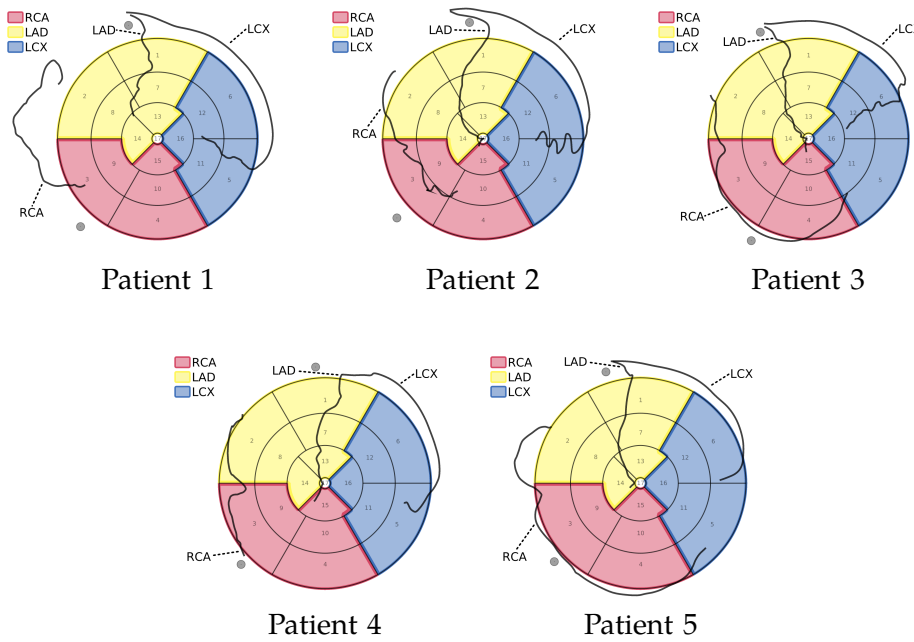
Patient 4



Patient 5

### A.2 Territories Based on the 17-Segment Model

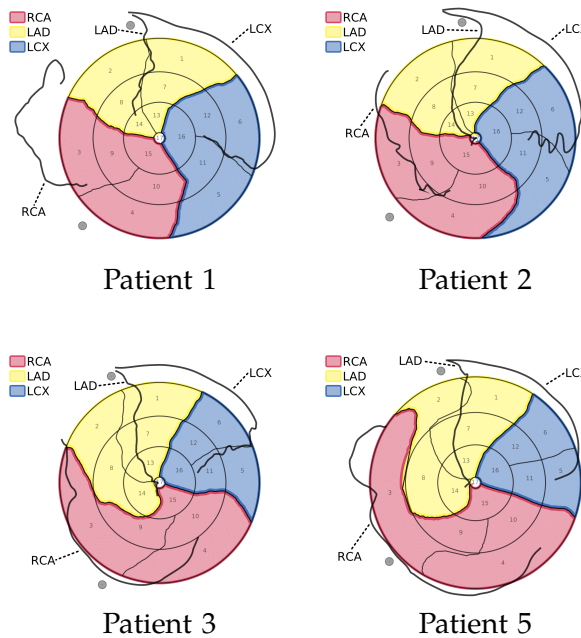
Below five bull's eye plots are shown, corresponding to the same patients as in the first part. In this part, the 17-segment model as defined by the American Heart Association is shown in each bull's eye plot. Your task is to judge the correspondence between the coronary territories as defined by the model and the patient-specific coronary anatomy. In other words, indicate how good you consider the assignment of segments of the myocardium to coronary arteries.



	1 (very bad)	2 (bad)	3 (moderate)	4 (good)	5 (very good)
Patient 1:					
Patient 2:					
Patient 3:					
Patient 4:					
Patient 5:					

### A.3 Territories Based on an Adapted 17-Segment Model

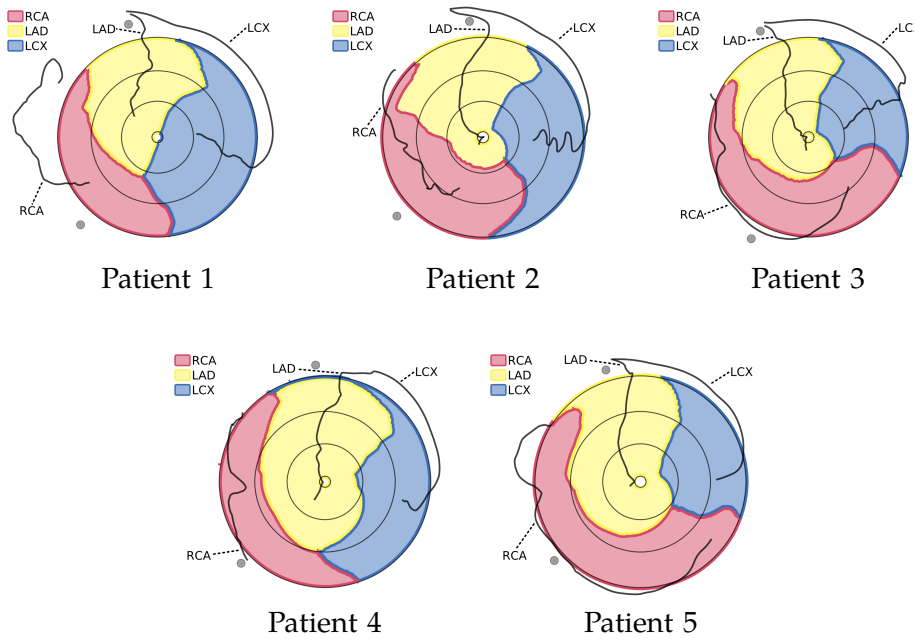
Below five bull's eye plots are shown, corresponding to the same patients as in the first two parts. In this part, the 17-segment model is adapted using the patient-specific coronary anatomy and is shown in each bull's eye plot. The topology of the coronary territories is forced to correspond to that of the 17-segment model. This is implemented by connecting the end of each coronary artery path to the apex. Your task is to judge the correspondence between the computed coronary territories and the patient-specific coronary anatomy. In other words, indicate how good you consider the assignment of segments of the myocardium to coronary arteries. This approach was not applied to patient 4. The coronary territories of this patient varied too much to force correspondence to the 17-segment model.



	1 (very bad)	2 (bad)	3 (moderate)	4 (good)	5 (very good)
Patient 1:					
Patient 2:					
Patient 3:					
Patient 5:					

### A.4 Territories Based on the Patient-Specific Coronary Anatomy

Below five bull’s eye plots are shown, corresponding to the same patients as in the first three parts. In this part, the coronary territories are computed using only the patient-specific coronary anatomy and are shown in each bull’s eye plot. No additional constraints were set to force correspondence to the 17-segment model. This approach allows for greater variation in shape and even allows for territories to be disjoint. An incomplete segmentation of an artery however has a greater impact on the shape of the territory. Your task is to judge the correspondence between the computed coronary territories and the patient-specific coronary anatomy. In other words, indicate how good you consider the assignment of segments of the myocardium to coronary arteries.



	1 (very bad)	2 (bad)	3 (moderate)	4 (good)	5 (very good)
Patient 1:					
Patient 2:					
Patient 3:					
Patient 4:					
Patient 5:					



## Bibliography

- [1] Stephan Achenbach and Werner G. Daniel. Noninvasive coronary angiography — an acceptable alternative? *New England Journal of Medicine*, 345(26):1909–1910, 2001. (Cited on page 7.)
- [2] Nidal Al-Saadi, Eike Nagel, Michael Gross, Axel Bornstedt, Bernhard Schnackenburg, Christoph Klein, Waldemar Klimek, Helmut Oswald, and Eckart Fleck. Noninvasive detection of myocardial ischemia from perfusion reserve based on cardiovascular magnetic resonance. *Circulation*, 101:1379–83, 2001. (Cited on page 11.)
- [3] American Society of Nuclear Cardiology. Imaging guidelines for nuclear cardiology procedures. *Journal of Nuclear Cardiology*, 6:G47–G48, 1999. (Cited on page 51.)
- [4] American Heart Association. Heart disease and stroke statistics — 2008 update. [www.americanheart.org](http://www.americanheart.org), 2008. Dallas TX, USA. (Cited on page 1.)
- [5] Pascale Beliveau, Randolph Setser, Farida Cheriet, and Thomas O'Donnell. Patient-specific coronary territory maps. *Proceedings of SPIE 2007*, 6511:65111J, 2007. (Cited on pages 52 and 69.)
- [6] Pascale Beliveau, Randolph M. Setser, Farida Cheriet, Richard D. White, and Thomas O'Donnell. Computation of coronary perfusion territories from CT angiography. *Computers in Cardiology*, 34:753–756, 2007. (Cited on pages 52 and 69.)
- [7] David Bessems. *On the propagation of pressure and flow waves through the patient-specific arterial system*. PhD thesis, Eindhoven University of Technology, 2007. (Cited on page 69.)
- [8] Jan Bogaert and Steven Dymarkowski. Delayed contrast-enhanced MRI: Use in myocardial viability assessment and other cardiac pathology. *European Radiology Supplements*, 15:52–58, 2005. (Cited on pages 10 and 15.)
- [9] René M. Botnar, Matthias Stuber, and Peter G. Danias. A fast 3D approach for coronary MRA. *Journal of Magnetic Resonance Imaging*, 10(5):821–825, 1999. (Cited on page 7.)

- [10] Evangelos Boutsianis, Dave Hitendu, Thomas Frauenfelder, Dimos Poulidakos, Simon Wildermuth, Marko Turina, Yiannis Ventikos, and Gregor Zund. Computational simulation of intracoronary flow based on real coronary geometry. *European Journal of Cardio-thoracic Surgery*, 26:248–256, 2004. (Cited on page 69.)
- [11] Marcel Breeuwer. Quantification of atherosclerotic heart disease with cardiac MRI. *MedicaMundi*, 49(2):30–38, 2005. (Cited on page 9.)
- [12] Marcel Breeuwer, Igno Paetsch, Eike Nagel, Raja Muthupillai, Scott Flamm, Sven Plein, and John P. Ridgway. The detection of normal, ischemic and infarcted myocardial tissue using MRI. In *Proceedings of International Congress and Exhibition on Computer Assisted Radiology and Surgery, CARS 2003*, volume 6, pages 1153–1158, 2003. (Cited on pages 10 and 13.)
- [13] Marcel Breeuwer, Marcel Quist, and Luuk J. Spreeuwers. Towards automatic quantitative analysis of cardiac MR perfusion images. In *Proceedings of International Congress and Exhibition on Computer Assisted Radiology and Surgery, CARS 2001*, pages 967–973, 2001. (Cited on page 11.)
- [14] Manuel D. Cerqueira, Neil J. Weissman, Vasken Dilsizian, Alice K. Jacobs, Sanjiv Kaul, Warren K. Laskey, Dudley J. Pennell, John A. Rumberger, Thomas Ryan, and Mario S. Verani. Standardized myocardial segmentation and nomenclature for tomographic imaging of the heart. *Circulation*, 105:539–542, 2002. (Cited on pages 17, 49, 50, 51, 69, and 79.)
- [15] Kelly M. Choi, Raymond J. Kim, George Gubernikoff, John D. Vargas, Michelle Parker, and Robert M. Judd. Transmural extent of acute myocardial infarction predicts long-term improvement in contractile function. *Circulation*, 104:1101–1107, 2001. (Cited on page 10.)
- [16] Alexandre Comte, Alain Lalande, Paul M. Walker, Alexandre Cochet, Louis Legrand, Yves Cottin, Jean-Eric Wolf, and François Brunotte. Visual estimation of the global myocardial extent of hyperenhancement on delayed contrast-enhanced MRI. *European Radiology*, 14:2182–2187, 2004. (Cited on page 10.)
- [17] Peter G. Danias, Arkadios Roussakis, and John P.A. Ioannidis. Diagnostic performance of coronary magnetic resonance angiography as compared against conventional X-ray angiography. *Journal of the American College of Cardiology*, 44:1867–1876, 2004. (Cited on page 7.)
- [18] E. Gordon DePuey, Margie E. Jones, and Ernest V. Garcia. Evaluation of right ventricular regional perfusion with technetium-99m-sestamibi



- SPECT. *Journal of Nuclear Medicine*, 32:1199–1205, 1991. (Cited on pages 69 and 77.)
- [19] James P. Earls, Vincent B. Ho, Thomas K. Foo, Ernesto Castillo, and Scott D. Flamm. Cardiac MRI: Recent progress and continued challenges. *Journal of Magnetic Resonance Imaging*, 16:111–127, 2002. (Cited on pages 6 and 101.)
- [20] Olivier Ecabert, Jochen Peters, and Jürgen Weese. Modeling shape variability for full heart segmentation in cardiac computed-tomography images. In *Proceedings of SPIE 2006*, volume 6144, pages 1199–1210, 2006. (Cited on pages 7, 13, 34, 36, 53, 70, 74, and 101.)
- [21] Alex Etienne, René M. Botnar, and Arianne M.C. van Muiswinkel. Soap-bubble visualization and quantitative analysis of 3D coronary magnetic resonance angiograms. *Magnetic Resonance in Medicine*, 48(4):658–666, 2002. (Cited on page 13.)
- [22] Cass Everitt. Interactive order-independent transparency. Technical report, NVIDIA Corporation, 2001. (Cited on page 37.)
- [23] Domenico Formica and Sergio Silvestri. Biological effects of exposure to magnetic resonance imaging: an overview. *BioMedical Engineering OnLine*, 3(11), 2004. (Cited on pages 5 and 6.)
- [24] Thomas Frauenfelder, Evangelos Boutsianis, Thomas Schertler, Lars Husmann, Sebastian Leschka, Dimos Poulidakos, Borut Marincek, and Hatem Alkadhi. In-vivo flow simulation in coronary arteries based on computed tomography datasets: feasibility and initial results. *European Radiology*, 17:1291–1300, 2007. (Cited on page 69.)
- [25] Y.C. Fung. *Biomechanics: Circulation*. Springer, 1996. (Cited on page 72.)
- [26] Mark G. Gunning, Constantinos Anagnostopoulos, Charles J. Knight, John Pepper, Elisabeth D. Burman, Glyn Davies, Kim M. Fox, Dudley J. Pennell, Peter J. Ell, and S. Richard Underwood. Comparison of 201-Tl, 99mTc-tetrofosmin and dobutamine magnetic resonance imaging for identifying hibernating myocardium. *Circulation*, 98:1869–1874, 1998. (Cited on page 13.)
- [27] Matthias Gutberlet, Ralph Noeske, Kerstin Schwinge, Patrick Freyhardt, Roland Felix, and Thoralf Niendorf. Comprehensive cardiac magnetic resonance imaging at 3.0 Tesla: Feasibility and implications for clinical applications. *Investigative Radiology*, 41(2):154–167, 2006. (Cited on page 5.)

- [28] Markus Hadwiger, Christoph Berger, and Helwig Hauser. High-quality two-level volume rendering of segmented data sets on consumer graphics hardware. In *Proceedings of IEEE Visualization 2003*, pages 301–308, 2003. (Cited on page 35.)
- [29] Gilion Hautvast, Steven Lobregt, Marcel Breeuwer, and Frans Gerritsen. Automatic contour propagation in cine cardiac magnetic resonance images. *Transactions on Medical Imaging*, 25(11):1472–1482, 2006. (Cited on pages 9 and 101.)
- [30] Anja Hennemuth, Sam Behrens, Caroline Kuehnel, Steffen Oeltze, Olaf Konrad, and Heinz-Otto Peitgen. Novel methods for parameter based analysis of myocardial tissue in MR-images. In *Proceedings of SPIE 2007*, volume 6511, pages 65111N–1–65111N–9, 2007. (Cited on pages 13 and 69.)
- [31] Anja Hennemuth, Achim Seeger, Ola Friman, Stephan Miller, Bernhard Klumpp, Steffen Oeltze, and Heinz-Otto Peitgen. A comprehensive approach to the analysis of contrast enhanced cardiac MR images. *Transactions on Medical Imaging*, 27(11):1592–1610, 2008. (Cited on page 13.)
- [32] Denis Hoa, Antoine Micheau, and Gerald Gahide. MRI step by step. <http://e-mri.com>, 2005. (Cited on page 5.)
- [33] Udo Hoffmann, Maros Ferencik, Ricardo C. Cury, and Antonio J. Pena. Coronary CT angiography. *Journal of Nuclear Medicine*, 47(5):797–806, 2006. (Cited on page 7.)
- [34] Joseph P. Hornak. The basics of MRI. <http://www.cis.rit.edu/htbooks/mri/>, 2006. (Cited on page 5.)
- [35] Nanaka Ishida, Hajime Sakuma, Munenobu Motoyasu, Tsutomu Okinaka, Naoki Isaka, Takeshi Nakano, and Kan Takeda. Noninfarcted myocardium: Correlation between dynamic first-pass contrast-enhanced myocardial MR imaging and quantitative coronary angiography. *Radiology*, 229(1):209–216, 2003. (Cited on page 11.)
- [36] Timothy Johnson, Dennis Kirch, and Bruce Hasegawa. A concentric polar display technique for emission cardiac tomography analysis (abstract). *Medical Physiology*, 8:567, 1981. (Cited on page 17.)
- [37] Thouis R. Jones, Frédo Durand, and Mathieu Desbrun. Non-iterative, feature-preserving mesh smoothing. In *Proceedings of SIGGRAPH 2003*, pages 943–949. ACM Press, 2003. (Cited on pages 37 and 93.)

- [38] Hong Jung, Jaeheung Yoo, and Jong Chul Ye. Generalized k-t BLAST and k-t SENSE using FOCUSS. In *Proceedings Biomedical Imaging: from nano to macro*, pages 145–148, 2007. (Cited on page 7.)
- [39] Armin Kanitsar, Dominik Fleischmann, Rainer Wegenkittl, Petr Felkel, and Eduard Gröller. CPR - Curved Planar Reformation. In *IEEE Visualization*, pages 37–44, 2002. (Cited on pages 13, 36, 40, and 69.)
- [40] Rufold Karch, Friederike Neumann, Martin Neumann, Paul Szawlowski, and Wolfgang Schreiner. Voronoi polyhedra analysis of optimized arterial tree models. *Annals of Biomedical Engineering*, 31:548–563, 2003. (Cited on page 52.)
- [41] Young Jin Kim, Jae-Seung Seo, Byoung Wook Choi, Kyu Ok Choe, Yangsoo Jang, and Young-Guk Ko. Feasibility and diagnostic accuracy of whole heart coronary MR angiography using free-breathing 3D balanced turbo-field-echo with SENSE and the half-fourier acquisition technique. *Korean Journal of Radiology*, 7:235–242, 2006. (Cited on pages 7 and 39.)
- [42] Arunark Kolipaka, George P. Chatzimavroudis, Richard D. White, Thomas P. O'Donnell, and Randolph M. Setser. Segmentation of non-viable myocardium in delayed enhancement magnetic resonance images. *The International Journal of Cardiovascular Imaging*, 21:303–311, 2005. (Cited on page 10.)
- [43] Caroline Kuehnel, Anja Hennemuth, Susanne Bock, Steffen Oeltze, Tobias Boskamp, Stefan Krass, Bernhard Preim, and Heinz-Otto Peitgen. New software assistants for cardiovascular diagnosis. In *GI-Workshop "Softwareassistenten - Computerunterstützung für die medizinische Diagnose und Therapieplanung" within the GI annual conference*, pages 491–498, 2006. (Cited on pages 19, 69, and 93.)
- [44] Dirkjan Kuijpers. Diagnosis of coronary artery disease with dobutamine-stress MRI. *European Radiology Supplements*, 15(0):B48–51, 2005. (Cited on page 9.)
- [45] C. De Lazzari, M.G. Trivella, M. Micalizzi, F. Bernini, M. Varanini, G. Ferrari, A. Macerata, D. Neglia, and A. L'Abbate. Coronary blood flow: Comparison between in vivo and numerical simulation data. *Computers in Cardiology*, 33:881–884, 2006. (Cited on page 69.)
- [46] Marc Levoy. Display of surfaces from volume data. *IEEE Computer Graphics and Applications*, 8(3):29–37, 1988. (Cited on pages 24 and 37.)
- [47] Martin J. Lipton, Jan Bogaert, and Larry M. Buxt. Imaging of ischemic heart disease. *European Radiology*, 12:1061–1080, 2002. (Cited on pages 6, 8, and 101.)

- [48] Charles Loop. Smooth subdivision surfaces based on triangles. Master's thesis, University of Utah, 1987. (Cited on page 74.)
- [49] William E. Lorensen and Harvey E. Cline. Marching cubes: A high resolution 3D surface construction algorithm. In *Proceedings of SIGGRAPH 1987*, pages 163–169, 1987. (Cited on page 55.)
- [50] Cristian Lorenz, Steffen Renisch, Thorsten Schlathoelter, and Thomas Buelow. Simultaneous segmentation and tree reconstruction of the coronary arteries in MSCT images. In *Proceedings of SPIE 2003*, volume 5031, pages 167–177, 2003. (Cited on pages 13, 21, 53, 70, and 101.)
- [51] Cristian Lorenz and Jens von Berg. A comprehensive shape model of the heart. *Medical Image Analysis*, 10:657–670, 2006. (Cited on page 34.)
- [52] Edward T. Martin, James A. Coman, Frank G. Shellock, Christopher C. Pulling, Robert Fair, and Kim Jenkins. Magnetic resonance imaging and cardiac pacemaker safety at 1.5-Tesla. *Journal of the American College of Cardiology*, 43(7):1315–1324, 2004. (Cited on page 6.)
- [53] Jennis Meyer-Spradow, Lars Stegger, Christian Döring, Timo Ropinski, and Klaus Hinrichs. Glyph-based SPECT visualization for the diagnosis of coronary artery disease. *IEEE Transactions on Visualization and Computer Graphics*, 14(6):1499–1506, 2008. (Cited on page 97.)
- [54] Eike Nagel and Eckart Fleck. Functional MRI in ischemic heart disease based on detection of contraction abnormalities. *Journal of Magnetic Resonance Imaging*, 10(3):411–417, 1999. (Cited on page 8.)
- [55] Eike Nagel, Christoph Klein, Ingo Paetsch, Sabine Hettwer, Bernhard Schnackenburg, Karl Wegscheider, and Eckart Fleck. Magnetic resonance perfusion measurements for the noninvasive detection of coronary artery disease. *Circulation*, 108:432–437, 2003. (Cited on pages 7, 11, and 12.)
- [56] Eike Nagel, Hans B. Lehmkuhl, Wolfgang Bocksch, Christoph Klein, Uta Vogel, Eckart Frantz, Axel Ellmer, Stefan Dreysse, and Eckart Fleck. Noninvasive diagnosis of ischemia-induced wall motion abnormalities with the use of high-dose dobutamine stress MRI. *Circulation*, 99:763–770, 1999. (Cited on page 8.)
- [57] Takeshi Nakaura, Daisuke Utsunomiya, Shinya Shiraishi, Seiji Tomiguchi, Tsuyoshi Honda, Hisao Ogawa, Kazuo Awai, and Yasuyuki Yamashita. Three-dimensional cardiac image fusion using new CT angiography and SPECT methods. *American Journal of Roentgenology*, 185:1554–1557, 2005. (Cited on page 70.)

- [58] Krishna S. Nayak, Charles H. Cunningham, and Juan M. Santos. Real-time cardiac MRI at 3 Tesla. *Magnetic Resonance in Medicine*, 51:655–660, 2004. (Cited on page 5.)
- [59] Nicholas M.I. Noble, Derek L.G. Hill, Marcel Breeuwer, and Reza Razavi. The automatic identification of hibernating myocardium. In *MICCAI*, volume 0, pages 890–898, 2004. (Cited on pages 13, 18, 34, 35, and 69.)
- [60] Steffen Oeltze, Helmut Doleisch, Helwig Hauser, Philipp Muigg, and Bernhard Preim. Interactive visual analysis of perfusion data. In *Proceedings of IEEE Visualization 2007*, 2007. (Cited on page 69.)
- [61] Steffen Oeltze, Anja Hennemuth, Sylvia Glaßer, Caroline Kühnel, and Bernhard Preim. Glyph-based visualization of myocardial perfusion data and enhancement with contractility and viability information. In *Proceedings of Visual Computing for Biomedicine 2008*, 2008. (Cited on pages 93 and 97.)
- [62] Steffen Oeltze, Anja Kuß, Frank Grothues, Anja Hennemuth, and Bernhard Preim. Integrated visualization of morphologic and perfusion data for the analysis of coronary artery disease. In *Proceedings of EuroVis 2006*, pages 131–138, 2006. (Cited on pages 19, 34, 35, 52, and 70.)
- [63] Steffen Oeltze, Arvid Malyszczuk, and Bernhard Preim. Intuitive mapping of perfusion parameters to glyph shape. In *Bildverarbeitung für die Medizin*, pages 262–266, 2008. (Cited on page 93.)
- [64] José T. Ortiz-Pérez, José Rodríguez, Sheridan N. Meyers, Daniel C. Lee, Charles Davidson, and Edwin Wu. Correspondence between the 17-segment model and coronary arterial anatomy using contrast-enhanced cardiac magnetic resonance imaging. *JACC: Cardiovascular Imaging*, 1(3):282–293, 2008. (Cited on pages 17, 52, 60, 64, and 69.)
- [65] Osvaldo Pereztol-Valdés, Jaume Candell-Riera, César Santana-Boado, Juan Angel, Santiago Aguadé-Bruix, Joan Castell-Conesa, Ernest V. Garcia, and Jordi Soler-Soler. Correspondence between left ventricular 17 myocardial segments and coronary arteries. *European Heart Journal*, 26:2637–2643, 2005. (Cited on pages 17, 51, 60, 63, and 69.)
- [66] Roderic I. Pettigrew, John N. Oshinski, George Chatzimavroudis, and W. Thomas Dixon. MRI techniques for cardiovascular imaging. *Journal of Magnetic Resonance Imaging*, 10:590–601, 1999. (Cited on pages 6 and 101.)
- [67] Guillem Pons-Llado. Assessment of cardiac function by CMR. *European Radiology Supplements*, 15(2):23–31, 2005. (Cited on page 9.)

- [68] Sandra Pujadas, Gautham P. Reddy, Oliver Weber, Jennifer J. Lee, and Charles B. Higgins. MR imaging assessment of cardiac function. *Journal of Magnetic Resonance Imaging*, 19:789–799, 2004. (Cited on page 8.)
- [69] Scott B. Reeder, Yiping P. Du, Joao A. C. Lima, and David A. Bluemke. Advanced cardiac MR imaging of ischemic heart disease. *Radiographics*, 21:1047–1074, 2001. (Cited on pages 6 and 101.)
- [70] Georgios Sakas, Marcus Grimm, and Alexandros Savopoulos. Optimized maximum intensity projection. In *Workshop on Rendering Techniques*, pages 51–63, 1995. (Cited on pages 36 and 39.)
- [71] Hajime Sakuma, Yasutaka Ichikawa, Shuji Chino, Tadanori Hirano, Katsutoshi Makino, and Kan Takeda. Detection of coronary artery stenosis with whole-heart coronary magnetic resonance angiography. *Journal of the American College of Cardiology*, 48:1946–1950, 2006. (Cited on page 7.)
- [72] Juerg Schwitter, Daniel Nanz, Stefan Kneifel, Katharina Bertschinger, Martin Büchi, Patrick R. Knüsel, Borut Marincek, Thomas F. Lüscher, and Gustav K. von Schulthess. Assessment of myocardial perfusion in coronary artery disease by magnetic resonance. *Circulation*, 103:2230–2235, 2001. (Cited on page 11.)
- [73] Susan Standring, editor. *Anatomy of the Human Body*. Elsevier/Churchill Livingstone, 1918. (Cited on pages 2 and 3.)
- [74] Matúš Straka, Michal Červeňanský, Alexandra La Cruz, Arnold Köchl, Miloš Šrámek, Eduard Gröller, and Dominik Fleischmann. The VesselGlyph: Focus & context visualization in CT-angiography. In *Proceedings of IEEE Visualization 2004*, pages 385–392, 2004. (Cited on page 40.)
- [75] Maurice Termeer, Javier Oliván Bescós, Marcel Breeuwer, Anna Vilanova, Frans Gerritsen, Meister Eduard Gröller, and Eike Nagel. Patient-specific mappings between myocardial and coronary anatomy. Technical report, Institute of Computer Graphics and Algorithms, Vienna University of Technology, Favoritenstrasse 9-11/186, A-1040 Vienna, Austria, 2008. (Cited on page 14.)
- [76] Maurice Termeer, Javier Oliván Bescós, and Alexandru Telea. Preserving sharp edges with volume clipping. In *Proceedings of Vision, Modeling and Visualization 2006*, pages 341–348, 2006. (Cited on page 37.)
- [77] Maurice Termeer, Javier Oliván Bescós, Marcel Breeuwer, Anna Vilanova, Frans Gerritsen, and Eduard Gröller. The volumetric bull’s

- eye plot. Poster at SCMR 11<sup>th</sup> annual scientific sessions, 2008. (Cited on page 14.)
- [78] Maurice Termeer, Javier Oliván Bescós, Marcel Breeuwer, Anna Vilanova, Frans Gerritsen, Eduard Gröller, and Eike Nagel. Patient-specific coronary artery supply territory AHA diagrams. Poster at SCMR 12<sup>th</sup> annual scientific sessions, 2009. (Cited on page 14.)
- [79] Maurice Termeer, Javier Oliván Bescós, Marcel Breeuwer, Anna Vilanova, Frans Gerritsen, and Meister Eduard Gröller. CoViCAD: Comprehensive visualization of coronary artery disease. *IEEE Transactions of Visualization and Computer Graphics*, 13(6):1632–1639, 2007. (Cited on pages 14 and 69.)
- [80] Maurice Termeer, Javier Oliván Oliván Bescós, Marcel Breeuwer, Anna Vilanova, Frans Gerritsen, M. Eduard Gröller, and Eike Nagel. Visualization of myocardial perfusion derived from coronary anatomy. *IEEE Transactions of Visualization and Computer Graphics*, 14(6):1595–1602, 2008. (Cited on page 14.)
- [81] Holger Thiele, Sven Plein, Marcel Breeuwer, John P. Ridgway, David Higgins, Penelope J. Thorley, Gerhard Schuler, and Mohan U. Sivananthan. Color-encoded semiautomatic analysis of multi-slice first-pass magnetic resonance perfusion: Comparison to tetrofosmin single photon emission computed tomography perfusion and X-ray angiography. *International Journal of Cardiovascular Imaging*, 20:371–384, 2004. (Cited on page 7.)
- [82] Jeffrey Tsao, Peter Boesiger, and Klaas P. Pruessmann. k-t BLAST and k-t SENSE: Dynamic MRI with high frame rate exploiting spatiotemporal correlations. *Magnetic Resonance In Medicine*, 50:1031–1042, 2003. (Cited on page 7.)
- [83] Stefan Tuchs Schmid. CoroViz: Visualization of 3D whole-heart coronary artery MRA data. Master’s thesis, University of California San Francisco, 2004. (Cited on page 13.)
- [84] Greg Turk. Generating textures on arbitrary surfaces using reaction-diffusion. *Computer Graphics*, 25(4):289–298, 1991. (Cited on page 97.)
- [85] Ivan Viola, Miquel Feixas, Mateu Sbert, and Meister Eduard Gröller. Importance-driven focus of attention. In *Proceedings of IEEE Visualization 2006*, pages 933–940, 2006. (Cited on page 46.)
- [86] Andreas Wahl, Ingo Paetsch, Albrecht Gollesch, Stefan Roethemeyer, Daniela Foell, Holger Langreck, Christoph Klein, Eckart Fleck, and Eike Nagel. Safety and feasibility of high-dose dobutamine-antropine

stress cardiovascular magnetic resonance for diagnosis of myocardial ischaemia: Experience in 1000 consecutive cases. *European Heart Journal*, 25:1230–1236, 2004. (Cited on pages 8 and 9.)

- [87] Jerold W. Wallis and Tom R. Miller. Three-dimensional display in nuclear medicine and radiology. *Journal of Nuclear Medicine*, 32(3):534–546, 1991. (Cited on page 24.)
- [88] Oliver M. Weber, Alastair J. Martin, and Charles B. Higgins. Whole-heart steady-state free precession coronary artery magnetic resonance angiography. *Magnetic Resonance in Medicine*, 50(6):1223–1228, 2003. (Cited on pages 7 and 50.)
- [89] Michael F. Wendland, Maythem Saeed, Gunnar Lund, and Charles B. Higgins. Contrast-enhanced MRI for quantification of myocardial viability. *Journal of Magnetic Resonance Imaging*, 10(5):694–702, 1999. (Cited on pages 10 and 15.)
- [90] W. Yong Kim, Peter G. Danias, Matthias Stuber, Scott D. Flamm, Sven Plein, Eike Nagel, Susan E. Langerak, Oliver M. Weber, Erik M. Pedersen, Matthias Schmidt, René Botnar, and Warren J. Manning. Coronary magnetic resonance angiography for the detection of coronary stenosis. *New England Journal of Medicine*, 345(26):1863–1869, 2001. (Cited on page 7.)




It has yet to be proven that intelligence has any survival value.

---

Arthur C. Clarke

## Curriculum Vitae

### Personal Details

Name	Maurice Alain Termeer	
Address	Lange Gasse 14 / 2 / 27, 1080 Wien, Austria, Europe	
Phone number	+43 69 911 846 227 & +31 6 15 473 769	
Email address	maurice@cg.tuwien.ac.at	
Date of Birth	4 <sup>th</sup> September 1982	
Nationality	Dutch	
Languages	Dutch (native), English (near native), German (moderate)	
Interests	Computer graphics, go & logic puzzles, cycling	

### Educational Background

**2005 - 2009** Vienna University of Technology, Austria. PhD in computer science on the topic of comprehensive visualization of cardiac MRI data at the Institute of Computer Graphics and Algorithms in collaboration with Philips Healthcare. Supervision by Prof. M. Eduard Gröller.

**2003 - 2005** Eindhoven University of Technology, The Netherlands. Masters program computing science & engineering. Master project at Philips Medical Systems on "Constructive Solid Geometry and Volume Rendering." Graduated cum laude.

**2000 - 2003** Eindhoven University of Technology, The Netherlands. Bachelors program computing science & engineering.

### Working Experience

**2005 - 2009** Assistant researcher at Vienna University of Technology.

**2003 - 2005** Developer of DamMentor (an online draughts tutoring program written in Java) at the Royal Dutch Draughts Association (KNDB).

**2002 - 2004** Various small computer science related projects such as supervising student projects and small freelance programming jobs.

**1997 - 2004** Various small jobs such as paper delivery boy and mailman.

## Professional Activities

Referee for international journals and conferences in the area of visualization and computer graphics.

**Journals** IEEE Transactions on Visualization and Computer Graphics, Computer Graphics Forum, Nondestructive Testing and Evaluation.

**Conferences** IEEE Visualization, Eurographics, EuroVis, VMV, GRAPHITE, CGIV, Pacific Graphics, Afrigraph, WSCG.

## Patent Applications

M. TERMEER, M. BREEUWER, J. OLIVÁN BESCÓS, "Volume Bull's Eye Plot," PH-008909-EP-1 (ID 680295), PCT/IB2008/053464, 2007.

M. TERMEER, M. BREEUWER, J. OLIVÁN BESCÓS, "Coronary-Artery Specific 17-Segment AHA Diagram," PH-010411-EP-1 (ID 676667), 2008.

## Publications

M. TERMEER, C. F. J. LANGE, A. TELEA, M. R. V. CHAUDRON, "Visual Exploration of Combined Architectural and Metric Information," in proceedings of VISSOFT 2005, pp. 21–26, 2005.

M. TERMEER, J. OLIVÁN BESCÓS, A. TELEA, "Preserving Sharp Edges with Volume Clipping," in proceedings of Vision, Modeling and Visualization 2006, pp. 341–348, 2006.

M. TERMEER, J. OLIVÁN BESCÓS, M. BREEUWER, A. VILANOVA, F. GERRITSEN, M. E. GRÖLLER, "CoViCAD: Comprehensive Visualization of Coronary Artery Disease," in IEEE Transactions on Visualization and Computer Graphics 13(6), pp. 1632–1639, 2007.

M. TERMEER, J. OLIVÁN BESCÓS, M. BREEUWER, A. VILANOVA, F. GERRITSEN, M. E. GRÖLLER, "The Volumetric Bulls Eye Plot," Poster at the SCMR 11th Annual Scientific Sessions, 2008.

M. TERMEER, J. OLIVÁN BESCÓS, M. BREEUWER, A. VILANOVA, F. GERRITSEN, M. E. GRÖLLER, E. NAGEL, "Visualization of Myocardial Perfusion Derived from Coronary Anatomy," in IEEE Transactions on Visualization and Computer Graphics 14(6), pp. 1595–1602, 2008.

M. TERMEER, J. OLIVÁN BESCÓS, M. BREEUWER, A. VILANOVA, F. GERRITSEN, M. E. GRÖLLER, E. NAGEL, "Patient-Specific Mappings between Myocardial and Coronary Anatomy," Technical report, Institute of Computer Graphics and Algorithms, Vienna University of Technology, Vienna, Austria, 2008.

M. TERMEER, J. OLIVÁN BESCÓS, M. BREEUWER, A. VILANOVA, F. GERRITSEN, M. E. GRÖLLER, E. NAGEL, "Patient-Specific Coronary Artery Supply Territory AHA Diagrams," Poster at the SCMR 12th Annual Scientific Sessions, 2009.